TARGETED PRINT® NANOPARTICLES FOR EFFECTIVE CANCER THERAPY

Kelly Marie McGowan

A dissertation submitted to the faculty of the University of North Carolina at Chapel Hill
in partial fulfillment of the requirements for the degree of Doctor of Philosophy in the
Department of Chemistry

Chapel Hill
2011

Approved by:

Joseph DeSimone

Nancy Allbritton

Moo Cho

Michael Rubinstein

Edward Samulski

# ABSTRACT

KELLY MCGOWAN: Targeted PRINT® Nanoparticles for Effective Cancer Therapy
(Under the direction of Joseph DeSimone)


Conventional therapeutics for the treatment of cancer are often faced with challenges such as systemic biodistribution within the body, drug degradation *in vivo*, low bioavailability at the site of disease, and off-target toxicity.  As such, particulate drug delivery systems have been developed with the aim of minimizing these limitations of current therapies.  Through the PRINT® (Particle Replication in Non-wetting Templates) technology, hydrogel nanoparticles, prepared from biocompatible poly(ethylene glycol) and acid-sensitive silyl ether crosslinkers, were functionalized and conjugated with targeting ligands for the folate receptor (FR), HER2 receptor, and transferrin receptor (TfR).  By conjugating specific ligands to nanoparticles to impart specificity, highly selective targeting and internalization ($>80\%$) of nanoparticles were demonstrated in various cancer cell lines.  The extent of cellular uptake of targeted nanoparticles was dependent on the surface characteristics of the nanoparticles, particle concentration, and kinetics.  Because a negative surface charge reduces nonspecific cellular uptake, attaching monoclonal antibodies to the surface of negatively charged PRINT nanoparticles facilitated specific binding of the antibodies to cellular surface receptors that subsequently triggered receptor-mediated endocytosis.  Additionally, the multivalent nature of nanoparticles influenced cellular uptake.  Specifically, nanoparticles with a

higher valence internalized more rapidly and efficiently than those with a lower valence. Nanoparticles that selectively target and accumulate within diseased cells have the potential of minimizing drug degradation under physiological conditions, enhancing bioavailability at the tumor, improving the efficacy of the drug, and reducing toxicity from systemic biodistribution.

Drug delivery through targeted nanoparticles was achieved by loading nanoparticles with silyl ether-modified gemcitabine prodrugs. Covalently reacting the prodrug into the nanoparticle matrix minimized drug loss, while the acid-sensitive silyl ether moiety enabled release of gemcitabine at a low pH. Targeted nanoparticles appeared to accumulate intracellularly, through TfR-mediated endocytosis, within acidic vesicles whose environment could trigger degradation of the prodrug and thus, release of gemcitabine. Leveraging the specificity of targeted nanoparticles and acid-sensitive silyl ether-based gemcitabine, targeted nanoparticles ($IC_{50} = 1.8 \times 10^{-2}$ nM) were far more potent than free gemcitabine ($IC_{50} = 4.1 \times 10^{4}$ nM). Therefore, this system demonstrates the tremendous potential of targeted PRINT nanoparticles as advanced drug delivery agents.

**TABLE OF CONTENTS**

# LIST OF TABLES

# LIST OF FIGURES

# LIST OF ABBREVIATIONS AND SYMBOLS

| | |
|---|---|
| ° C | degrees Celsius |
| μg | microgram |
| μL | microliter |
| μm | micrometer |
| μM | micromolar |
| % | percent |
| ® | registered |
| ζ-potential | zeta potential |
| Ab | antibody |
| AR | aspect ratio |
| bTf | bovine transferrin |
| cyto D | cytochalasin D |
| *d* | diameter |
| dCK | deoxycytidine kinase |
| DES | diethyl silyl ether crosslinker |
| DIS | diisopropyl silyl ether crosslinker |
| DLS | dynamic ligh scattering |
| DMF | dimethylformamide |
| DMS | dimethyl silyl ether crosslinker |
| DNA | deoxyribonucleic acid |
| DOG | 2-deoxyglucose |

| | |
|---|---|
| DPBS | Dulbecco's phosphate buffered saline |
| DTS | di-*tert*-butyl silyl ether crosslinker |
| DTT | dithiothreitol |
| EEA1 | early endosome antigen 1 |
| EGFR | epidermal growth factor receptor |
| EPR | enhanced permeability and retention |
| FA | folic acid |
| FDA | US Food and Drug Administration |
| FR | folate receptor |
| *h* | height |
| h | hour |
| hENT1 | human equilibrative nucleoside transporter 1 |
| HER1 | human epidermal growth factor receptor 1 |
| HER2 | human epidermal growth factor receptor 2 |
| HIV | human immunodeficiency virus |
| HPLC | high-performance liquid chromatography |
| HPMA | *N*-(2-hydroxypropyl)methacrylamide |
| hTf | human transferrin |
| $IC_{50}$ | half maximal inhibitory concentration |
| IgG | immunoglobulin G |
| $K_d$ | dissociation constant |
| kPa | kilopascal |
| MβCD | β-cyclodextrin |

| | |
|---|---|
| mAb | monoclonal antibody |
| mg | milligram |
| mL | milliliter |
| ms | millisecond |
| mV | millivolts |
| MW | molecular weight |
| NaN$_3$ | sodium azide |
| NHS-PEG-biotin | biotin-poly(ethylene glycol)-succinimidyl carboxymethyl ester |
| NHS-PEG-Mal | maleimide-poly(ethylene glycol)-succinimidyl carboxymethyl ester |
| nm | nanometer |
| nM | nanomolar |
| NP-7mer | heptamer-targeted nanoparticles |
| NP-bTf | bovine transferrin-targeted nanoparticles |
| NP-FR | anti-folate receptor antibody-targeted nanoparticles |
| NP-Herc | Herceptin-targeted nanoparticles |
| NP-hTf | human holo-transferrin-targeted nanoparticles |
| NP-IgG | IgG-targeted nanoparticles |
| NP-OKT9 | anti-transferrin receptor antibody-targeted nanoparticles |
| NTs | nucleoside transporters |
| OKT9 | anti-human transferrin receptor monoclonal antibody |
| PBS | phosphate buffered saline |
| PDI | polydispersity index |
| PEG | poly(ethylene glycol) |

| | |
|---|---|
| PEG$_8$DES | poly(ethylene glycol) diethyl silyl ether crosslinker |
| PEG$_8$DTS | poly(ethylene glycol) di-*tert*-butyl silyl ether crosslinker |
| PET | poly(ethylene terephthalate) |
| PLA | poly-L-glutamic acid |
| PLGA | poly(lactic acid-*co*-glycolic acid) |
| PRINT | Particle Replication In Non-wetting Templates |
| pyr | pyridine |
| RES | reticulo-endothelial system |
| RGD | arginine-glycine-aspartic acid |
| RNA | ribonucleic acid |
| RT | room temperature |
| SEM | scanning electron microscopy |
| TES | triethyl silyl ether |
| TfR | transferrin receptor |
| TIS | triisopropyl silyl ether |
| TMS | trimethyl silyl ether |
| UV | ultra violet |
| wt % | weight percent |

# CHAPTER 1

## ENGINEERING PARTICLES AS POTENT DRUG DELIVERY SYSTEMS

## 1.1 Designing Nanoparticles as Cancer Therapeutics

Conventional chemotherapeutic drugs are effective in the treatment of cancers but also have limitations. They are distributed nonspecifically throughout the body, affecting both normal and cancerous cells.[1] This lack of specificity and thus bioavailability decreases the efficacy of the drugs. However, toxicity to normal tissue limits the dose and frequency of treatment. Thus, nanotechnology has been employed to address these issues for therapeutic drug delivery.[2] Several parameters, such as particle size, shape, modulus, surface charge, surface chemistry, and drug release, must be considered in the rational design of drug nanocarriers and are discussed below.

## 1.1.1 Nanoparticle Therapeutics

Through nanotechnology, researchers have developed methods for improving the therapeutic efficacy and functionality of cancer treatments.[3] Some extensively researched nanovectors include nanoparticles,[4] liposomes,[5] dendrimers,[6] and micelles[7] (Figure 1.1).
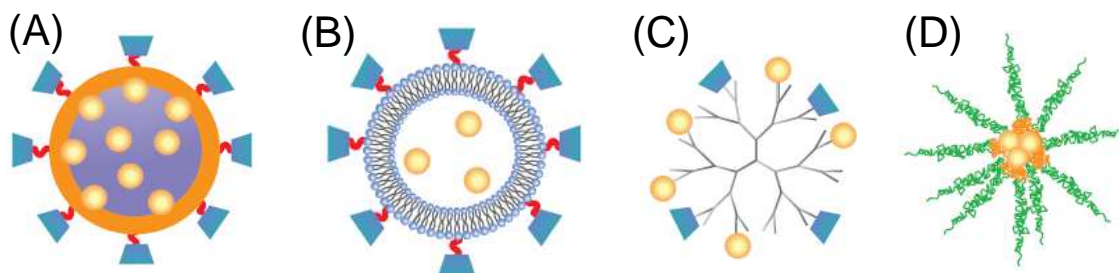
**Figure 1.1** Examples of nanocarrier systems for drug delivery: (A) nanoparticles, (B) liposomes, (C) dendrimers, and (D) micelles. Adapted from [8].

Liposomes are spherical, self-assembled colloidal vesicles produced from lipid bilayers with an inner aqueous phase. The lipids consist of a hydrophilic head and a hydrophobic tail. They are appealing as nanocarriers because of their general biocompatibility, biodegradability, and amphiphilicity.[9] Both hydrophilic and hydrophobic molecules have been incorporated into liposomal strategies with success. Doxil and Myocet are liposomal formulations of the chemotherapeutic doxorubicin and are approved for the treatment of metastatic breast cancer, ovarian cancer, and multiple myeloma.[10-12] DaunoXome is daunorubicin formulated within liposomes and is indicated as a therapeutic for advanced HIV-associated Kaposi's sarcoma.[13]

Micelles are another class of lipid-based nanocarriers. Commonly prepared from amphiphilic block copolymers, micelles are self-assembled closed colloidal structures that consist of a lipid monolayer with a hydrophobic core and hydrophilic shell.[14] The hydrophilic outer region stabilizes the hydrophobic core while rendering the system soluble under aqueous conditions. The hydrophobic core serves as a reservoir for hydrophobic or water-insoluble drugs.[15] By this approach, Genexol-PM and NK105 are

currently in clinical trials as polymeric micelle formulations of paclitaxel for the treatment of various cancers, including breast, pancreatic, and gastric cancer.[16,17]

Dendrimers are synthetic, branched macromolecules of nanometer dimensions (average diameter of 1.5-14.5 nm) with arms that extend radially from a central core.[18] They are biocompatible, monodisperse, multivalent, highly water soluble, and possess a modifiable surface.[6,19] Polyamidoamine dendrimers are one of the most commonly used platform in this area and have demonstrated improved efficacy as cancer treatments over free systemic drugs such as cisplatin and methotrexate.[20,21] Dendrimers can be conjugated with targeting molecules, imaging agents, or drugs for multifunctional drug delivery systems, but they require numerous synthetic steps, which can be difficult to translate into large-scale production.[8,18,22]

Nanoparticles have also been explored as pharmaceutical vehicles for cancer therapy. While they can be prepared from organic and inorganic materials, polymers are among the most common scaffolds for nanoparticles. Synthetic polymers, such as *N*-(2-hydroxypropyl)methacrylamide copolymer (HPMA), poly(ethylene glycol) (PEG), and poly-L-glutamic acid (PLA), have been conjugated to therapeutics for polymer-drug conjugates.[23,24] They can be formulated to incorporate hydrophobic or hydrophilic cargo, both small molecule drugs and macromolecules such as nucleic acids and proteins.[25-27] Nanoparticles can also be tailored to release therapeutic cargo at a controlled rate in a time- or condition-dependent fashion.[28-30] The surface of nanoparticles can be functionalized to influence *in vivo* circulation and accumulation at the target site.[31,32] Naturally occurring polymers, such as albumin, chitosan, and heparin, have also been utilized to deliver chemotherapeutic drugs.[1] For example, Abraxane is a nanoparticulate

formulation of paclitaxel in which the drug is bound by albumin. It is approved for the treatment of metastatic breast cancer and is being investigated in clinical trials for the treatment of other cancers including non-small-cell lung cancer.[33,34]

### 1.1.2 Particle Size and Shape

The size of particles plays an important role in biodistribution *in vivo* and mechanisms of cellular internalization. Most studies have investigated the effect of size with spherical particles. Nanoparticles in the size range of 10-100 nm are generally accepted as effective drug delivery agents, determined by *in vivo* clearance and biodistribution. Particles less than 5-10 nm are typically cleared rapidly from circulation through renal clearance,[35,36] and larger particles up to around 15 µm generally collect in the liver and spleen and are removed from circulation by the reticulo-endothelial system (RES).[37,38] Kupffer cells in the liver are actively involved in removal of particles, as well as mechanical filtration of particles by sinusoids in the spleen.[39]

Particle size is also a key factor in the mechanism of cellular internalization. Particles can be internalized into cells through phagocytosis, macropinocytosis, caveolae-mediated endocytosis, or clathrin-mediated endocytosis.[40-42] The mode of particle entry into cells influences subsequent intracellular microenvironments of the particle. Understanding the mechanism of internalization allows particles to be engineered to accumulate in particular intracellular regions for site specific triggers or drug delivery.

As the field of nanomedicine continues to advance, the shape of particles is emerging as a key factor in biodistribution and cellular internalization. It has been reported that prolate elliposoids can effectively attach to macrophages but are not well

4

internalized.[43,44] Also, the geometry of interaction between the particle and cell is critical to inducing or inhibiting internalization. Tangent angles of the particle at the point in contact with macrophages must be less than 45° for particle internalization.[45] Furthermore, filomicelles, filamentous particles with lengths up to 18 µm, have been reported to circulate *in vivo* for up to one week whereby the circulation time correlated with the length of the particle.[46]

### 1.1.3 Particle Modulus

The modulus of particles is another significant factor in designing particulate drug delivery systems that has not been thoroughly investigated. One study reported the low uptake of soft polyacrylamide beads (1-6 µm) by macrophages while their rigid counterparts were readily phagocytosed.[47] They found that the soft particles frustrated actin filament formation by macrophages, thereby preventing internalization. Conversely, another report of rigid liposomes decreased complement activation and thus, reduced internalization by macrophages.[48] This area requires additional research but has shown to be an important parameter for consideration in designing therapeutic particles.

### 1.1.4 Particle Surface Charge

The surface charge of particles can influence cellular internalization and *in vivo* circulation. Generally, positively charged particles are efficiently internalized by cells because of electrostatic interactions between the positively charged particle surface and the negatively charged cellular membrane.[49,50] Particles with a positive surface charge

also undergo more phagocytosis by macrophages and accumulate in the liver and spleen.[51,52]  Conversely, particles with negative surface charges typically exhibit low cellular internalization.[53]  It has also been reported that negatively charged particles can circulate longer *in vivo* and thus, better accumulate in the tumor.[54]

### 1.1.5  Particle Surface Chemistry

Surface properties of particles influence their interactions with proteins and cells in vivo.  Poly(ethylene glycol) (PEG) is often conjugated to the surface of particles to impart stealthing properties in circulation.  PEG reduces adsorption by serum proteins, minimizes nonspecific cellular uptake, and decreases phagocytosis by macrophages, thereby extending circulation time *in vivo*.[55]  In addition to prolonging circulation within the body for accumulation of particles in the tumor, selective interaction with cells is important.  It is desirable for particles to specifically internalize into cancerous cells so as to deliver therapeutic cargo to the site of interest, thereby maximizing drug efficacy while minimizing any adverse side effects.  Thus, targeting ligands are conjugated to the surface of particles to promote cellular internalization at the disease site.[56]

### 1.2  PRINT Particles as Cancer Therapeutics

The PRINT (Particle Replication In Non-wetting Templates) technology is a robust particle fabrication approach that facilitates independent control over particle size, shape, matrix composition, and surface chemistry.  It has been described previously[57-64] and is illustrated in Figure 1.2.  Photopolymerizable low surface energy prepolymers,

such as perfluoropolyethers, are used to generate elastomeric molds that replicate features on a silicon master produced by photolithographic techniques. These molds become the template for the fabrication of particles prepared from proteins,[59] monomers,[58,60-64] or polymers.[57] A preparticle solution is applied to the PRINT mold, provided by Liquidia Technologies, with a sheet of poly(ethylene terephthalate) (PET). The mold and PET are laminated together under pressure to fill the cavities in the mold with the preparticle solution. As the sheet of PET is separated from the mold, excess preparticle solution is effectively removed from the mold because of the higher surface energy of the PET, and thus, enables the formation of individual particles. Solidified particles can then be transferred to a sacrificial adhesive layer for collection.
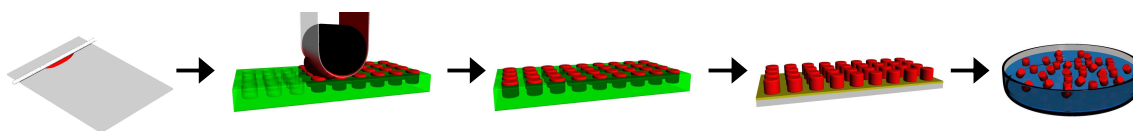


**Figure 1.2** Schematic illustration of the PRINT process.

Through the PRINT platform, a variety of particles (Figure 1.3) have been fabricated to investigate the rational design of particles for delivery of therapeutics. Particles of different shapes and sizes from 80 nm to 20 $\mu$m, composed of biocompatible polymers such as poly(ethylene glycol) (PEG), poly(D-lactic acid), and proteins, have been fabricated.[57,59,62] Additionally, particles were prepared from novel silyl ether-based materials and disulfide crosslinkers to produce stimuli responsive nanocarriers for advanced drug delivery.[61,65] PRINT particles have also been readily loaded with chemotherapeutic drugs and imaging agents as therapeutic and imaging particle

7

systems.[61,65-67] Furthermore, particle surfaces have been modified for specific targeting, imaging, and enhancing *in vivo* circulation.[63,68] Through the PRINT process, various factors in engineering model particles as drug delivery vehicles have been investigated and will be discussed below.
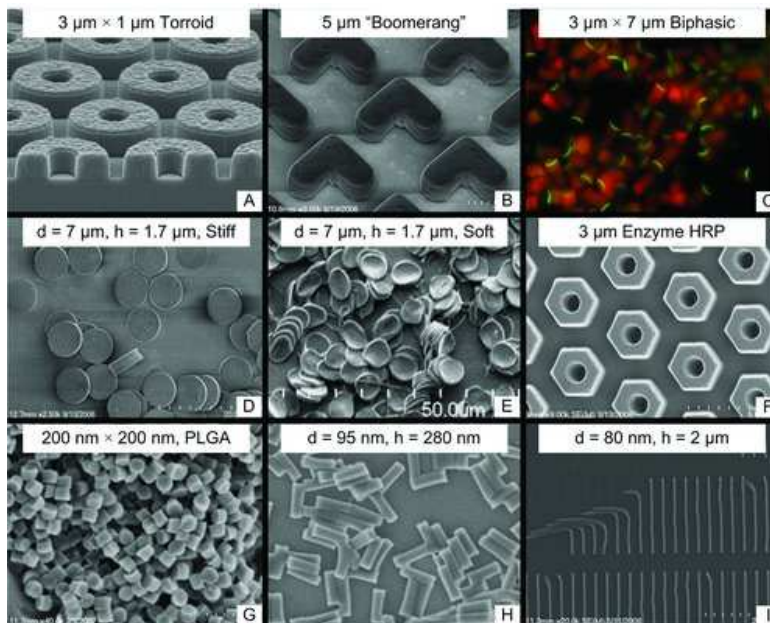


**Figure 1.3** Diverse array of hydrogel (unless noted otherwise) particles fabricated through the PRINT platform.[69]

### 1.2.1 Particle Size and Shape

Employing the PRINT technology and its independent control over particle shape and size, hydrogel particles over a range of sizes (100 nm to 5 µm) and shapes (cylinders and cubes) were fabricated, and the interdependent effect on internalization in HeLa cells was investigated.[58] Generally, large microparticles internalized more slowly than smaller nanoparticles, with 3 µm and 5 µm cubic particles internalizing minimally in HeLa cells. HeLa cells internalized more cylindrical particles (~75%) with diameters of 500 nm and

1 µm ($h$ = 1 µm for both particles) than 2 µm cubic particles (~45%). For the nanoparticles, cylindrical nanoparticles with dimension of $d$ = 150 nm and $h$ = 450 nm (aspect ratio, AR = 3) internalized most rapidly and effectively. Despite a similar volume, the more symmetric, low AR, cylindrical counterparts ($d$ = 200 nm and $h$ = 200 nm, AR = 1) were internalized more slowly. Cylindrical nanoparticles with a diameter of 100 nm and an AR of 3 were also internalized more slowly than nanoparticles with a diameter of 150 nm and AR of 3 (Figure 1.4). This demonstrates that the internalization kinetics of nanoparticles by HeLa cells is dependent on both the size of the particles and the shape (elongated, rod-like vs. symmetric cylinder).
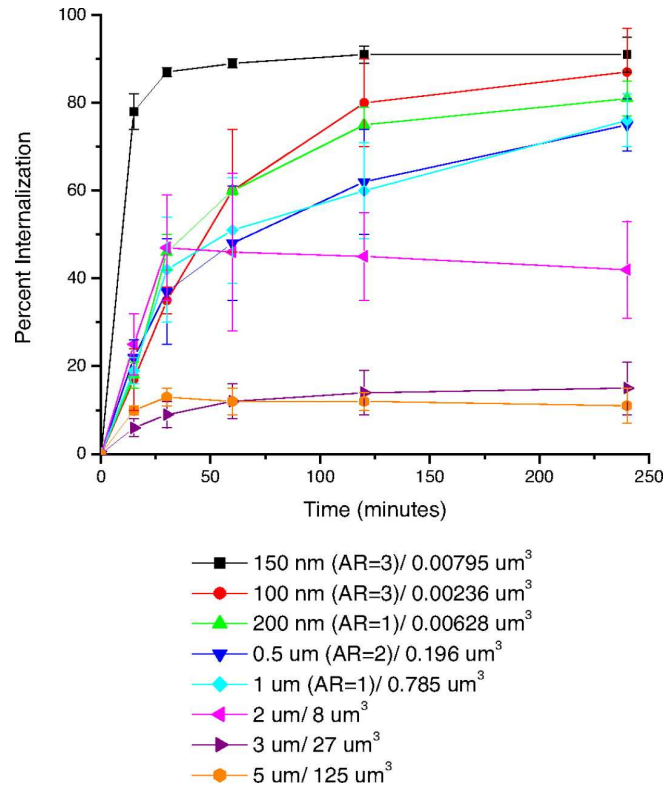


**Figure 1.4** Internalization of PRINT particles into HeLa cells at 15 µg/mL and 37 °C up to 4 h. Legend depicts particle dimater and volume.[58]

Internalization of these hydrogel particles by HeLa cells was mostly mediated by a combination of clathrin and caveolae pathways (Figure 1.5).[58] Prior to incubation with particles, HeLa cells were incubated with various biochemical inhibitors of energy-dependent processes, clathrin-mediated endocytosis, caveolae-mediated endocytosis, and macropinocytosis. Inhibition of cellular uptake by cells pretreated with sodium azide/2-deoxyglucose ($NaN_3$/DOG) suggests that all particles are internalized through an energy-dependent process. Decreased uptake of particles was observed for cells preincubated with cytochalasin D (cyto D), an inhibitor of macropinocytosis/phagocytosis and also clathrin- and caveolae-mediated endocytosis. In the presence of inhibitors for clathrin-mediated endocytosis, Dynasore, chlorpromazine, and genistein, cellular uptake of cylindrical nanoparticles (150 nm, AR = 3 and 200 nm, AR = 1) decreased markedly. For 1 µm (AR = 1) particles, only chlorpromazine significantly inhibited uptake of the particles. Although the mechanism of internalization is unclear for larger particles, nanoparticles are clearly internalized, in part, by clathrin-mediated pathways. In the presence of inhibitors for caveolae-mediated endocytosis, β-cyclodextrin (MβCD) and genistein, internalization of nanoparticles was affected more significantly than uptake of microparticles, which was expected as caveolae generally can only endocytose particles in the range of 50-100 nm.[70] This work suggests that clathrin- and caveolae-mediated endocytosis, and to a lesser extent, macropinocytosis are all involved in cellular uptake of nanoparticles and microparticles. These mechanisms appear to play a larger role with the internalization of 150 nm (AR = 3) and 200 nm (AR = 1) nanoparticles. Nonetheless, none of the biochemical inhibitors that were studied inhibited particle internalization to

>95%, suggesting that the possibility of non-clathrin- and non-caveolae-mediated mechanisms of internalization.
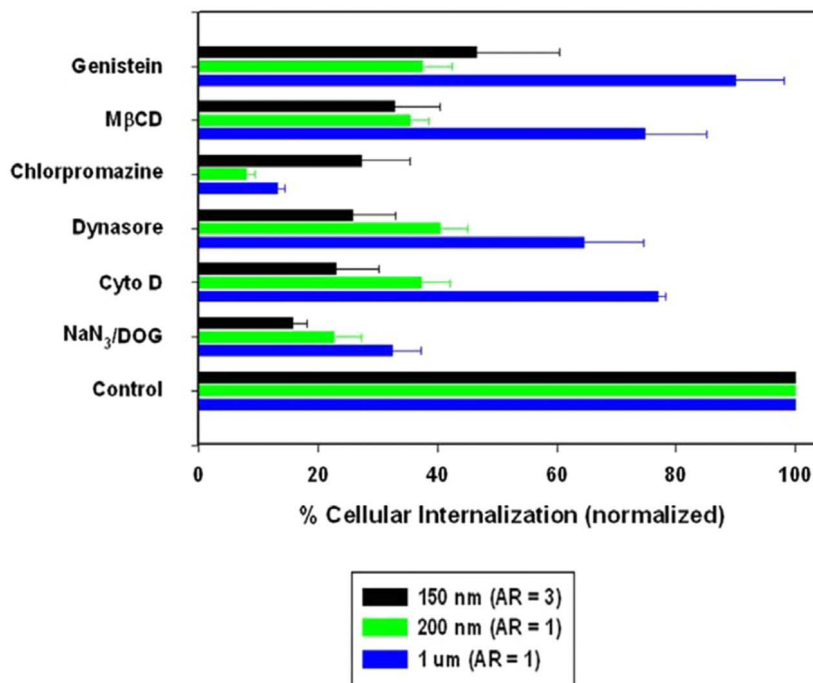


**Figure 1.5** Internalization of PRINT particles into HeLa cells preincubated with various inhibitors of endocytosis.[58]

### 1.2.2 Particle Modulus

Modulus is a factor for consideration in the design of particles for cancer therapy. It has not been extensively explored, scientific thought is that the modulus of particles dictates the *in vivo* biodistribution and circulation time. Red blood cells are extraordinarily flexible, able to deform as they circulate *in vivo* and pass through restrictions in vasculature that are smaller than their diameter.[71] To investigate the effect of particle modulus, we fabricated hydrogel microparticles, with tunable elasticity, in the shape (biconcave disks) and size (6 µm) resembling red blood cells (Figure 1.6A).[60]

11

Macroscopic coupons of the hydrogels with varied amounts of crosslinker resulted in moduli that ranged from 64 to 8 kPa, including the modulus of red blood cells (26 kPa). In microfluidic models of vascular constrictions, the low crosslinked, soft microparticles readily navigated channels that were 3 µm wide and 50 µm long, while rigid microparticles clogged the channels (Figure 1.6).
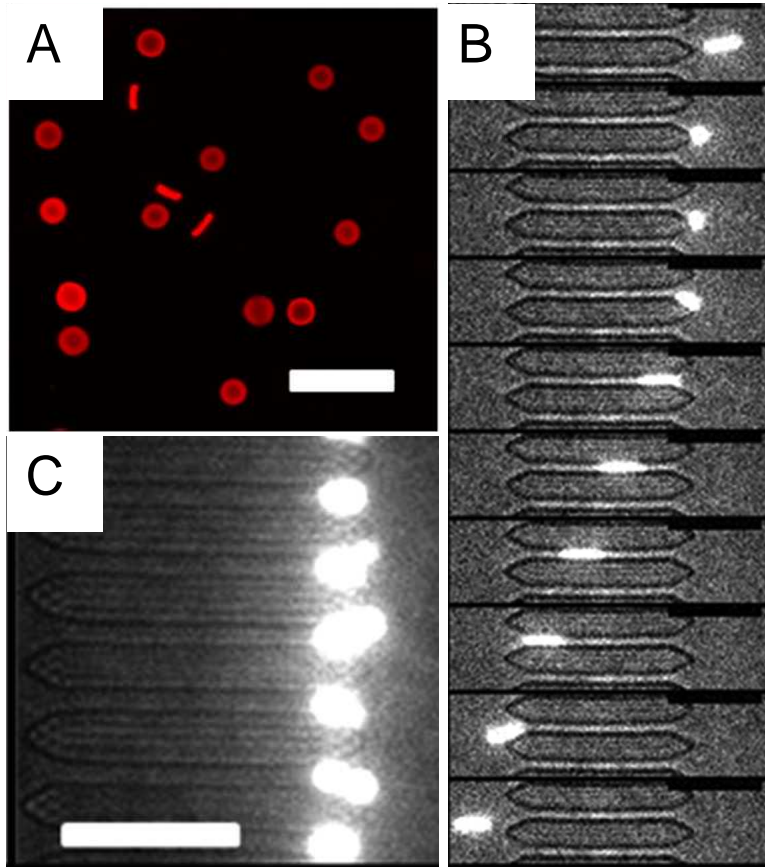


**Figure 1.6** Deformable red blood cell mimics. (A) Fluorescent image of hydrated 10% crosslinked particles. Scale bar is 20 µm. (B) Image sequence of 1% crosslinked particles deforming to pass through 3 µm × 3.5 µm channel (25 ms between frames). (C) 10% crosslinked particles stuck at entrance of channels in microfluidic device. Scale bars are 30 µm.[60]

For *in vivo* studies, it was found that microparticles with low modulus bypassed *in vivo* filtration mechanisms in various organs, such as the lung, and were able to circulate for several days with a 30-fold increase in elimination half-life relative to their rigid counterparts. While flexible microparticles were mostly sequestered into the spleen, rigid microparticles were largely accumulated in the lungs (Figure 1.7).[60] This study demonstrates that the modulus of particles is an important design parameter that affects pharmacokinetics and biodistribution.
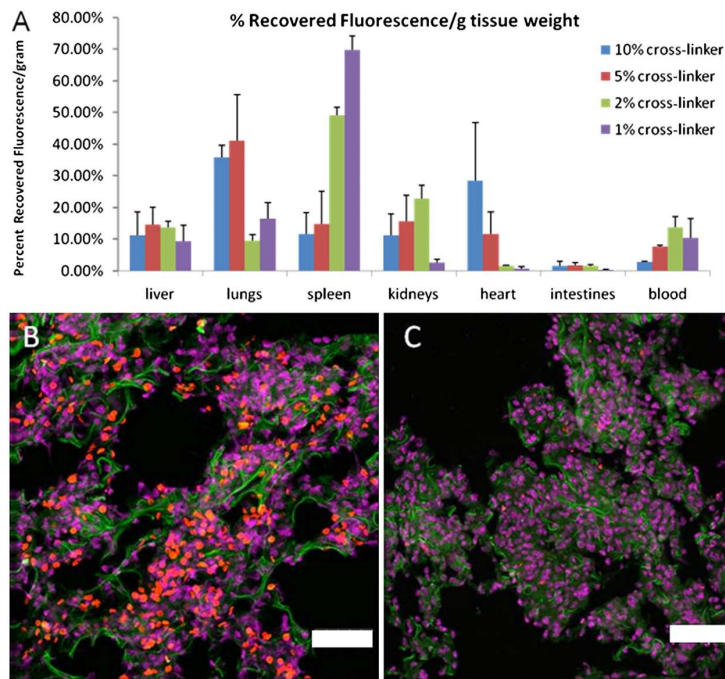


**Figure 1.7** Biodistribution of red blood cell mimics. (A) Distribution of particles in various tissues 2 h after dosing. (B) Lung tissue of a mouse dosed with 10% crosslinked particles (red). Cell nuclei are stained purple and the cytoskeleton (F-actin) is stained green. (C) Lung tissue of a mouse dosed with 1% crosslinked particles. Scale bars are 50 μm.[60]

### 1.2.3 Particle Surface Charge

Studies have demonstrated that the surface charge of particles plays an important role in cellular internalization.[49-54]  So the effect of $\zeta$-potential of PRINT particles on cellular uptake was explored.  Cylindrical hydrogel PRINT nanoparticles ($d = 150$ nm and $h = 450$ nm) were fabricated, and their cellular uptake was investigated *in vitro* with HeLa cells.[58]  Nanoparticles were reacted with acetic anhydride to passivate protonated surface amine groups, shifting the $\zeta$-potential from +35 mV to -34 mV.  Positively charged nanoparticles internalized into 84% of cells after an incubation period of 1 h.  However, less than 5% of cells internalized the negatively charged counterparts.  This suggests that the surface charge of particles is a critical factor in cellular internalization and the design of drug delivery agents.

### 1.2.4 Particle Surface Chemistry

Surface modification of particles is an extensively researched area, particularly with the aim of extending in vivo circulation and delivering therapeutics specifically to diseased cells.  Through the PRINT platform, we have fabricated nanoparticles to investigate the effect of multivalency on targeting and cell biology.[63]  The surface of cylindrical ($d = 200$ nm and $h = 200$ nm) hydrogel nanoparticles were conjugated with ligands specific for the transferrin receptor (TfR).  Human holo-transferrin-targeted nanoparticles (NP-hTf) and anti-TfR antibody-targeted nanoparticles (NP-OKT9) selectively internalized into HeLa, Ramos, H460, SKOV3, HepG2, and LNCaP cancer cell lines with varying levels of overexpression of the TfR, as well as HEK293 cells, a transformed normal human cell line with low expression of the TfR (Figure 1.8A).

Cellular uptake of targeted nanoparticles was found to correlate with the expression level of TfR in the cell lines, in addition to being dependent on nanoparticle concentration, targeting ligand density, and incubation times. In contrast, control nanoparticles (NP-bTf and NP-IgG1) were minimally internalized (<10%) in all cell lines investigated. When the viability of cells treated with nanoparticles was investigated, no cytotoxicity to targeted nanoparticles was observed for HeLa, H460, SKOV3, HepG2, or LNCaP cells. However, both NP-hTf and NP-OKT9 exhibited dose dependent cytotoxicity to Ramos Burkitt's lymphoma cells (Figure 1.8B). It is believed that this cytotoxicity is due to the multivalent nature of the nanoparticles with numerous copies of specific TfR ligands hTf and OKT9. By functionalizing the surface of nanoparticles with specific targeting ligands, selective internalization was achieved, demonstrating the potential of targeted PRINT nanoparticles as site-specific drug nanocarriers. Moreover, the cytotoxicity of NP-hTf and NP-OKT9 to Ramos cells only suggests the potential of targeted nanoparticles as effective therapeutics without an additional chemotherapeutic payload.
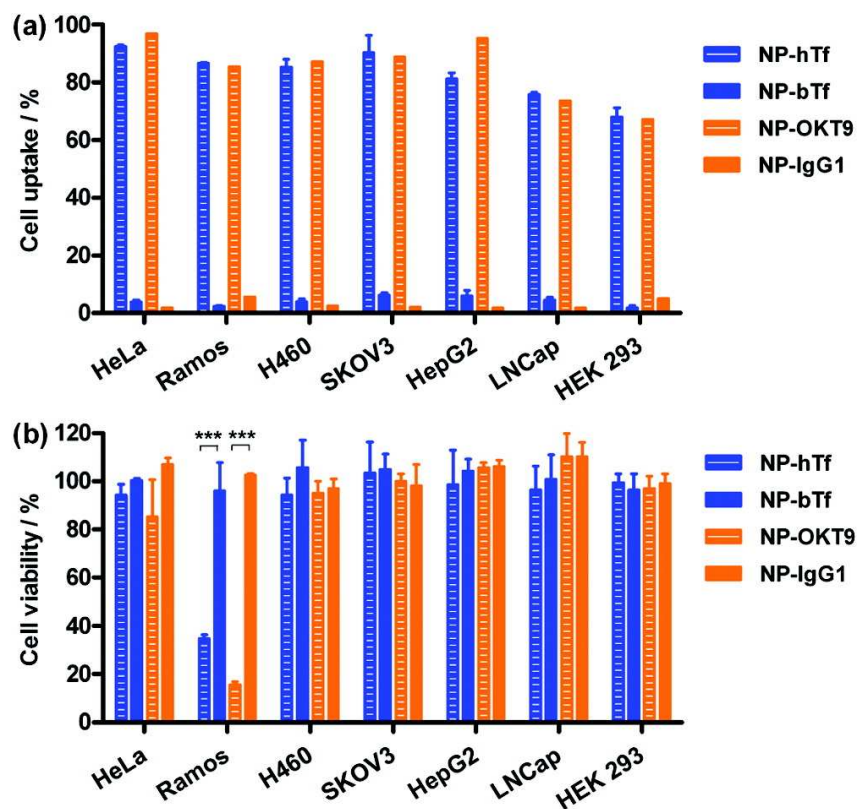
**Figure 1.8** Transferrin receptor-targeted delivery of nanoparticles. (A) Cellular uptake and (B) cytotoxicity of nanoparticles in various cancer cell lines. ***, $P < 0.001$.[63]

## 1.2.5 Delivery of Therapeutics

Effective drug delivery systems are biocompatible, target specific, and can deliver and release a therapeutic payload at the tumor site. One such system includes poly(lactic acid-*co*-glycolic acid) (PLGA) PRINT particles with high loading of docetaxel, up to 40%.[57] We demonstrated the facile fabrication of particles, in various shapes and sizes, from PLGA, a biocompatible and bioabsorbable polymer that has proven promise in biomedical devices and applications.[72,73] Docetaxel was easily and efficiently encapsulated into PLGA cylindrical ($d$ = 200 nm and $h$ = 200 nm) nanoparticles. When investigated *in vitro* with SKOV3 cells, nanoparticles loaded with 40% of docetaxel were

16

more efficacious ($IC_{50}$ = 0.013 nM) than nanoparticles of lower loadings (10%, 20%, and 30%), as well as Taxotere, the clinical formulation of docetaxel ($IC_{50}$ = 0.103 nM, Table 1.1 and Figure 1.9). This suggests that docetaxel is released from the nanoparticles and can be delivered intracellularly to trigger cytotoxic effects that are more potent than the current therapy.

**Table 1.1** $IC_{50}$ values of docetaxel-loaded PLGA PRINT nanoparticles and Taxotere.[57]

|  | $IC_{50}$ (nM of Docetaxel) |
| --- | --- |
| Taxotere | 0.103 |
| 10% Docetaxel Nanoparticles | 0.379 |
| 20% Docetaxel Nanoparticles | 0.158 |
| 30% Docetaxel Nanoparticles | 0.072 |
| 40% Docetaxel Nanoparticles | 0.013 |
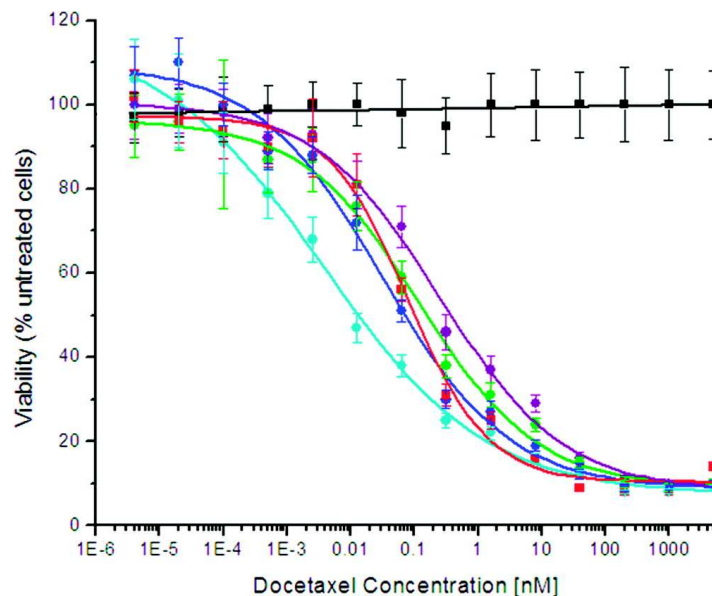
**Figure 1.9** Cytotoxicity of Taxotere (red) and PLGA PRINT nanoparticles with 0% docetacel (black), 10% docetaxel (purple), 20% docetaxel (green), 30% docetaxel (dark blue), and 40% docetaxel (light blue) to SKOV3 cells after 72 h. Blank nanoparticles (0% docetaxel) were dosed at equal nanoparticle concentrations to 10% docetaxel nanoparticles.[57]

To minimize release of chemotherapeutics from nanocarriers until the drug delivery agents reach cancerous cells, particles are often engineered to be responsive to acidic and reducing environments within cells. We investigated the delivery of the encapsulated doxorubicin in microparticles designed to release cargo under intracellular reducing environments such as the cytosol.[65] Cubic (2 µm) hydrogel particles were fabricated with and without the reductively labile disulfide crosslinker *N,N'*-cystaminebisacrylamide (Table 1.2). Particles with the disulfide crosslinker released doxorubicin when incubated with the reductant dithiothreitol (DTT), but when stirred only in phosphate buffered saline (PBS), doxorubicin was not released from the microparticles. For particles without the disulfide crosslinker, no release of doxorubicin was observed in the presence of DTT.

**Table 1.2** Composition of reductively labile PRINT microparticles.  Adapted from [65].

| Composition | A | B | C |
|---|---|---|---|
| Trimethylolpropane ethyoxylate (14/3 EO/OH) triacrylate | 57 | 87 | 57 |
| *N*,*N'*-Cystaminebisacrylamide | 30 | 0 | 30 |
| Doxorubicin HCl | 2 | 2 | 0 |
| 2-Aminoethylmethacrylate HCl | 10 | 10 | 10 |
| 1-Hydroxycyclohexyl phenyl ketone | 1 | 1 | 1 |

When cytotoxicity of the particles was investigated *in vitro* in HeLa cells, particles containing the disulfide crosslinker and doxorubicin were markedly more cytotoxic (only 10% viable cells) than those without the reductively labile disulfide crosslinker and were also nearly as potent as free doxorubicin (Figure 1.10).  This work suggests that the reducing intracellular environment triggered release of doxorubicin from the microparticles.  It is believed that the reduction of the disulfide crosslinker decreased the mesh density of the particles, thereby increasing the porosity of the particles for passive diffusion of the cargo.
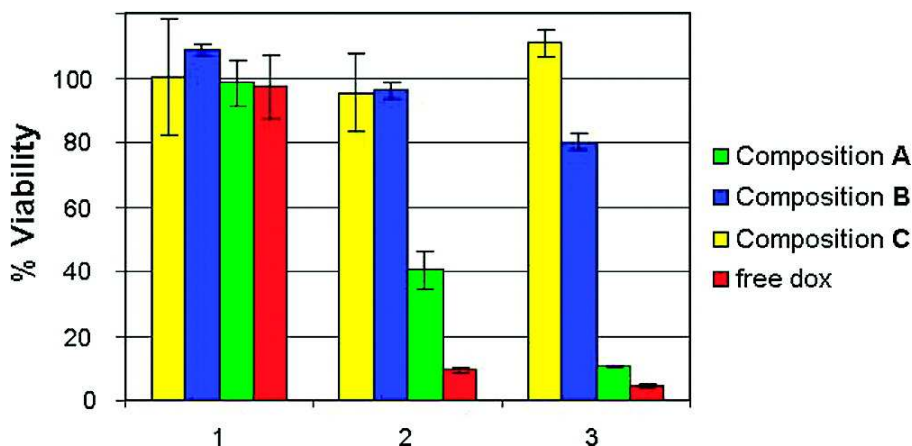
**Figure 1.10** Cytotoxicity of doxorubicin (dox) and doxorubicin-loaded PRINT microparticles to HeLa cells. Dosing of 1-3 was 2.5, 160, 640 µg/mL for particles and 0.05, 3.2, and 12.8 µg/mL for doxorubicin.[65]

Along the same lines, stimuli responsive microparticles, composed of acid sensitive bifunctional silyl ether crosslinkers, were fabricated.[61] A collection of novel crosslinkers based upon silyl ether chemistry was designed and synthesized: dimethyl (DMS), diethyl (DES), diisopropyl (DIS), and di-*tert*-butyl (DTS) silyl ether crosslinkers. Silyl ethers are acid labile, and their sensitivity is tunable.[74] Large, bulky substituents on the silicon atom create more stable materials, whereas small substituents on the silicon atom produce molecules that are more sensitive to acid. When 5 µm cubic microparticles, fabricated from these bifunctional silyl ether crosslinkers, were incubated under conditions to mimic lysosomal, endosomal, and physiological pH (pH 5.0, 6.0, and 7.4, respectively),[75] all microparticles preferentially degraded under acidic conditions whereby the rate of degradation was accelerated at lower pH (Figure 1.11). The rate of acid catalyzed hydrolysis was also varied amongst the particles fabricated from the various silyl ether crosslinkers. Particles fabricated from the DMS crosslinker degraded most rapidly, on the order of hours, while particles fabricated from the DES crosslinker

were 13.6 times more stable, degrading over days. Particles fabricated from the DIS crosslinker were most stable with a degradation half-life of 30.7 days, fully degrading over months. This demonstrates the acid sensitivity of these bifunctional silyl ether crosslinkers as well as their tunability. Silyl ether crosslinkers are a promising material in the delivery of therapeutic drugs in a controlled manner.
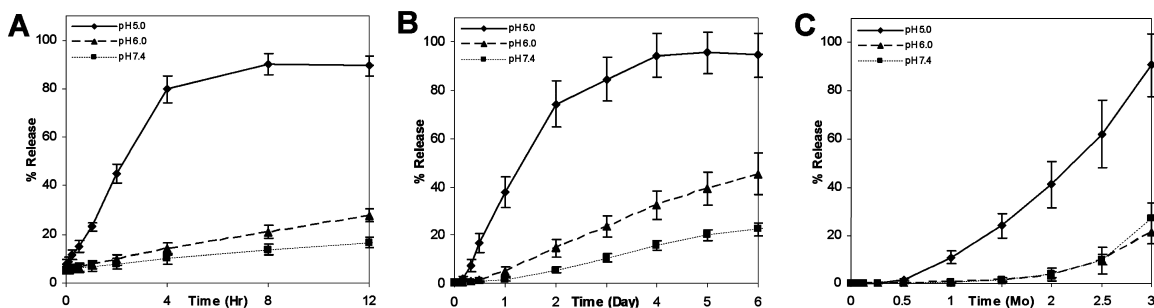


**Figure 1.11** Release of rhodamine-B from PRINT microparticles, fabricated from (A) DMS, (B) DES, and (C) DIS crosslinkers, at various pHs.[61]

## 1.3 References

(1)     Cho, K.; Wang, X.; Nie, S.; Chen, Z.; Shin, D. M. *Clin Cancer Res* **2008**, *14*, 1310-1316.

(2)     Ferrari, M. *Nat Rev Cancer* **2005**, *5*, 161-171.

(3)     Misra, R.; Acharya, S.; Sahoo, S. K. *Drug Discovery Today* **2010**, *15*, 842-850.

(4)     Brigger, I.; Dubernet, C.; Couvreur, P. *Adv Drug Deliv Rev* **2002**, *54*, 631-51.

(5)     Malam, Y.; Loizidou, M.; Seifalian, A. M. *Trends Pharmacol Sci* **2009**, *30*, 592-599.

(6)     Wolinsky, J. B.; Grinstaff, M. W. *Advanced Drug Delivery Reviews* **2008**, *60*, 1037-1055.

(7)     Natalya, R. *Progress in Polymer Science* **2007**, *32*, 962-990.

(8)     Peer, D.; Karp, J. M.; Hong, S.; Farokhzad, O. C.; Margalit, R.; Langer, R. *Nat Nano* **2007**, *2*, 751-760.

(9)     Torchilin, V. P. *Nature Reviews Drug Discovery* **2005**, *4*, 145-160.

(10)    O'Brien, M. E. R.; Wigler, N.; Inbar, M.; Rosso, R.; Grischke, E.; Santoro, A.; Catane, R.; Kieback, D. G.; Tomczak, P.; Ackland, S. P.; Orlandi, F.; Mellars, L.; Alland, L.; Tendler, C. *Ann Oncol* **2004**, *15*, 440-449.

(11)    Hussein, M. A.; Anderson, K. C. *Semin Oncol* **2004**, *31, Supplement 13*, 147-160.

(12)    Thigpen, J. T.; Aghajanian, C. A.; Alberts, D. S.; Campos, S. M.; Gordon, A. N.; Markman, M.; McMeekin, D. S.; Monk, B. J.; Rose, P. G. *Gynecol Oncol* **2005**, *96*, 10-18.

(13)    Rosenthal, E.; Poizot-Martin, I.; Saint-Marc, T.; Spano, J.-P.; Cacoub, P.; the, D. N. X. S. G. *Am J Clin Oncol* **2002**, *25*, 57-59.

(14)    Kataoka, K.; Harada, A.; Nagasaki, Y. *Advanced Drug Delivery Reviews* **2001**, *47*, 113-131.

(15)    Adams, M. L.; Lavasanifar, A.; Kwon, G. S. *J Pharm Sci* **2003**, *92*, 1343-1355.

(16)    Kim, T.-Y.; Kim, D.-W.; Chung, J.-Y.; Shin, S. G.; Kim, S.-C.; Heo, D. S.; Kim, N. K.; Bang, Y.-J. *Clin Cancer Res* **2004**, *10*, 3708-3716.

17) Hamaguchi, T.; Kato, K.; Yasui, H.; Morizane, C.; Ikeda, M.; Ueno, H.; Muro, K.; Yamada, Y.; Okusaka, T.; Shirao, K.; Shimada, Y.; Nakahama, H.; Matsumura, Y. *Br J Cancer* **2007**, *97*, 170-176.

(18) Patri, A. K.; Majoros, I. n. J.; Baker Jr, J. R. *Curr Opin Chem Biol* **2002**, *6*, 466-471.

(19) Svenson, S.; Tomalia, D. A. *Advanced Drug Delivery Reviews* **2005**, *57*, 2106-2129.

(20) Malik, N.; Evagorou, E. G.; Duncan, R. *Anticancer Drugs* **1999**, *10*, 767-776.

(21) Kukowska-Latallo, J. F.; Candido, K. A.; Cao, Z.; Nigavekar, S. S.; Majoros, I. J.; Thomas, T. P.; Balogh, L. P.; Khan, M. K.; Baker, J. R. *Cancer Res* **2005**, *65*, 5317-5324.

(22) Gillies, E. R.; Fréchet, J. M. J. *Drug Discovery Today* **2005**, *10*, 35-43.

(23) Duncan, R. *Nat Rev Cancer* **2006**, *6*, 688-701.

(24) Chun, L. *Advanced Drug Delivery Reviews* **2002**, *54*, 695-713.

(25) Panyam, J.; Labhasetwar, V. *Advanced Drug Delivery Reviews* **2003**, *55*, 329-347.

(26) Zhang, L.; Gu, F. X.; Chan, J. M.; Wang, A. Z.; Langer, R. S.; Farokhzad, O. C. *Clin Pharmacol Ther* **2007**, *83*, 761-769.

(27) Perez, C.; Sanchez, A.; Putnam, D.; Ting, D.; Langer, R.; Alonso, M. J. *J Controlled Release* **2001**, *75*, 211-224.

(28) Brannon-Peppas, L. *Int J Pharm* **1995**, *116*, 1-9.

(29) Soppimath, K. S.; Aminabhavi, T. M.; Kulkarni, A. R.; Rudzinski, W. E. *J Controlled Release* **2001**, *70*, 1-20.

(30) Huang, G.; Gao, J.; Hu, Z.; St. John, J. V.; Ponder, B. C.; Moro, D. *J Controlled Release* **2004**, *94*, 303-311.

(31) Owens III, D. E.; Peppas, N. A. *Int J Pharm* **2006**, *307*, 93-102.

(32) Gu, F. X.; Karnik, R.; Wang, A. Z.; Alexis, F.; Levy-Nissenbaum, E.; Hong, S.; Langer, R. S.; Farokhzad, O. C. *Nano Today* **2007**, *2*, 14-21.

(33) Gradishar, W. J.; Tjulandin, S.; Davidson, N.; Shaw, H.; Desai, N.; Bhar, P.; Hawkins, M.; O'Shaughnessy, J. *J Clin Oncol* **2005**, *23*, 7794-7803.

(34) Green, M. R.; Manikhas, G. M.; Orlov, S.; Afanasyev, B.; Makhson, A. M.; Bhar, P.; Hawkins, M. J. *Ann Oncol* **2006**, *17*, 1263-1268.

(35)     Choi, H. S.; Liu, W.; Misra, P.; Tanaka, E.; Zimmer, J. P.; Ipe, B. I.; Bawendi, M. G.; Frangioni, J. V. *Nat Biotech* **2007**, *25*, 1165-1170.

(36)     Vinogradov, S. V.; Bronich, T. K.; Kabanov, A. V. *Advanced Drug Delivery Reviews* **2002**, *54*, 135-147.

(37)     Moghimi, S. M.; Hedeman, H.; Muir, I. S.; Illum, L.; Davis, S. S. *Biochimica et Biophysica Acta (BBA) - General Subjects* **1993**, *1157*, 233-240.

(38)     Ilium, L.; Davis, S. S.; Wilson, C. G.; Thomas, N. W.; Frier, M.; Hardy, J. G. *Int J Pharm* **1982**, *12*, 135-146.

(39)     Moghimi, S. M.; Hunter, A. C.; Murray, J. C. *Pharmacol Rev* **2001**, *53*, 283-318.

(40)     Hillaireau, H.; Couvreur, P. *Cell Mol Life Sci* **2009**, *66*, 2873-2896.

(41)     Rejman, J.; Oberle, V.; Zuhorn, I. S.; Hoekstra, D. *Biochem J* **2004**, *377*, 159-169.

(42)     Conner, S. D.; Schmid, S. L. *Nature* **2003**, *422*, 37-44.

(43)     Sharma, G.; Valenta, D. T.; Altman, Y.; Harvey, S.; Xie, H.; Mitragotri, S.; Smith, J. W. *J Controlled Release* **2010**, *147*, 408-412.

(44)     Decuzzi, P.; Ferrari, M. *Biophys J* **2008**, *94*, 3790-3797.

(45)     Champion, J. A.; Mitragotri, S. *Proc Natl Acad Sci U S A* **2006**, *103*, 4930-4934.

(46)     Geng, Y.; Dalhaimer, P.; Cai, S.; Tsai, R.; Tewari, M.; Minko, T.; Discher, D. E. *Nature Nanotechnology* **2007**, *2*, 249-255.

(47)     Beningo, K. A.; Wang, Y.-l. *J Cell Sci* **2002**, *115*, 849-856.

(48)     Allen, T. M.; Austin, G. A.; Chonn, A.; Lin, L.; Lee, K. C. *Biochimica et Biophysica Acta (BBA) - Biomembranes* **1991**, *1061*, 56-64.

(49)     Harush-Frenkel, O.; Altschuler, Y.; Benita, S. *Crit Rev Ther Drug Carrier Syst* **2008**, *25*, 485-544.

(50)     Harush-Frenkel, O.; Debotton, N.; Benita, S.; Altschuler, Y. *Biochem Biophys Res Commun* **2007**, *353*, 26-32.

(51)     Alexis, F.; Pridgen, E.; Molnar, L. K.; Farokhzad, O. C. *Molecular Pharmaceutics* **2008**, *5*, 505-515.

(52)     Yamamoto, Y.; Nagasaki, Y.; Kato, Y.; Sugiyama, Y.; Kataoka, K. *J Controlled Release* **2001**, *77*, 27-38.

(53)     Verma, A.; Stellacci, F. *Small* **2010**, *6*, 12-21.

(54) He, C.; Hu, Y.; Yin, L.; Tang, C.; Yin, C. *Biomaterials* **2010**, *31*, 3657-3666.

(55) Fang, C.; Shi, B.; Pei, Y.-Y.; Hong, M.-H.; Wu, J.; Chen, H.-Z. *Eur J Pharm Sci* **2006**, *27*, 27-36.

(56) Byrne, J. D.; Betancourt, T.; Brannon-Peppas, L. *Advanced Drug Delivery Reviews* **2008**, *60*, 1615-1626.

(57) Enlow, E. M.; Luft, J. C.; Napier, M. E.; DeSimone, J. M. *Nano Letters* **2011**, *11*, 808-813.

(58) Gratton, S. E. A.; Ropp, P. A.; Pohlhaus, P. D.; Luft, J. C.; Madden, V. J.; Napier, M. E.; DeSimone, J. M. *Proceedings of the National Academy of Sciences* **2008**, *105*, 11613-11618.

(59) Kelly, J. Y.; DeSimone, J. M. *Journal of the American Chemical Society* **2008**, *130*, 5438-5439.

(60) Merkel, T. J.; Jones, S. W.; Herlihy, K. P.; Kersey, F. R.; Shields, A. R.; Napier, M.; Luft, J. C.; Wu, H.; Zamboni, W. C.; Wang, A. Z.; Bear, J. E.; DeSimone, J. M. *Proceedings of the National Academy of Sciences* **2010**.

(61) Parrott, M. C.; Luft, J. C.; Byrne, J. D.; Fain, J. H.; Napier, M. E.; DeSimone, J. M. *Journal of the American Chemical Society* **2010**, *132*, 17928-17932.

(62) Rolland, J. P.; Maynor, B. W.; Euliss, L. E.; Exner, A. E.; Denison, G. M.; DeSimone, J. M. *Journal of the American Chemical Society* **2005**, *127*, 10096-10100.

(63) Wang, J.; Tian, S.; Petros, R. A.; Napier, M. E.; DeSimone, J. M. *Journal of the American Chemical Society* **2010**, *132*, 11306-11313.

(64) Zhang, H.; et al. *New Journal of Physics* **2009**, *11*, 075018.

(65) Petros, R. A.; Ropp, P. A.; DeSimone, J. M. *J Am Chem Soc* **2008**, *130*, 5008-5009.

(66) Nunes, J.; Herlihy, K. P.; Mair, L.; Superfine, R.; DeSimone, J. M. *Nano Letters* **2010**, *10*, 1113-1119.

(67) Canelas, D. A.; Herlihy, K. P.; DeSimone, J. M. *Wiley Interdisciplinary Reviews: Nanomedicine and Nanobiotechnology* **2009**, *1*, 391-404.

(68) Gratton, S. E. A.; Pohlhaus, P. D.; Lee, J.; Guo, J.; Cho, M. J.; DeSimone, J. M. *J Controlled Release* **2007**, *121*, 10-18.

(69) Wang, J.; Byrne, J. D.; Napier, M. E.; DeSimone, J. M. *Small* **2011**, *7*, 1919-1931.

(70) Simionescu, N.; Siminoescu, M.; Palade, G. E. *The Journal of Cell Biology* **1975**, *64*, 586-607.

(71) Sutera, S. P.; Mehrjardi, M. H. *Biophys J* **1975**, *15*, 1-10.

(72) Jain, R. A. *Biomaterials* **2000**, *21*, 2475-2490.

(73) Anderson, J. M.; Shive, M. S. *Advanced Drug Delivery Reviews* **1997**, *28*, 5-24.

(74) Wuts, P. G. M.; Greene, T. W. *Greene's Protective Groups in Organic Synthesis*; 4th ed.; Wiley-Interscience: New York, 2006.

(75) Mellman, I.; Fuchs, R.; Helenius, A. *Annu Rev Biochem* **1986**, *55*, 663-700.

# CHAPTER 2

## TARGETING PRINT® NANOPARTICLES FOR ENGINEERED DRUG DELIVERY CARRIERS

### 2.1 Targeting Nanoparticles for Cancer Therapeutics

One method of improving nanoparticles for therapeutic delivery systems is targeting. The goal of targeting is to specifically deliver therapeutics to the disease site so as to improve both the bioavailability and the efficacy of the drug, while minimizing adverse systemic effects. Delivery of the drug to the desired tissue is primarily achieved by two approaches: passive and active targeting.[1-3]

### 2.1.1 Passive Targeting

Passive targeting exploits the leaky vasculature and poor lymphatic drainage of the tumor microenvironment. It is based upon the enhanced permeability and retention (EPR) effect. The EPR effect describes the accumulation of particles and payload in the tumor as a result of highly permeable vasculature and defective lymphatic drainage (Figure 2.1).[4] Through this method, the concentration of macromolecules in tumor tissue can reach levels up to 100 times higher than in normal tissue.[3] Extravasation of particles into the tumor and subsequent release of drug from the carrier are essential to passive

targeting. The extent of nanoparticle deposition and drug accumulation is dependent upon the size of the fenestrations and pathways in the tumor. Liposomes have shown that the threshold for extravasation into tumors is around 400 nm.[5]

Through passive targeting, therapeutic nanoparticle formulations have demonstrated improved efficacy over small molecule chemotherapeutics and become the basis for clinical therapy.[6] One such success is Doxil, composed of doxorubicin encapsulated within liposomes that are coated with poly(ethylene glycol) (PEG). It is approved for use in treating refractory Kaposi's sarcoma, breast, and ovarian cancer and has been shown to be more effective than free doxorubicin.[7] Formulation of the drug within liposomes reduced uptake by the reticuloendothelial system and extended circulation, thereby promoting tumor accumulation.[8] Such advancements have prompted extensive research into passively targeting drug nanocarriers.
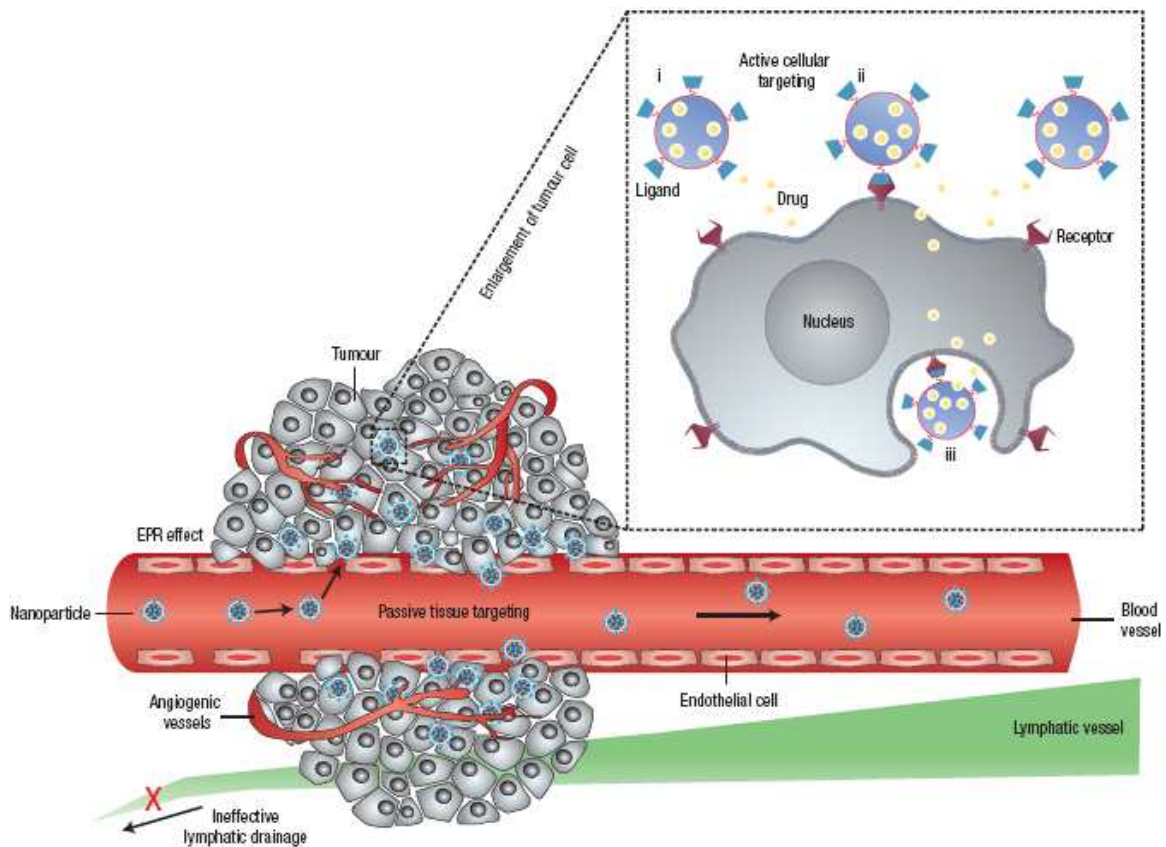
**Figure 2.1** Model of the two approaches of nanoparticle targeting: passive and active (inset). Adapted from [1].

## 2.1.2 Active Targeting

Active targeting is an approach that involves the conjugation of specific ligands to the surface of nanoparticles. These ligands recognize and bind specifically to tumor tissue through cellular surface receptors. To achieve target specificity, the biomarker is uniquely expressed on the tumor cells with minimal expression on normal cells.[9] Some receptors that have been investigated include the folate receptor, transferrin receptor, and human epidermal growth factor receptors.[10] Through the ligand-receptor interactions, nanoparticles can internalize into target cells where the cargo can be released so as to minimize toxicity to adjacent healthy tissue.

A variety of ligands have been explored as targeting molecules for cancerous cells. Most prominent are antibodies, their fragments, and derivatives. Within the last couple decades, antibody therapeutics have emerged as potential targeting agents in cancer therapy. Numerous monoclonal antibodies (mAb) have been approved by the US Food and Drug Administration (FDA), including rituximab, trastuzumab, cetuximab, and bevacizumab.[11] Despite clinical success as monotherapies, many antibody therapeutics are being investigated as adjuvant therapies in combination with chemotherapeutic drugs. As adjuvant therapies, improved effects are observed over treatment by antibody or chemotherapeutic alone.[12-15] Thus, nanoparticles encapsulated with a high drug loading and targeted with specific antibodies may prove to be an advanced, more potent cancer therapy than either chemotherapy- or antibody-based treatments.

An advantage of targeting with whole monoclonal antibodies is the divalent nature present on a single antibody that allows for higher binding avidity. Whole antibodies are also stable during long-term storage. Furthermore, when immune cells bind to the Fc portion of antibodies on target cells, a signaling cascade is triggered to kill cancer cells. Conversely, the Fc domain of antibodies can bind to receptors on normal cells and result in immunogenicity and uptake of nanoparticles in the liver and spleen. Thus, antibody-based targeting efforts also include antibody fragments such as antigen-binding fragments (Fab), dimers of antigen-binding fragments (F(ab')$_2$), and single-chain fragment variables (scFv), seen in Figure 2.2. Despite their safer systemic profiles due to diminished nonspecific binding, antibody and engineered fragments are less stable than their whole counterparts.[16,17]
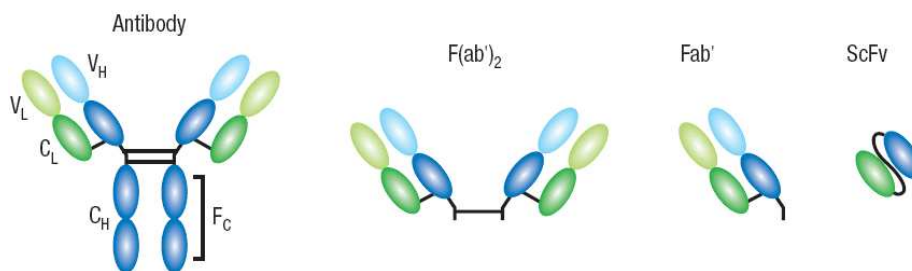
**Figure 2.2** Various targeting ligands based upon antibodies. Adapted from [1].

Aptamers, nucleic acid-based ligands, have also been explored as targeting agents for nanoparticles.[18] They are DNA or RNA oligonucleotides that fold by intramolecular interaction into conformations that have binding properties. They can be developed to bind antigens with high affinity and specificity.[19] They can also be selected to bind to various targets such as transmembrane and intracellular proteins, carbohydrates, and small molecules.[20] Thus, aptamers have been investigated as targeting agents and have demonstrated potential to improve nanoparticulate drug carrier systems. For instance, nanoparticles encapsulated with chemotherapeutics have demonstrated increased efficacy *in vivo* as a result of aptamers targeting prostate cancer cells.[21,22]

Peptides have also demonstrated potential as targeting agents. Through combinatorial libraries, short peptides of 10-15 amino acids have been developed to bind specifically to proteins and cells.[23,24] They are attractive alternatives to antibodies because of their small size, increased stability, lower immunogenicity, and ease of manufacturing. One of the most widely studied peptides is the RGD (arginine-glycine-aspartic acid) peptide, which binds to the $\alpha_v\beta_3$ cell adhesion integrin on endothelial cells. It has been shown to enhance intracellular accumulation of nanoparticles in neuroblastoma and breast cancer models *in vivo*.[25-27] Cilengitide is a cyclic RGD peptide

that is being studied in clinical trials for the treatment of glioblastoma, pancreatic, and non-small cell lung cancer.[28-30] Despite the promise of the RGD peptide, it is nonspecific and binds to other integrins, including $\alpha_5\beta_1$ and $\alpha_4\beta_1$, so it is not specific to cancer cells and can also target healthy tissue.[1]

Utilizing nanoparticles to target receptors associated with metabolic rates has been extensively researched. As cancer cells grow rapidly, receptors including the epidermal growth factor receptor (EGFR),[31] folate receptor (FR),[32] and transferrin receptor (TfR)[33] are commonly overexpressed. Specific protein ligands for these receptors have been conjugated onto nanoparticles to achieve specific targeting in diseased cells. Nanoparticles targeted with epidermal growth factor[34,35] or transferrin[36,37] have demonstrated increased delivery in cancer cells for improved therapeutic efficacy. Similarly, folic acid has been employed as a targeting agent for the FR, and nanoparticles targeted with the small molecule have shown greater intracellular accumulation and enhanced therapeutic potency.[38-40]

## 2.2 Nanoparticles Targeting the Folate Receptor

### 2.2.1 Introduction

The folate receptor (FR) is a cellular membrane glycoprotein with limited expression on healthy tissue but amplified expression on cancer cells, such as ovarian, breast, lung, and prostate cancers.[41-43] Expression of the FR has been correlated with the stage or grade of the cancer. Metastatic cancers generally express significantly more FR

than localized tumors, and high overexpression of the FR is associated with poor prognosis.[44,45] Although generally absent from most normal tissues, the FR is found at significant levels in the choroid plexus, placenta, lung, intestine, and kidney. However, these receptors are largely inaccessible to plasma folates.[46] Consequently, the FR is an attractive biomarker for targeted nanotherapeutics because of its prevalence amongst a variety of cancer cells but limited expression on normal cells.

Two general strategies for targeting the FR involve folic acid or monoclonal antibodies. Folic acid is a small molecule (MW 441) with high affinity for the FR ($K_d$ ~0.1 nM) because it is necessary for the synthesis of nucleotide bases. Thus, it plays a critical role in cellular survival and proliferation.[47,48] Folic acid is an attractive targeting ligand because of its low molecular weight, solubility, stability, lack of immunogenicity, commercial availability, and facile conjugation to nanocarriers.[49] Consequently, nanoparticles conjugated with folic acid as a targeting ligand have been widely researched and have demonstrated selective intracellular uptake in diseased cells for delivery of therapeutics.[39,50,51] Similarly, monoclonal antibodies against the FR (i.e., MOv18, MOv19) have also been explored as targeting ligands for drug and diagnostic nanocarriers.[42] Through either targeting ligand, nanoparticles targeting the FR bind to cancer cells and are delivered intracellularly through receptor-mediated endocytosis.

## 2.2.2 Experimental

### 2.2.2.1 Chemicals and Reagents

Biotinylated isotype control mouse IgG was purchased from eBioscience. Anti-folate receptor (FR) monoclonal antibody (mAb; MOv18) was purchased from Axxora. UltraAvidin was purchased from Leinco Technologies. Biotin-poly(ethylene glycol)-succinimidyl carboxymethyl ester (941 g/mol; NHS-PEG$_{12}$-biotin) was purchased from Thermo Scientific. Biotin-poly(ethylene glycol)-succinimidyl carboxymethyl ester (3400 g/mol for PEG; NHS-PEG$_{3400}$-biotin) was purchased from Laysan Bio. Anhydrous dimethylformamide (DMF) and pyridine were purchased from Acros. Acetic anhydride was purchased from Fisher Scientific. All other reagents were purchased from Sigma Aldrich.

### 2.2.2.2 Cells and Culture

SKOV3, MCF7, OVCAR3, and HeLa, cells were from UNC LCCC Tissue Culture Facility. SKOV3 cells were maintained in McCoy's 5A with 10% FBS. OVCAR3 cells were maintained in RPMI 1640 with 10% FBS. MCF7 and HeLa cells were maintained in MEM with 10% FBS. All media and supplements were from Gibco except McCoy's 5A, which was from Mediatech.

### 2.2.2.3 Fabrication of PRINT Nanoparticles

Cylindrical nanoparticles ($d$ = 200 nm and $h$ = 200 nm) were fabricated using the PRINT technique. Nanoparticles were prepared from a starting monomer solution (5% wt/vol in DMF) consisting of 87 wt % of trimethyloylpropane ethoxylate triacrylate (MW = 428 g/mol; PEG$_{428}$ triacrylate), 10 wt % of 2-aminoethyl methacrylate hydrochloride, 2

wt % of fluorescein *o*-acrylate, and 1 wt % of 2,2-diethoxyacetophenone. A monomer film was cast upon a sheet of poly(ethylene terephthalate) (PET) by spreading 90 µL of monomer solution with a mayer rod (#2, R.D. Specialties), and it was dried with heat using a heat gun to remove the solvent DMF. The monomer film and patterned mold, provided by Liquidia Technologies, were laminated together under pressure (40 PSI) and then delaminated, by gently splitting the mold and PET, to yield a mold with filled cavities. The filled mold was laminated with a fresh sheet of PET and then exposed to UV irradiation ($\lambda = 365$ nm, power 90 mW/cm$^2$) for 4 min under a nitrogen purge. The mold was removed, leaving nanoparticles transferred on the sheet of PET. This was due to the higher surface energy of the PET. Milli-Q filtered water (400 µL) was placed on the PET, and nanoparticles were collected mechanically with a cell scraper. The harvested particles were washed twice with water by centrifugation.

### 2.2.2.4  Labeling anti-FR mAb with Biotin

Anti-FR mAb (1 mL, 0.5 mg/mL in PBS) was reacted with NHS-PEG$_{12}$-biotin (2.5 µL, 25 mg/mL in DMF) for 30 min at RT. The reaction solution was then dialyzed in a Slide-A-Lyzer dialysis cassette (10k molecule weight cut-off; Thermo Scientific) against cold DPBS for 24 h at 4 °C to remove excess NHS-PEG$_{12}$-biotin. The biotinylated antibody was then collected and stored at 4 °C.

**2.2.2.5  Determining the Biological Activity of Biotinylated anti-FR mAb**

MCF7 cells were trypsinized and seeded at 50,000 cells in 50 µL of DPBS per well in a round-bottom 96-well plate.  The primary antibody (anti-FR mAb, biotinylated anti-FR mAb, or IgG), at 0.5 mg/mL, was diluted 1:50 in DPBS, and 50 µL of the primary antibody was added to the cells and incubated for 30 min at 4 °C.  Cells were washed twice with cold DPBS by centrifugation.  The secondary antibody Alexa Fluor 488 goat anti-mouse IgG (Invitrogen), at 2 mg/mL, was diluted 1:400 in DPBS.  The diluted secondary antibody (100 µL/well) was then incubated with the cells for 30 min at 4 °C.  Subsequently, cells were washed twice with cold DPBS by centrifugation. Samples were resuspended in DPBS and analyzed using a Dako CyAn flow cytometer.

**2.2.2.6  Conjugation of anti-FR mAb/IgG to PRINT Nanoparticles**

Nanoparticles were conjugated with anti-FR mAb or IgG through a biotin-avidin linkage.  Nanoparticles in anhydrous DMF (500 µL at 2 mg/mL) were reacted with 5 mg of NHS-PEG$_{3400}$-biotin in the presence of 10 µL anhydrous of pyridine; the nanoparticle dispersion was shaken on a vortex for 2 h.  Acetic anhydride (10 µL) was added to the dispersion, which was shaken for 10 min, to quench unreacted amines on the nanoparticle surface.  The nanoparticles were washed twice with Dulbecco's phosphate buffered saline (DPBS) by centrifugation.  UltraAvidin (50 µL, 10 mg/mL) was added to the nanoparticles in DPBS (2 mg/mL).  The dispersion was shaken for 1 h.  The nanoparticles were washed twice with DPBS by centrifugation.  To target the nanoparticles, 50 µg of anti-FR mAb or IgG was added to the nanoparticle dispersion and was shaken for 30 min at room temperature and then kept overnight at 4 °C.  The

nanoparticles were washed twice with DPBS by centrifugation and then resuspended in DPBS.

### 2.2.2.7  Physical Characterization of Nanoparticles

Scanning electron microscopy samples were prepared by pipetting 10 µL of nanoparticle solution onto a glass slide.  Samples were dried and coated with 2 nm of gold palladium with a Cressington 108 auto sputter coater (Cressington Scientific Instruments).  Samples were imaged with a scanning electron microscope (Hitachi S-4700).  The size (dynamic light scattering, DLS) and charge ($\zeta$-potential) of the nanoparticles were determined for 20 µg/mL nanoparticle samples in a 1 mM potassium chloride solution with a Malvern Instruments Nano ZS.

### 2.2.2.8  Determining the FR Expression in Cells

HeLa, SKOV3, MCF7, and OVCAR3 cells were analyzed for expression of the FR following the same protocol described above for the determination of the biological activity of biotinylated anti-FR mAb.

### 2.2.2.9  Quantitative *In Vitro* Cellular Targeting

SKOV3 and HeLa cells were plated at 50,000 cells/well in a 24-well plate and allowed to adhere overnight at 37 °C and 5% $CO_2$.  Nanoparticles in OPTI-MEM were incubated with cells at 37 °C and 5% $CO_2$ for specified amounts of time and then removed.  The cells were washed twice with DPBS, trypsinized, and prepared for

analysis by flow cytometry with a 0.2% trypan blue solution containing 10% FBS in DPBS. Samples were analyzed with a Dako CyAn flow cytometer.

### 2.2.2.10  Inhibition of Cellular Internalization of Nanoparticles

SKOV3 cells were plated at 50,000 cells/well in a 24-well plate and allowed to adhere overnight at 37 °C and 5% $CO_2$. Free anti-FR mAb or IgG, in varying amounts in OPTI-MEM, was dosed onto cells. The cells were incubated at 37 °C for 1 h, after which free targeting ligands were removed. Nanoparticles in OPTI-MEM, at 5 µg/mL, were incubated with cells at 37 °C for 4 h and then removed. The cells were washed twice with DPBS, trypsinized, and prepared for analysis by flow cytometry with a 0.2% trypan blue solution containing 10% FBS in DPBS. Samples were analyzed with a Dako CyAn flow cytometer.

### 2.2.2.11  Confocal Microscopy

SKOV3 cells (50,000) were seeded in T-25 flasks and allowed to adhere overnight at 37 °C and 5% $CO_2$. Cells were incubated with 15 µg/mL of nanoparticles in OPTI-MEM for 4 h at 37 °C. Cells were washed by detachment with trypsin, resuspended in complete media, replated onto 35-$mm^2$ glass bottom dishes with 1.5G cover slips (MatTek Corp.), and allowed to adhere overnight at 37 °C. Nuclei were stained with 2.5 µM DRAQ5 (Biostatus Ltd.). Cells were fixed with 4% paraformaldehyde. Cells were imaged with a confocal laser scanning microscope (Olympus Fluoview FV500).

## 2.2.3 Results and Discussion

### 2.2.3.1 Nanoparticle Fabrication and Conjugation with Anti-FR Antibodies

The PRINT technology is a versatile platform for the fabrication of particles because it affords precise control over particle size, shape, composition, and surface chemistry.[52-60] Through this technique, cylindrical nanoparticles ($d = 200$ nm and $h = 200$ nm), primarily composed of poly(ethylene glycol) (PEG; 428 g/mol) triacrylate were fabricated (Figure 2.3).
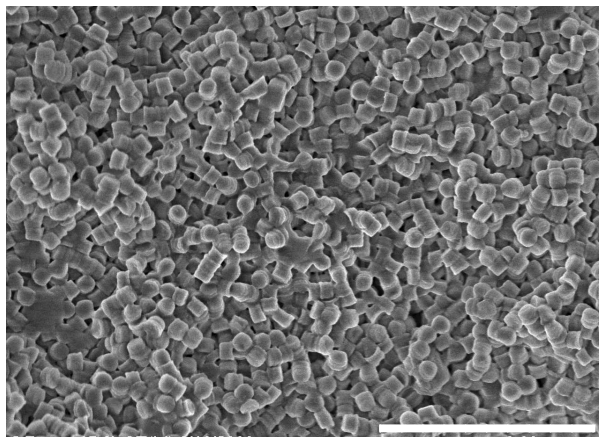


**Figure 2.3** SEM of 200 nm cylindrical PRINT nanoparticles. Scale bar is 3 µm.

Also included within the nanoparticles were 2-aminoethyl methacrylate hydrochloride, fluorescein *o*-acrylate, and 2,2-diethoxyacetophenone (Table 2.1). The 2-aminoethyl methacrylate hydrochloride provided amine functionalities for nanoparticle surface

modification, while fluorescein *o*-acrylate fluorescently labeled the nanoparticles to be tracked and visualized *in vitro*.

**Table 2.1**  Composition of PEG-based PRINT nanoparticles for targeting with anti-FR antibodies.

| Monomers | Wt % |
|---|---|
| PEG$_{428}$ triacrylate | 87 |
| 2-Aminoethyl methacrylate hydrochloride | 10 |
| Fluorescein *o*-acrylate | 2 |
| 2,2-Diethoxyacetophenone | 1 |

Pre-functionalized nanoparticles with no surface modifications had a hydrodynamic diameter of 297 nm with a narrow polydispersity index of 0.039.  They were cationic and possessed a positive ζ-potential of +29.2 ± 0.6 mV because of the amine functional groups at the surface of the nanoparticles (Table 2.2).

**Table 2.2**  Hydrodynamic diameters and zeta potentials of 200 nm cylindrical PRINT nanoparticles.

| Nanoparticle | Diameter (nm) | PDI | ζ-Potential (mV) |
|---|---|---|---|
| Pre-functionalized | 297 | 0.039 | +29.2 ± 0.6 |
| Biotinylated | 300 | 0.010 | -20.6 ± 0.5 |
| NP-FR | 298 | 0.08 | -23.1 ± 0.8 |
| NP-IgG | 298 | 0.07 | -26.6 ± 1.4 |

Previously demonstrated, positively charged particles can internalize into cells quickly albeit nonspecifically[53,61,62] and can also induce cytotoxicity.[63] Thus, such particles are not ideal as drug delivery systems. However, negatively charged particles can circumvent these issues because they exhibit decreased cellular uptake.[53,61,62] Therefore, conjugating targeting ligands to negatively charged particles can achieve specific cellular internalization that is better suited for improved drug delivery agents.[59]

For this reason, the surface of PRINT nanoparticles were functionalized and targeted with anti-human folate receptor (FR) monoclonal antibodies (mAb; Figure 2.4). Cationic pre-functionalized nanoparticles were initially reacted with $NHS-PEG_{3400}$-biotin. This was followed by acetic anhydride to quench any unreacted amines, thereby shifting the $\zeta$-potential to negative (-20.6 mV for biotinylated nanoparticles, Table 2.2) so that nonspecific cellular internalization could be avoided. Targeted antibodies were conjugated to the nanoparticles through biotin-avidin linkages, so avidin was first reacted with biotinylated nanoparticles, followed by the targeting ligands, anti-FR antibody and IgG. Nanoparticles functionalized with the anti-FR antibodies (NP-FR) were designed to specifically target cancer cells that overexpress the FR, while nanoparticles targeted with IgG (NP-IgG) were tailored as control nanoparticles. Targeted nanoparticles maintained hydrodynamic diameters around 300 nm and negative $\zeta$-potentials of about -25 mV so that nonspecific cellular internalization and cytotoxicity could be avoided.
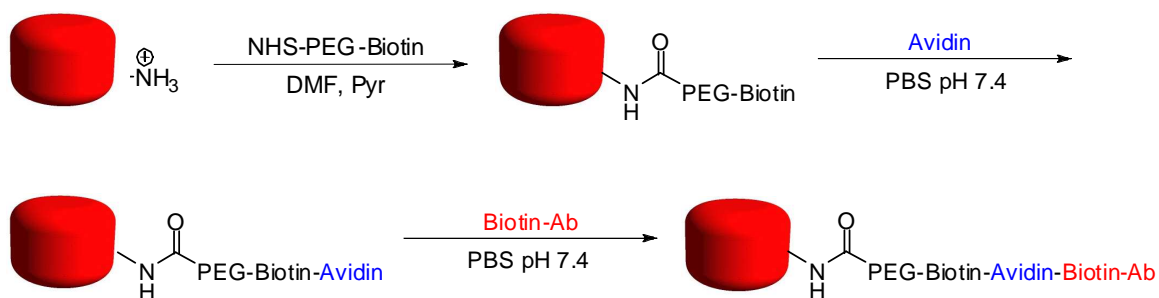
**Figure 2.4** Scheme of nanoparticle surface modification for targeting with antibodies.

As the anti-FR antibody was attached onto nanoparticles through biotin-avidin linkages, the antibody was first modified with biotin to enable conjugation. The antibody was reacted with NHS-PEG$_{12}$-biotin, which randomly labeled the antibody with biotin. Because biotinylation of the antibody was indiscriminate, biological activity of the antibody was investigated by flow cytometry before conjugation to nanoparticles. Binding of the original antibody and the biotinylated antibody to the FR on MCF7 (human breast cancer) cells was studied using a secondary antibody labeled with the fluorescent dye Alexa Fluor 488. Histograms in Figure 2.5 illustrate similar shifts in fluorescence for both the unmodified antibody and the biotinylated antibody. This demonstrates that the biotinylated antibody maintained its biological function. Labeling the anti-FR antibody with biotin did not disrupt the binding of the antibody to the FR, so the biotinylated antibodies were utilized in targeting PRINT nanoparticles.
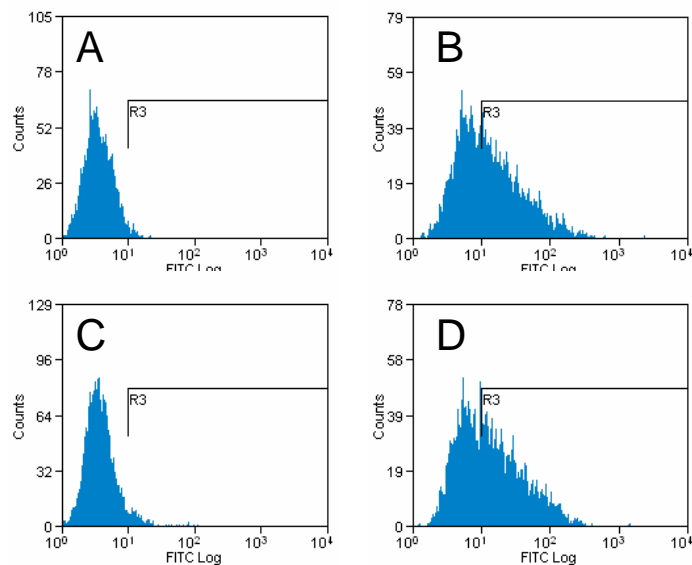
**Figure 2.5** Flow cytometry histograms of (A) MCF7 cells, (B) anti-FR mAb binding, (C) no nonspecific binding of the fluorescent secondary Ab, and (D) binding of biotinylated anti-FR mAb.

### 2.2.3.2 Determination of FR-Positive Cell Lines

Before investigating cellular internalization of the nanoparticles, a variety of cell lines were investigated for the expression of the FR to determine appropriate *in vitro* models. HeLa (human cervical cancer), MCF7 (human breast adenocarcinoma), and SKOV3 and OVCAR3 (human ovarian adenocarcinoma) cells were probed for the expression of the FR. Cells were stained for the FR with anti-FR mAb and a secondary antibody labeled with the fluorescent Alexa Fluor 488 dye and then analyzed by flow cytometry. SKOV3, MCF7, and OVCAR3 cells exhibited amplified expression of the FR, while HeLa cells had minimal levels (Figure 2.6). Based on these results, SKOV3 cells were chosen as a FR-positive cell line for *in vitro* studies, and HeLa cells were selected as a FR-negative cell line.
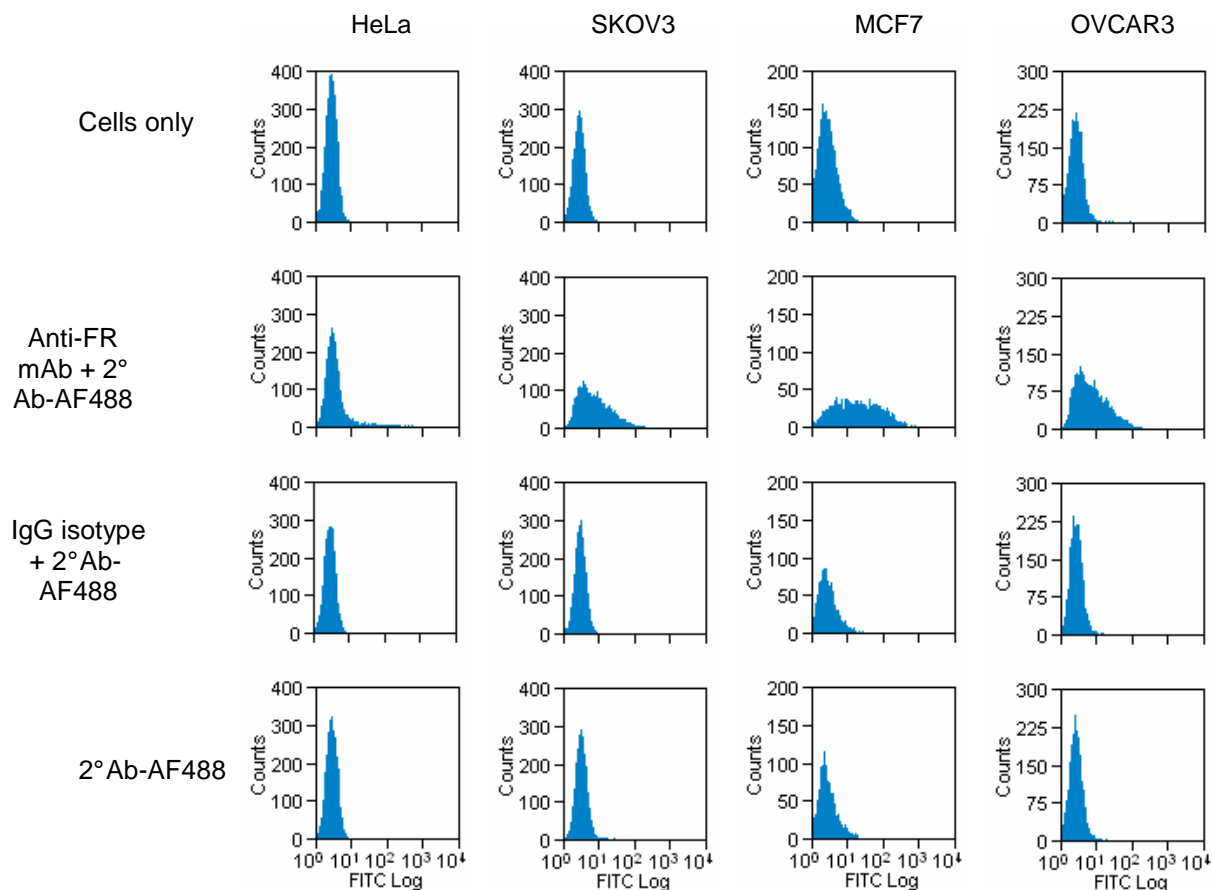
**Figure 2.6** Histograms illustrating the level of expression of the FR in HeLa, SKOV3, MCF7, and OVCAR3 cells.

### 2.2.3.3  Quantitative *In Vitro* Cellular Uptake

Cellular internalization of the nanoparticles was investigated in SKOV3 and HeLa cells.  SKOV3 cells overexpress the FR, but HeLa cells have negligible levels of the receptor.  Initially, pre-functionalized nanoparticles were studied.  Nanoparticles were incubated at 37 °C with the cells at varied nanoparticle concentrations and incubation times (2 and 4 h).  Uptake of pre-functionalized nanoparticles was analyzed by a flow

cytometry technique to quantify the percentage of cells with internalized nanoparticles.[64] In both SKOV3 and HeLa cells, pre-functionalized nanoparticles were rapidly internalized in a dose dependent fashion (Figure 2.7). There was a high amount of nanoparticle internalization, over 95% in HeLa cells and over 85% in SKOV3 cells at 4 h. In 2 h, there was only a slight decrease in uptake with 94% of HeLa cells and 75% of SKOV3 cells with internalized nanoparticles. Rapid internalization of pre-functionalized nanoparticles in both cell lines was due to the positive ζ-potential that induces nonspecific cellular binding and uptake. Rapid, nonspecific internalization of positively charged PRINT particles has also been demonstrated previously.[53,65]
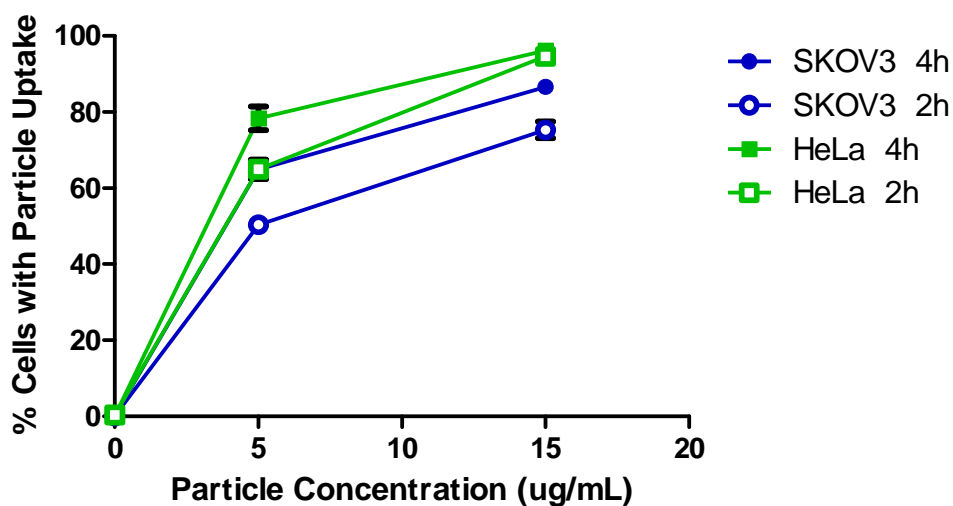


**Figure 2.7** Internalization of pre-functionalized nanoparticles in SKOV3 and HeLa cells as a function of nanoparticle concentration and incubation time.

Positively charged particles can internalize into cells nonspecifically[53,61,62] and potentially induce cytotoxicity.[63] To avoid these issues, targeting ligands are often conjugated to the surface of nanoparticles to promote specific intracellular accumulation.

Thus, pre-functionalized nanoparticles were functionalized for a negative ζ-potential to evade nonspecific cellular uptake and then conjugated with targeting ligands for the FR to support specific internalization. Targeted nanoparticles NP-FR and NP-IgG were incubated with SKOV3 cells at varied nanoparticle concentrations and incubation times. In SKOV3 cells, which overexpress the FR, NP-FR was selectively internalized into cells, in a dose and time dependent manner, to over 70% at 4 h and over 55% in 2 h, while minimal cells (<14%) internalized NP-IgG (Figure 2.8). Low uptake of NP-IgG was attributed to the negative charge of the nanoparticles as well as the nonspecific IgG ligands. In contrast, despite the negative ζ-potential, NP-FR exhibited higher uptake due to the specific binding of the anti-FR mAb to the FR, which induced receptor-mediated endocytosis of the nanoparticles. By conjugating a targeting ligand to the surface of the nanoparticles, NP-FR were able to overcome the low uptake of negatively charged particles to specifically internalize into FR-expressing SKOV3 cells.
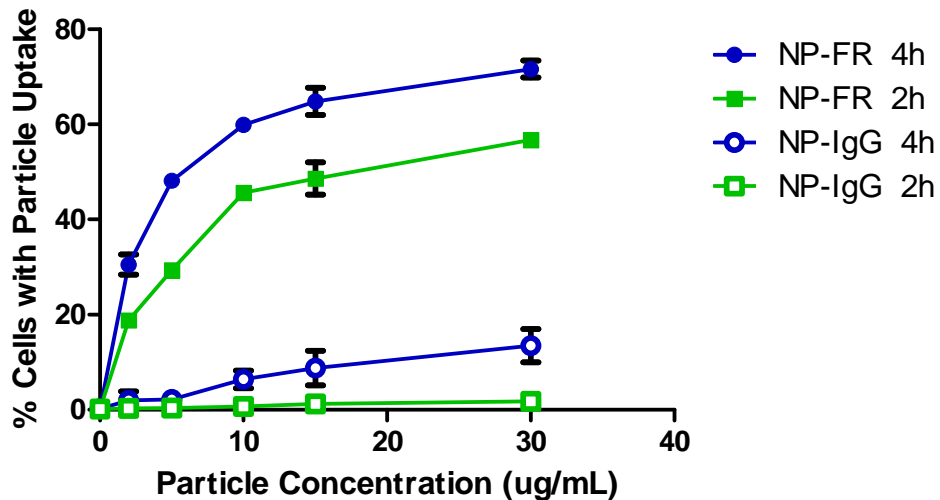


**Figure 2.8** Internalization of anti-FR mAb-targeted nanoparticles into SKOV3 cells as a function of nanoparticle concentration and incubation time.

Additionally, NP-FR and NP-IgG were incubated with HeLa cells, which have minimal expression of the FR. Uptake of targeted nanoparticles was low as compared to that in SKOV3 cells (Figure 2.9). There was also an insignificant difference between NP-FR and NP-IgG, attributed to the low level of the FR in HeLa cells. As observed between SKOV3 and HeLa cells, the level of the FR in the cell lines strongly influences the specific uptake of NP-FR. The amount of internalization of NP-FR correlates well to the expression level of the FR on the cell lines.
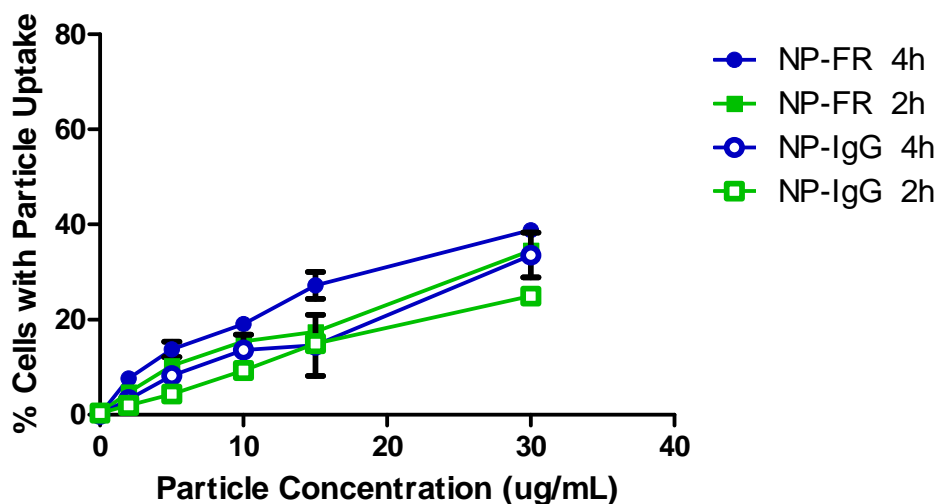


**Figure 2.9** Internalization of anti-FR mAb-targeted nanoparticles in HeLa cells as a function of nanoparticle concentration and incubation time.

## 2.2.3.4  Inhibition of Nanoparticle Cellular Targeting

Specific targeting and uptake of NP-FR was confirmed in SKOV3 cells through competition with free anti-FR mAb. SKOV3 cells were incubated with free anti-FR mAb prior to addition of NP-FR to allow the cellular FR to be bound by free ligands and thus,

decrease those available for binding with targeted nanoparticles. As seen in Figure 2.10, SKOV3 cells preincubated with free anti-FR mAb internalized less NP-FR, with only 37% of cells having internalized nanoparticles. Addition of the nonspecific IgG control antibody to SKOV3 cells prior to incubation with NP-FR did not influence the binding and internalization of the targeted nanoparticles. Specific targeting and inhibition of uptake with only free anti-FR mAb indicate that NP-FR selectively bind to the FR and internalize through receptor-mediated endocytosis.
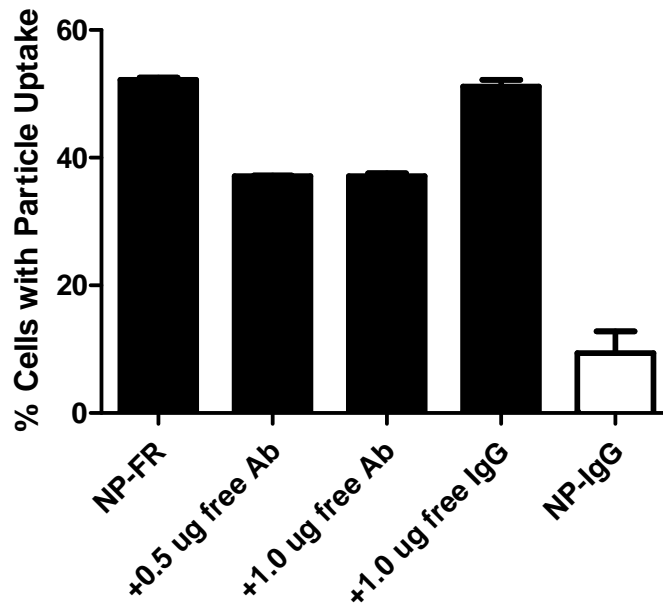


**Figure 2.10** Inhibition of internalization of anti-FR mAb-targeted nanoparticles with free ligand in SKOV3 cells.

### 2.2.3.5  Confocal Microscopy

Targeting and internalization of NP-FR in SKOV3 cells was also visualized by confocal microscopy.  Cells were incubated with fluorescein-labeled NP-FR.  As expected, targeted nanoparticles bound and internalized into SKOV3 cells (Figure 2.11). NP-FR specifically targeted the FR on the surface of the cells, and through FR-mediated endocytosis, targeted nanoparticles were internalized into the cells.  Based on the data, PRINT nanoparticles targeted with anti-FR mAb are potential drug delivery vehicles that can selectively bind to cells that overexpress the FR and accumulate intracellularly for localized delivery of a therapeutic payload.
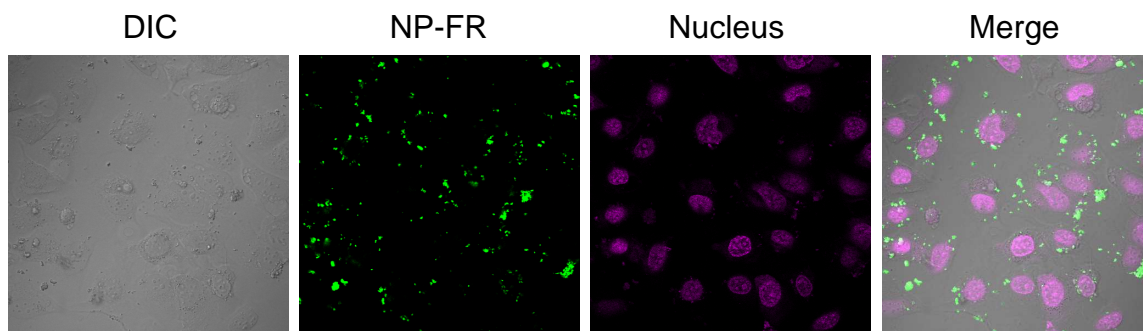


**Figure 2.11**  Confocal microscopy images of specific targeting and internalization of NP-FR in SKOV3 cells.

### 2.2.3.6  Effect of Targeted Ligand Density on Nanoparticle Uptake

To better understand the influence of multivalency on targeting, nanoparticles were fabricated with varying densities of anti-FR mAb (100% to 0%) by substituting the targeting ligand with the control ligand IgG during the process of conjugation to nanoparticles.  Nanoparticles were incubated with SKOV3 cells for 4 h at 37 °C, and SKOV3 cells were analyzed for nanoparticle uptake by flow cytometry.  As the density

of anti-FR mAb was decreased on the nanoparticles, internalization of the nanoparticles also began to decrease (Figure 2.12). When the density of anti-FR mAb was lowered from 100% to 60%, uptake of NP-FR decreased slightly from 56% to 50%. This may suggest that nanoparticles functionalized with 60% of the targeting ligand can achieve a nearly similar extent of nanoparticle internalization as those with 100% of anti-FR mAb. Therefore, other targeting or therapeutic ligands may be conjugated to nanoparticles, in addition to anti-FR mAb, to increase target specificity or therapeutic efficacy while maintaining high selective targeting of the nanoparticles to cancer cells. However, when the density of anti-FR mAb was further decreased to 20%, a more prominent effect was observed with only 25% of SKOV3 cells having internalized nanoparticles. At 10% of the targeting anti-FR mAb, effects from the nonspecific ligand IgG were more prevalent as uptake of these nanoparticles were nearly similar to those with 0% of the anti-FR mAb (or 100% of IgG). In both cases, less than 7% of cells internalized nanoparticles.
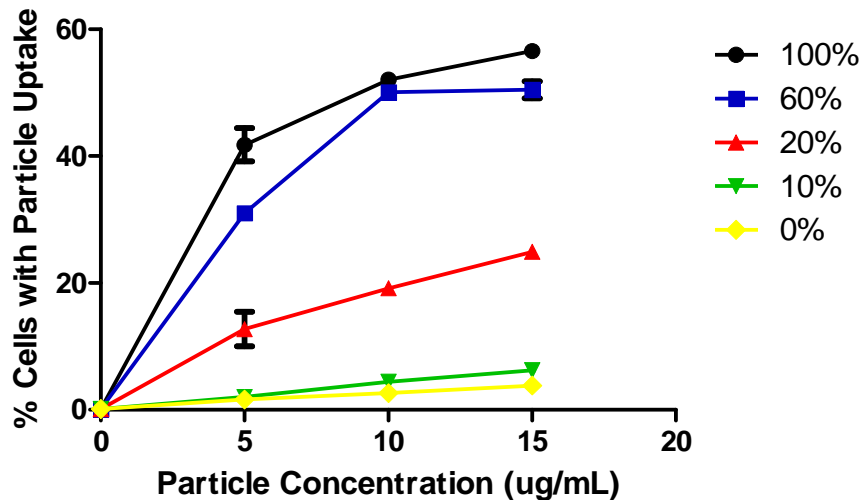


**Figure 2.12** Internalization of NP-FR with varied density of the anti-FR mAb targeting ligand in SKOV3 cells.

50

### 2.2.4 Conclusions

PRINT nanoparticles were created and investigated for active targeting as possible drug delivery agents. Cylindrical nanoparticles, composed primarily of biocompatible PEG, were successfully fabricated and converted from a positive surface charge to a negative $\zeta$-potential to avoid nonspecific cellular uptake. They were further engineered with anti-FR mAb targeting ligands on the surface to facilitate specific targeting and internalization into cancer cells with an amplified level of the FR. When investigated *in vitro* by flow cytometry and confocal microscopy, NP-FR exhibited specific targeting and internalization into FR-expressing SKOV3 cells. The targeted nanoparticles internalized in a dose and time dependent manner. It was also shown that NP-FR internalized into SKOV3 cells through FR-mediated endocytosis, triggered by the binding of anti-FR mAb with the receptor, because internalization of NP-FR was inhibited by free targeting ligands. Additionally, uptake of NP-FR correlated with the expression level of FR in cells. SKOV3 cells readily internalized NP-FR, while the targeted nanoparticles did not heavily accumulate in HeLa cells. Moreover, NP-FR, with a decreased density of targeting ligands on the nanoparticle surface, still internalized into SKOV3 cells, suggesting that nanoparticles with decreased multivalency can still target and accumulate in cancer cells. In contrast to NP-FR, NP-IgG were minimally influenced by all these factors, exhibiting low cellular internalization, because of their negative surface charge and nonspecific surface ligands. By utilizing the PRINT platform, biocompatible nanoparticles were fabricated and developed into potential drug nanocarriers that actively target FR-expressing cancer cells.

**2.2.5 Future Work**

Conjugating antibodies to the surface of nanocarriers as a method to enhance specific targeting of the drug delivery system is commonly employed by researchers. For the FR, targeting is primarily achieved with anti-FR mAb or folic acid, a small molecule ligand for the FR.[42] Because of its small size, it can be easily manipulated for conjugation and may be nonimmunogenic as well.[49] Thus, it is an appealing ligand for targeting the FR that has been researched by others.[39,42,50,51] Cylindrical PRINT nanoparticles were fabricated and conjugated with folic acid and investigated *in vitro* with FR-expressing KB cells. After 4 h at 37 °C, nanoparticles targeted with folic acid were internalized into 85% of cells, while just 26% of KB cells internalized untargeted nanoparticles (Figure 2.13).
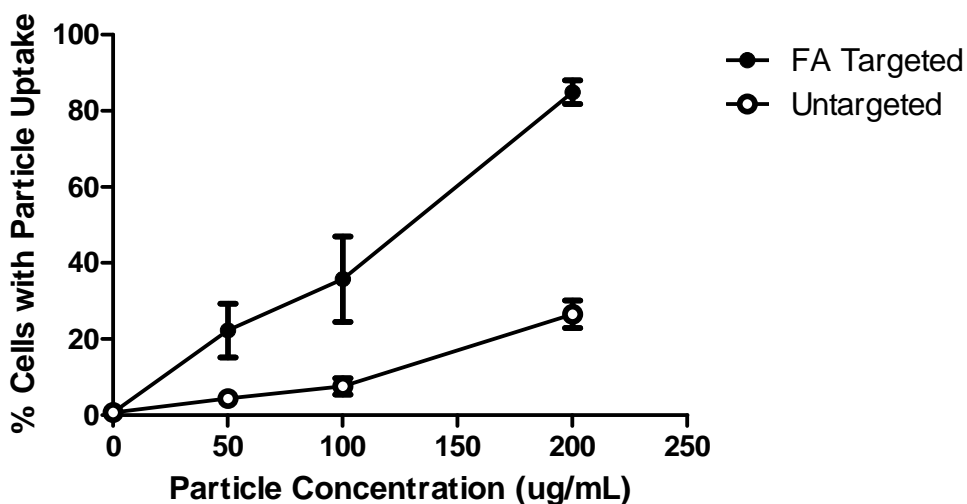


**Figure 2.13** Internalization of nanoparticles targeted with folic acid in KB cells.

While the results are promising, further studies are required to confirm targeting and internalization mechanisms of folic acid-targeted nanoparticles. Additionally, future investigations with nanoparticles targeted with the small molecule folic acid compared to those targeted with anti-FR mAb would help to elucidate differences in nanoparticle targeting between the targeting ligands. The PRINT platform is an ideal technique for such a study as nanoparticles can be readily fabricated and studied with independent control of the surface chemistry and targeting ligands. These basic studies would benefit and advance efforts to develop improved targeted therapeutic nanocarriers.

## 2.3  Nanoparticles Targeting the HER2 Receptor

### 2.3.1  Introduction

The human epidermal growth factor receptor 2 (HER2, HER2/*neu*, ErbB2) is a transmembrane tyrosine kinase receptor of the epidermal growth factor receptor (EGFR) family.[66] It is minimally expressed in normal tissue but is overexpressed in ovarian, lung, and about 30% of breast cancers and is largely associated with poor prognosis.[67-70] There are no known ligands for the HER2 receptor, but Herceptin (trastuzumab; Genentech) is a humanized monoclonal antibody approved for the treatment of metastatic breast cancer that binds the receptor with specificity. Herceptin inhibits tumor growth as a monotherapy, but when administered in combination with cytotoxic agents, it acts synergistically.[71,72] As such, Herceptin is an appealing targeting ligand for the delivery of nanoparticles containing chemotherapeutic drugs for a dual functional nanocarrier.

Thus, researchers have studied the targeting of nanoparticles with Herceptin and found that nanoparticles effectively and specifically target HER2-positive cancer cells and internalize through receptor-mediated endocytosis.[73-76] When loaded with cytotoxic agents, such as paclitaxel, methotrexate, and doxorubicin, targeted nanoparticles still demonstrated specific targeting and internalization into cells and were generally more potent than the free drug.[77-79]

Herein, we describe the fabrication and modification of PRINT nanoparticles with ligands specific for the HER2 receptor and the *in vitro* targeting properties of the nanoparticles. We investigated nanoparticles that were conjugated with Herceptin through noncovalent biotin-avidin linkages. Additionally, nanoparticles were covalently modified with an engineered heptameric ligand for the HER2 receptor. These nanoparticles were studied for targeting and accumulation in various HER2-positive cancer cell lines. Through these two ligands, we studied the implications of the multivalent nature of the nanoparticles on targeting to emphasize that such considerations are necessary in the rational design of targeted nanoparticles for cancer therapeutics.

### 2.3.2 Experimental

### 2.3.2.1 Chemicals and Reagents

Control mouse IgG and biotinylated IgG were purchased from eBioscience. Herceptin (Genentech) was purchased from the UNC Hospitals. The engineered heptameric ligand for the HER2 receptor was provided by Professor Rihe Liu (UNC

Eshelman School of Pharmacy). UltraAvidin was purchased from Leinco Technologies. Biotin-poly(ethylene glycol)-succinimidyl carboxymethyl ester (3400 g/mol for PEG; NHS-PEG$_{3400}$-biotin) and maleimide-poly(ethylene glycol)- succinimidyl carboxymethyl ester (5000 g/mol for PEG; NHS-PEG$_{5000}$-Mal) were purchased from Laysan Bio. Biotin-poly(ethylene glycol)-succinimidyl carboxymethyl ester (941 g/mol; NHS-PEG$_{12}$-biotin) and borate buffer were purchased from Thermo Scientific. Anhydrous dimethylformamide (DMF) and pyridine were purchased from Acros. Acetic anhydride was purchased from Fisher Scientific. All other reagents were purchased from Sigma Aldrich.

### 2.3.2.2 Cells and Culture

BT474, SKOV3, MCF7, OVCAR3, and HeLa cells were from UNC LCCC Tissue Culture Facility. BT474 cells were maintained in RPMI 1640 with 10% FBS, 1.5 g/L sodium bicarbonate, 4.5 g/L glucose, 10 mM HEPES, 1.0 mM sodium pyruvate, and 0.02 mg/mL human insulin. SKOV3 cells were maintained in McCoy's 5A with 10% FBS. OVCAR3 cells were maintained in RPMI 1640 with 10% FBS. MCF7 and HeLa cells were maintained in MEM with 10% FBS. All media and supplements were from Gibco except McCoy's 5A, which was from Mediatech.

### 2.3.2.3 Fabrication of PRINT Nanoparticles

Cylindrical nanoparticles ($d$ = 200 nm and $h$ = 200 nm) were fabricated using the PRINT technique. Nanoparticles were prepared from a starting monomer solution (5%

wt/vol in DMF) consisting of 77 wt % of $PEG_{700}$ diacrylate, 20 wt % of 2-aminoethyl methacrylate hydrochloride, 2 wt % of fluorescein $o$-acrylate, and 1 wt % of 2,2-diethoxyacetophenone.  A monomer film was cast upon a sheet of poly(ethylene terephthalate) (PET) by spreading 90 µL of monomer solution with a mayer rod (#2, R.D. Specialties), and it was dried with heat using a heat gun to remove the solvent DMF.  The monomer film and patterned mold, provided by Liquidia Technologies, were laminated together under pressure (40 PSI) and then delaminated, by gently splitting the mold and PET, to yield a mold with filled cavities.  The filled mold was laminated with a fresh sheet of PET and then exposed to UV irradiation ($\lambda$ = 365 nm, power 90 $mW/cm^2$) for 4 min under a nitrogen purge.  The mold was removed, leaving nanoparticles transferred on the sheet of PET.  This was due to the higher surface energy of the PET.  Milli-Q filtered water (400 µL) was placed on the PET, and nanoparticles were collected mechanically with a cell scraper.  The harvested particles were washed twice with water by centrifugation.

### 2.3.2.4  Labeling Herceptin with Biotin

Herceptin (1 mL, 2 mg/mL in PBS) was reacted with NHS-$PEG_{12}$-biotin (2.5 µL, 25 mg/mL in DMF) for 30 min at RT.  The reaction solution was then dialyzed in a Slide-A-Lyzer dialysis cassette (10k molecule weight cut-off; Thermo Scientific) against cold DPBS for 24 h at 4 °C to remove excess NHS-$PEG_{12}$-biotin.  The biotinylated antibody was then collected and stored at 4 °C.

### 2.3.2.5  Determining the Biological Activity of Biotinylated Herceptin

BT474 cells were trypsinized and seeded at 50,000 cells in 50 µL of DPBS per well in a round-bottom 96-well plate.  The primary antibody Herceptin or biotinylated Herceptin, at 2 mg/mL, was diluted 1:200 in DPBS, and IgG, at 0.5 mg/mL, was diluted 1:50 in DPBS.  The diluted primary antibody (50 µL/well) was added to the cells and incubated for 30 min at 4 °C.  Cells were washed twice with cold DPBS by centrifugation.  The secondary antibody Alexa Fluor 488 goat anti-human IgG or Alexa Fluor 488 goat anti-mouse IgG (Invitrogen), at 2 mg/mL, was diluted 1:400 in DPBS.  The diluted secondary antibody (100 µL/well) was then incubated with the cells for 30 min at 4 °C.  Subsequently, cells were washed twice with cold DPBS by centrifugation.  Samples were resuspended in DPBS and analyzed using a BD LSRII flow cytometer with an HTS system.

### 2.3.2.6  Noncovalent Conjugation of Herceptin/IgG to PRINT Nanoparticles

Nanoparticles were conjugated with Herceptin or IgG through a biotin-avidin linkage.  Nanoparticles in anhydrous DMF (500 µL at 2 mg/mL) were reacted with 5 mg of NHS-PEG$_{3400}$-biotin in the presence of 10 µL anhydrous of pyridine; the nanoparticle dispersion was shaken on a vortex for 2 h.  Acetic anhydride (10 µL) was added to the dispersion, which was shaken for 10 min, to quench unreacted amines on the nanoparticle surface.  The nanoparticles were washed twice with Dulbecco's phosphate buffered saline (DPBS) by centrifugation.  UltraAvidin (50 µL, 10 mg/mL) was added to the nanoparticles in DPBS (2 mg/mL).  The dispersion was shaken for 1 h.  The nanoparticles were washed twice with DPBS by centrifugation.  To target the

nanoparticles, 50 µg of biotinylated Herceptin or IgG was added to the nanoparticle dispersion and was shaken for 30 min at room temperature and then kept overnight at 4 °C. The nanoparticles were washed twice with DPBS by centrifugation and then resuspended in DPBS.

### 2.3.2.7 Covalent Conjugation of Herceptin/Heptamer/IgG to PRINT Nanoparticles

Nanoparticles in anhydrous DMF (500 µL at 2 mg/mL) were reacted with 5 mg of NHS-PEG$_{5000}$-maleimide in the presence of 10 µL anhydrous of pyridine; the nanoparticle dispersion was shaken on a vortex for 2 h. Acetic anhydride (10 µL) was added to the dispersion, which was shaken for 10 min, to quench unreacted amines on the nanoparticle surface. Nanoparticles were washed twice with Milli-Q filtered water by centrifugation. To target nanoparticles with antibodies, 50 µg of Herceptin or IgG was added to the nanoparticle dispersion (500 µL at 2 mg/mL in 50 mM borate buffer pH 8.5). To target nanoparticles with the heptamer, 50 µg of the heptamer was added to the nanoparticle dispersion (500 µL at 2 mg/mL in DPBS pH 7.4). All nanoparticle dispersions were shaken for 4 h at room temperature. Nanoparticles were washed twice with DPBS by centrifugation and then resuspended in DPBS.

### 2.3.2.8 Physical Characterization of Nanoparticles

Scanning electron microscopy samples were prepared by pipetting 10 µL of nanoparticle solution onto a glass slide. Samples were dried and coated with 2 nm of gold palladium with a Cressington 108 auto sputter coater (Cressington Scientific

Instruments). Samples were imaged with a scanning electron microscope (Hitachi S-4700). The size (dynamic light scattering, DLS) and charge ($\zeta$-potential) of the nanoparticles were determined for 20 µg/mL nanoparticle samples in a 1 mM potassium chloride solution with a Malvern Instruments Nano ZS.

### 2.3.2.9 Determining the Expression of the HER2 Receptor in Cells

BT474, SKOV3, MCF7, OVCAR3, and HeLa cells were analyzed for expression of the HER2 receptor following the same protocol described above for the determination of the biological activity of biotinylated Herceptin.

### 2.3.2.10 Quantitative *In Vitro* Cellular Targeting

BT474, SKOV3, and MCF7 cells were plated at 10,000 cells/well in a 96-well plate and allowed to adhere overnight at 37 °C and 5% $CO_2$. Nanoparticles in OPTI-MEM were incubated with cells at 37 °C and 5% $CO_2$ for specified amounts of time and then removed. The cells were washed twice with DPBS, trypsinized, and prepared for analysis by flow cytometry with a 0.2% trypan blue solution containing 10% FBS in DPBS. Samples were analyzed with a BD LSRII flow cytometer with an HTS system.

For kinetic studies, BT474 cells were plated at 10,000 cells/well in a 96-well plate and allowed to adhere for 24 h at 37 °C and 5% $CO_2$. Nanoparticles in OPTI-MEM (200 µg/mL) were incubated with cells at 37 °C and 5% $CO_2$ for specified amounts of time and then removed. Cells were then processed for flow cytometry analysis as described above.

### 2.3.2.11 Confocal Microscopy

BT474 cells were plated on cover slips in a 6-well plate ($5 \times 10^4$ cells/well) overnight at 37 °C and 5% $CO_2$. Cells were incubated with 50 µg/mL of nanoparticles in OPTI-MEM for 4 h at 37 °C. Cells were fixed, made permeable with 0.1% triton-X100 in PBS for 3 min, and incubated with 1 µM of TO-PRO-3 (Invitrogen) in DPBS for 15 min. Cells were washed with DPBS, and cover slips were mounted onto glass slides with FluorSave Reagent (Calbiochem), and cells were imaged with a confocal laser scanning microscope (Olympus Fluoview FV500).

### 2.3.2.12 Inhibition of Cellular Internalization of Nanoparticles

BT474 cells were plated at 10,000 cells/well in a 96-well plate and allowed to adhere overnight at 37 °C and 5% $CO_2$. Free Herceptin, heptamer, or IgG (6 µg) was dosed onto cells. The cells were incubated at 37 °C for 1 h, after which free targeting ligands were removed. Nanoparticles in OPTI-MEM, at 200 µg/mL, were incubated with cells at 37 °C for 4 h and then removed. The cells were washed twice with DPBS, trypsinized, and prepared for analysis by flow cytometry with a 0.2% trypan blue solution containing 10% FBS in DPBS. Samples were analyzed with a BD LSRII flow cytometer with an HTS system.

### 2.3.3 Results and Discussion

### 2.3.3.1 Particle Fabrication and Noncovalent Conjugation with Herceptin/IgG

As the PRINT technology affords independent control over particle size, shape, matrix, and surface chemistry,[52-55,57-60,80] cylindrical ($d$ = 200 nm and $h$ = 200 nm) nanoparticles, primarily comprised of biocompatible poly(ethylene glycol) (PEG), were fabricated through this process (Figure 2.14).
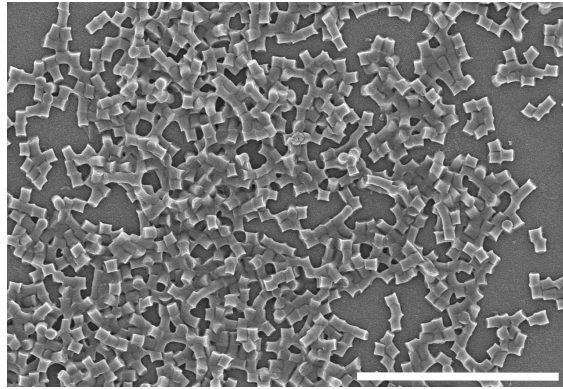


**Figure 2.14** SEM of cylindrical ($d$ = 200 nm and $h$ = 200 nm) nanoparticles. Scale bar is 3 µm.

Nanoparticles were mostly composed of the crosslinker $PEG_{700}$ diacrylate, and also 2-aminoethyl methacrylate hydrochloride for functional handles in surface modification, and fluorescein $o$-acrylate to fluorescently label nanoparticles for tracking *in vitro* (Table 2.3).

**Table 2.3** Composition of PRINT nanoparticles for targeting.

| Monomers | Wt % |
| --- | --- |
| PEG$_{700}$ diacrylate | 77 |
| 2-Aminoethyl methacrylate hydrochloride | 20 |
| Fluorescein $o$-acrylate | 2 |
| 2,2-Diethoxyacetophenone | 1 |

Cylindrical pre-functionalized nanoparticles with no surface modification had a hydrodynamic diameter of 288 nm with a PDI of 0.114. As seen in Table 2.4, they also possessed a positive ζ-potential +26 mV. The cationic nature of the pre-functionalized nanoparticles was due to amine functional groups. Positively charged particles have been reported to internalize rapidly though nonspecifically into cells[53,61,62] and can also induce cytotoxicity.[63] Alternately, negatively charged particles show low intracellular internalization.[53,61,62] Thus, for the purposes of drug delivery, nanoparticles are often designed to have a negative charge. The use of negatively charged nanoparticles helps to minimize nonspecific uptake and in conjunction with targeting ligands, aids in achieving specific accumulation within the disease site.[59]

**Table 2.4** Hydrodynamic diameters and zeta potentials of PRINT nanoparticles throughout surface modifications to noncovalently conjugate Herceptin.

| Nanoparticle | Diameter (nm) | PDI | $\zeta$-Potential (mV) |
|---|---|---|---|
| Pre-functionalized | 288 | 0.114 | $+26.0 \pm 0.5$ |
| Biotinylated | 284 | 0.111 | $-23.6 \pm 0.5$ |
| NP-Herc | 329 | 0.213 | $-20.1 \pm 0.3$ |
| NP-IgG | 310 | 0.214 | $-18.7 \pm 0.2$ |

Consequently, pre-functionalized nanoparticles were functionalized and conjugated with targeting ligands as described previously. Pre-functionalized nanoparticles were reacted with NHS-PEG$_{3400}$-biotin and then with acetic anhydride to quench any unreacted amines. As shown in Table 2.4, biotinylated nanoparticles still maintained their size (284 nm) after surface modification. However, their surface charges shifted to negative $\zeta$-potentials (-23.6 mV) so as to inhibit nonspecific cellular internalization. Through biotin-avidin linkages, targeting ligands were conjugated onto the surfaces of nanoparticles. Biotinylated nanoparticles were first reacted with avidin and then with the targeting ligands biotinylated Herceptin or IgG. Herceptin is a humanized monoclonal antibody that binds with HER2, while IgG is a nonspecific control antibody. For Herceptin-targeted nanoparticles (NP-Herc) and IgG-targeted nanoparticles (NP-IgG), the $\zeta$-potentials were negative (around -20 mV) so as to minimize nonspecific cellular uptake while targeting ligands could facilitate specific accumulation within tumor cells.

Because Herceptin was conjugated onto nanoparticles though biotin-avidin linkages, it was first labeled with biotin to facilitate attachment. Herceptin was reacted with NHS-PEG$_{12}$-biotin, resulting in antibody that was randomly labeled with biotin.

The biological integrity of biotinylated Herceptin was determined prior to conjugation with nanoparticles. Binding of biotinylated Herceptin with HER2 was investigated to ensure that antibody activity was maintained and was not disturbed by the arbitrary reaction with biotin. Binding of unmodified and biotinylated Herceptin in BT474 (human breast carcinoma) cells was studied by flow cytometry using a secondary antibody labeled with the fluorescent dye Alexa Fluor 488. Shown in Figure 2.15, there were similar shifts in fluorescence for unmodified and biotinylated Herceptin, suggesting that biotinylated Herceptin maintained its activity and could still bind to the HER2 receptor on BT474 cells. There was also minimal nonspecific binding of the fluorescent secondary antibody. Based on this data, labeling Herceptin with biotin did not adversely alter its binding with HER2. That being the case, biotinylated Herceptin was used to functionalize and target nanoparticles.
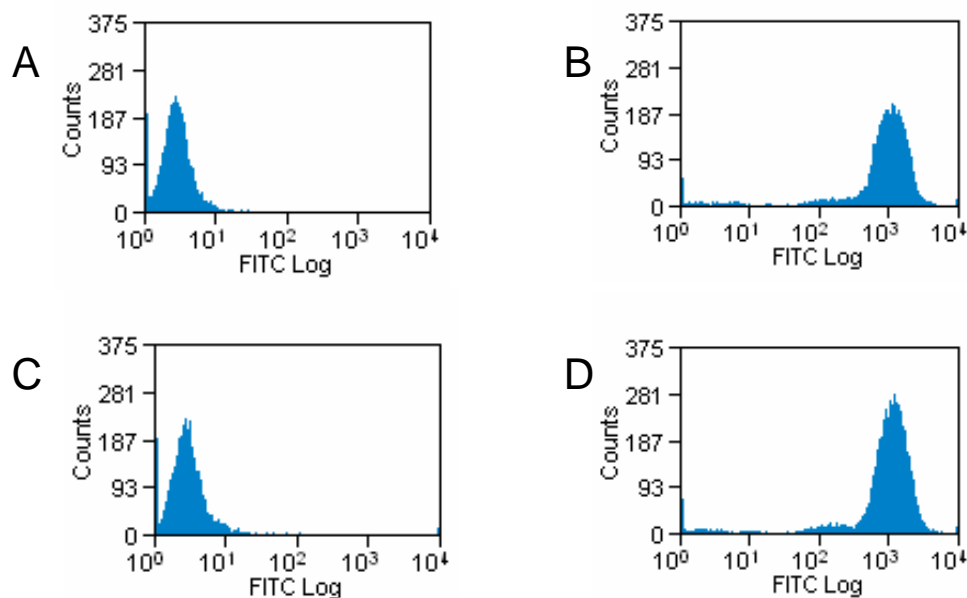
**Figure 2.15** Flow cytometry histograms of (A) BT474 cells, (B) binding of Herceptin, (C) no nonspecific of the fluorescent secondary antibody, and (D) binding of biotinylated Herceptin.

### 2.3.3.2 Determination of HER2-Positive Cell Lines

Numerous cancer cell lines were investigated for expression of the HER2 receptor. In a similar manner used to check the integrity of biotinylated Herceptin, HeLa (human cervical cancer), MCF7 (human breast adenocarcinoma), OVCAR3 and SKOV3 (human ovarian adenocarcinoma), and BT474 (human breast carcinoma) cells were probed for HER2 with Herceptin as a primary antibody and an Alexa Fluor 488 fluorescently-labeled secondary antibody. As shown in flow cytometry histograms in Figure 2.16, BT474 and SKOV3 cells strongly expressed the HER2 receptor. HeLa, MCF7, and OVCAR3 cells demonstrated less intense shifts in fluorescence, indicating decreased

expression of the receptor. Based on these results, BT474, SKOV3, and MCF7 cells were selected for further investigations with Herceptin-targeted PRINT nanoparticles.
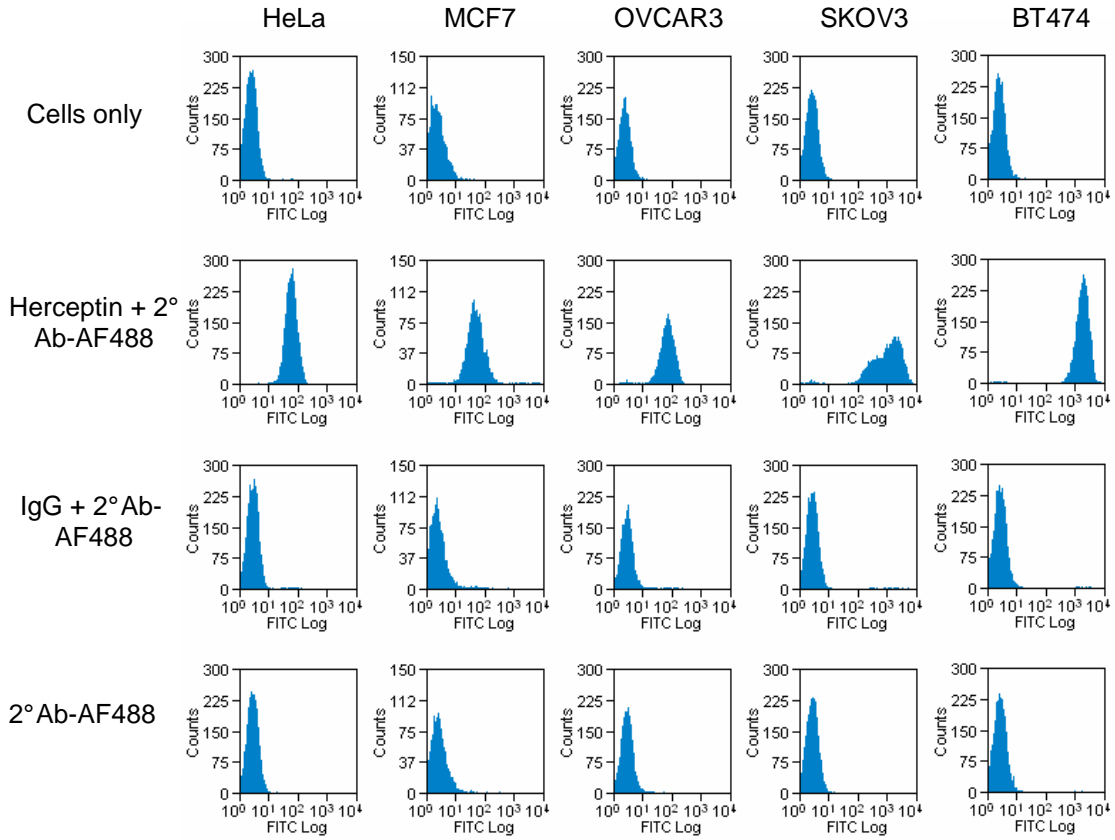


**Figure 2.16** Flow cytometry histograms of HER2 expression in various cancer cell lines by labeling with Herceptin and a fluorescent (Alexa Fluor 488) secondary antibody.

## 2.3.3.3 Cellular Internalization of Nanoparticles with Noncovalently Conjugated Herceptin/IgG

Targeting specificity of nanoparticles targeted with Herceptin and IgG through noncovalent methods was investigated in various cancer cell lines of differing HER2 expression. NP-Herc and NP-IgG, in increasing concentration up to 200 μg/mL, were

incubated with BT474, SKOV3, and MCF7 cells for 4 h at 37 °C. Samples were analyzed by a flow cytometry technique to quantify the percentage of cells with internalized nanoparticles.[64] As seen in Figure 2.17, BT474 cells readily internalized NP-Herc with nearly 95% of cells containing nanoparticles. Uptake of NP-Herc was slightly lower in SKOV3 cells (75%), and MCF7 cells internalized a minimal amount of NP-Herc. This trend correlates with the expression level of the HER2 receptor in each cell line. BT474 cells express more HER2 receptors than SKOV3 cells, which have more HER2 than MCF7 cells. Increased level of cellular HER2 receptors facilitates greater nanoparticle internalization. However, for NP-IgG, there was negligible accumulation in all cell lines (<2%). This demonstrates the high specificity of NP-Herc as a targeted nanoparticle system, which can discriminate cancer cells with high overexpression of the HER2 receptor from those with minimal levels of the receptor.
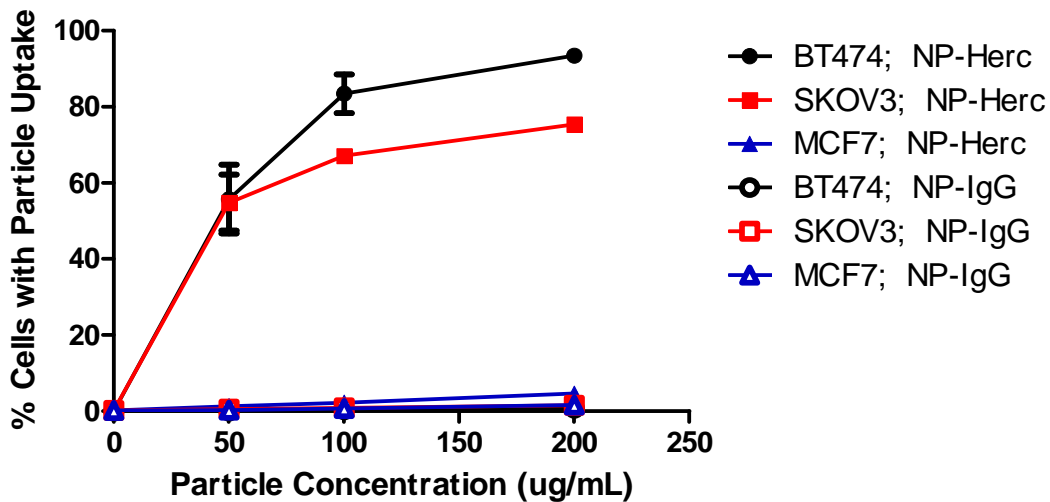


**Figure 2.17** Cellular internalization of cylindrical 200 nm nanoparticles targeted with Herceptin or IgG in BT474, SKOV3, and MCF7 cells.

In addition to flow cytometry, targeting and internalization of 200 nm cylindrical NP-Herc were visualized by confocal microscopy. Fluorescein-labeled nanoparticles were incubated with BT474 cells for 4 h at 37 °C. Based on flow cytometry results, NP-Herc were anticipated to be readily internalized into BT474 cells, and indeed, the targeted nanoparticles bound to the HER2 receptor and internalized into cells (Figure 2.18). Conjugation with the HER2 receptor presumably induced nanoparticle internalization through receptor-mediated endocytosis. Targeting results from both flow cytometry and confocal microscopy demonstrate the potential of PRINT nanoparticles as advanced nanomedicine through highly specific targeting of conjugated Herceptin to the HER2 receptor and subsequent cellular internalization in HER2-positive cells.
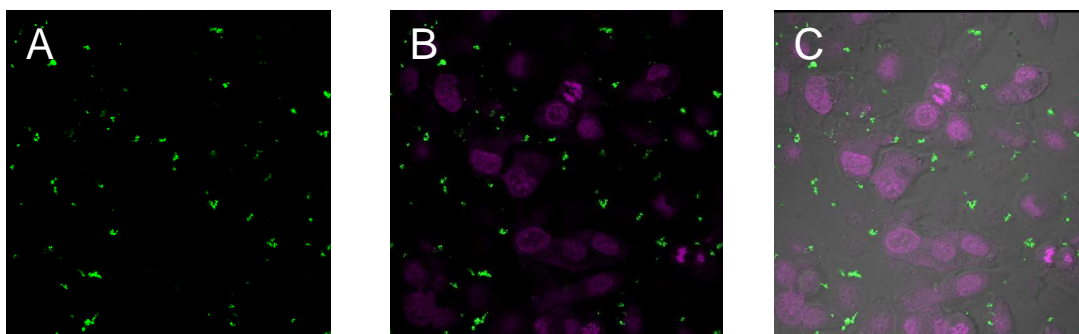


**Figure 2.18** Confocal microscopy images of (A) 200 nm cylindrical, fluorescein-labeled NP-Herc (green), (B) in BT474 cells (nuclei stained), and (C) merge of fluorescence and DIC.

### 2.3.3.4 Effect of Targeting Ligand Density on Targeted Cellular Internalization

The density of Herceptin on the nanoparticle surface was varied to further understand targeting specificity. Density was modulated from 100% of Herceptin to 0%,

with the total ligand concentration maintained by substituting Herceptin for the IgG control antibody. In other words, nanoparticles with 0% Herceptin were equivalent to nanoparticles with 100% of IgG (NP-IgG). Cells were incubated for 4 h at 37 °C with targeted nanoparticles (0-200 µg/mL) with varied ligand densities. In BT474 cells, all nanoparticles with Herceptin exhibited selective internalization in a dose dependent manner, while nanoparticles with 0% Herceptin (or NP-IgG) had negligible uptake (Figure 2.19). Over 85% of BT474 cells readily internalized nanoparticles with just 50% of Herceptin, achieving a similar uptake profile as nanoparticles with 75% and 100% of Herceptin. However, when the targeting antibody Herceptin accounted for only 25% of the ligands, cellular uptake decreased slightly to 75%. Nonetheless, all nanoparticles conjugated with some Herceptin specifically internalized into BT474 cells because of the overexpression of cellular HER2 receptor, while nanoparticles with 0% of Herceptin (or NP-IgG) demonstrated minimal uptake as a result of a negative $\zeta$-potential and nonspecific control ligand. Through this study, the high specificity and cellular internalization of nanoparticles with only 25% of Herceptin are promising indications for multimeric targeting of other overexpressed receptors to increase target specificity (i.e., nanoparticles with various ligands that target the HER2 and FR) or for addition of ligands with therapeutic effects (i.e, chemotherapeutic drugs).
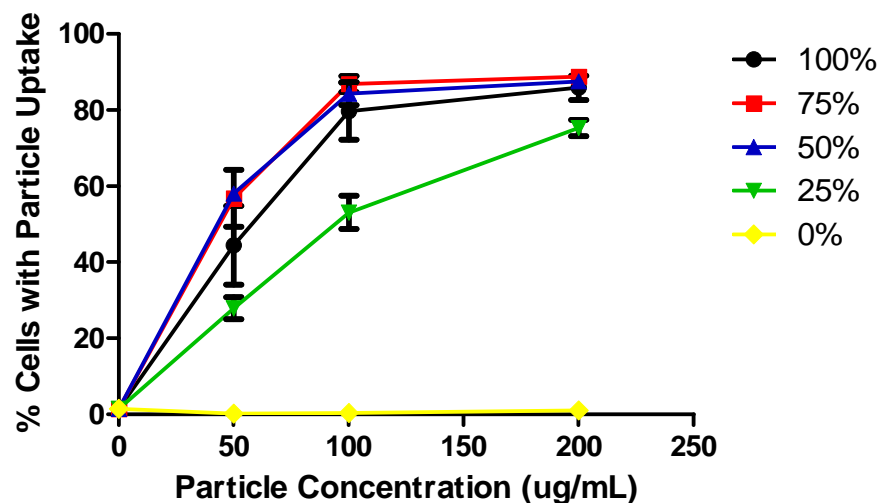
**Figure 2.19** Internalization of 200 nm cylindrical nanoparticles targeted with varied densities of Herceptin in BT474 cells.

Cellular uptake of these nanoparticles was further investigated in MCF7 cells, which have a differing level of HER2 than BT474 cells. As seen in Figure 2.20, less than 20% of MCF7 cells internalized nanoparticles labeled with any Herceptin. In fact, minimal differences in uptake were observed amongst nanoparticles targeted with 100%, 75%, 50%, or 25% of Herceptin. Low cellular uptake of these nanoparticles can be attributed to the minimal expression of the HER2 receptor in MCF7 cells. Based on nanoparticle internalization in BT474 and MCF7 cells, the extent of uptake of NP-Herc correlates well with the cellular expression of the HER2 receptor. This demonstrates the high degree of specificity with which PRINT nanoparticles functionalized with Herceptin can target diseased cells.
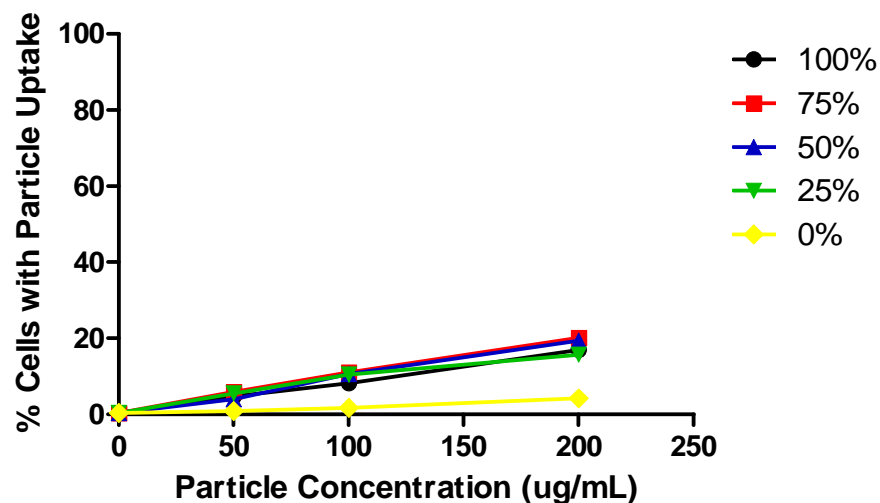
**Figure 2.20** Internalization of 200 nm cylindrical nanoparticles targeted with varied densities of Herceptin in MCF7 cells.

**2.3.3.5  Particle Fabrication and Covalent Conjugation of Ligands Targeting HER2**

In efforts to further understand the targeting of nanoparticles, 200 nm cylindrical nanoparticles were functionalized with Herceptin and an engineered heptameric ligand, both with binding affinity to the HER2 receptor.  Similar to previous NP-Herc, these nanoparticles were composed of $PEG_{700}$ diacrylate, 2-aminoethyl methacrylate, and fluorescein *o*-acrylate (Table 2.3).  Pre-functionalized nanoparticles without surface modifications had a hydrodynamic diameter of 295 nm and were positively charged (+32.4 mV, Table 2.5).

**Table 2.5** Hydrodynamic diameters and zeta potentials of 200 nm cylindrical PRINT nanoparticles for targeting with HER2 ligands.

| Nanoparticle | Diameter (nm) | PDI | $\zeta$-Potential (mV) |
|---|---|---|---|
| Pre-functionalized | 295 | 0.080 | $+32.4 \pm 0.2$ |
| Maleimide | 300 | 0.017 | $-31.3 \pm 0.6$ |
| NP-7mer | 301 | 0.062 | $-34.2 \pm 2.8$ |
| NP-Herc | 299 | 0.125 | $-31.8 \pm 0.6$ |
| NP-IgG | 298 | 0.058 | $-32.8 \pm 0.4$ |

However, positive $\zeta$-potentials can induce nonspecific cellular uptake of particles[53,61,62] and also cellular toxicity,[63] so pre-functionalized nanoparticles were functionalized for a negative $\zeta$-potential and conjugated with targeting ligands for the HER2 receptor. Unlike previously fabricated targeted PRINT nanoparticles, targeting ligands were covalently attached to the surface of nanoparticles through maleimide functional groups (Figure 2.21). Pre-functionalized nanoparticles were reacted with NHS-PEG$_{5000}$-maleimide, yielding nanoparticles with surface maleimide functional groups for further reaction with targeting ligands. After quenching unreacted amines with acetic anhydride, maleimide nanoparticles became negatively charged ($-31.3 \pm 0.6$ mV) so as to minimize nonspecific cellular internalization. Maleimide nanoparticles were then reacted with lysines in Herceptin or IgG under moderately basic conditions (pH 8.5) for covalent but arbitrary attachment of the antibodies. Conversely, maleimide nanoparticles were reacted under neutral conditions (pH 7.4) with heptameric ligands (7mer) consisting of a cysteine for site specific covalent conjugation of targeting ligands. Heptamer-targeted nanoparticles (NP-7mer), along with covalently linked NP-Herc and NP-IgG, maintained hydrodynamic diameters around 300 nm and negative $\zeta$-potentials around -30 mV.
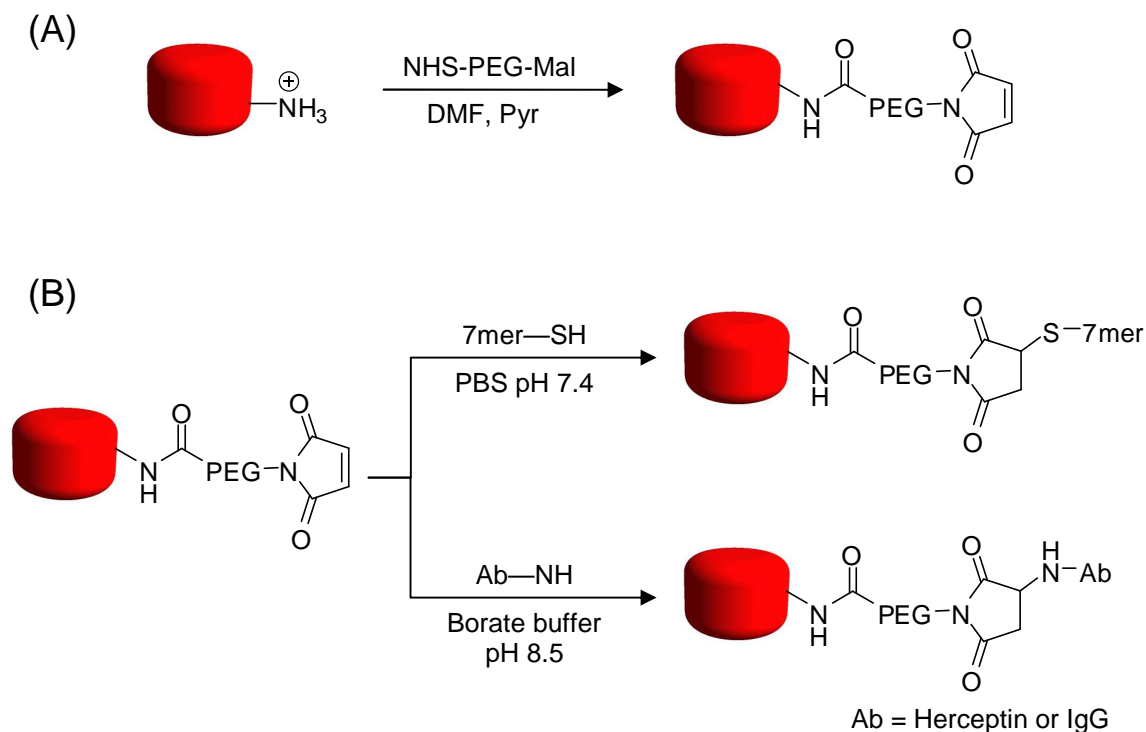
**Figure 2.21** Scheme of covalent conjugation of HER2 targeting ligands to the surface of nanoparticles. (A) Functionalizing pre-functionalized nanoparticles for surface maleimide functional groups. (B) Conjugating maleimide nanoparticles with targeting ligands.

### 2.3.3.6 Cellular Targeting of Nanoparticles with Covalently Conjugated Ligands

Nanoparticles were investigated in BT474 breast cancer cells for the effects of surface modification through covalent linkages and the targeting of the engineered heptameric ligand with seven sites for binding with HER2 receptors. After incubation with cells for 4 h at 37 °C, samples were analyzed by flow cytometry. HER2 receptor targeting nanoparticles NP-7mer and NP-Herc were internalized into cells, while NP-IgG showed minimal cellular uptake of <10% (Figure 2.22). About 80% of BT474 cells

internalized NP-7mer, while fewer cells (~40%) internalized NP-Herc, but both NP-7mer and NP-Herc demonstrated target specificity, binding to the HER2 receptor present on BT474 cells to induce internalization. Interestingly, NP-Herc fabricated through covalent conjugation methods did not achieve similar levels of cellular internalization as NP-Herc prepared through noncovalent biotin-avidin linkages (40% vs. 85%). However, NP-7mer reached 80% uptake in BT474 cells, comparable to NP-Herc formed with noncovalent bonds.
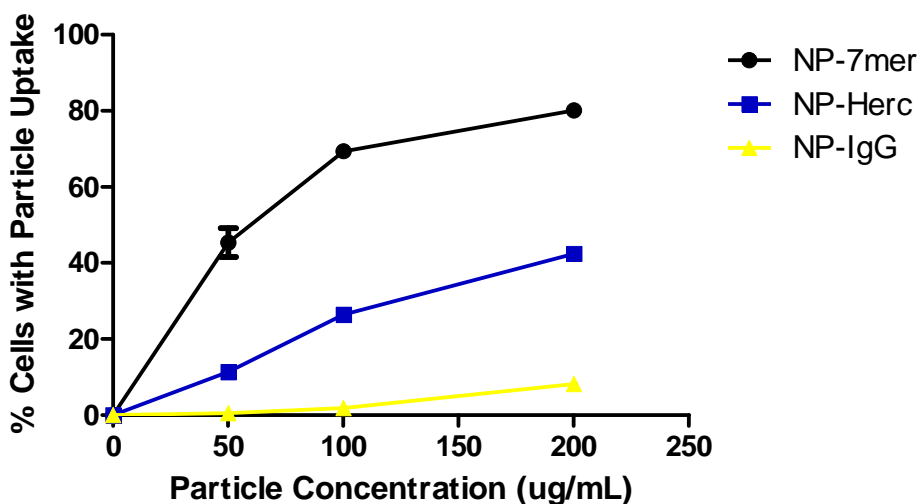


**Figure 2.22** Internalization of nanoparticles targeted with HER2 ligands or IgG in BT474 cells.

A possible explanation for this is the accelerated internalization of large cellular surface complexes formed by neighboring HER2 receptors interconnected by proteins (Figure 2.23).[81-83]

74
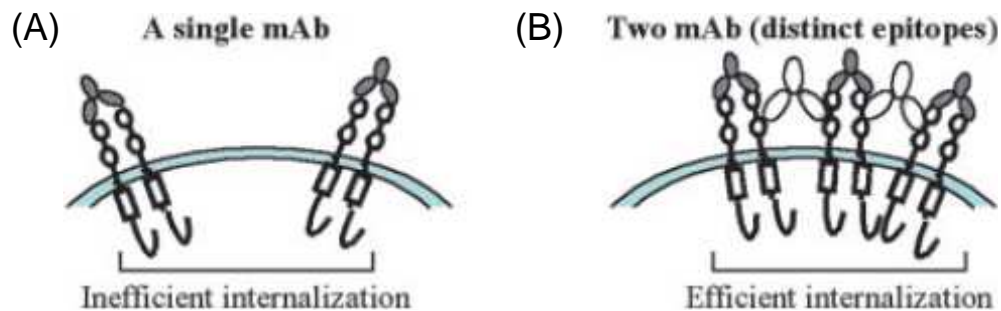
**Figure 2.23**  Models comparing the size of receptor-antibody complexes formed at cellular surfaces by (A) one or (B) two antibodies.  Adapted from [81].

The heptamer can bind with up to seven HER2 receptors, while Herceptin can only bind with a maximum of two receptors.  With multiple copies of the heptameric ligand, NP-7mer possess over three times as many binding sites for HER2 as NP-Herc.  The increased valency of NP-7mer enables larger cellular surface complexes to be formed, and thus, facilitates internalization of the nanoparticles.  Similarly, NP-Herc fabricated through biotin-avidin linkages likely formed large receptor-antibody complexes that enabled efficient uptake of nanoparticles because of their increased multivalent nature over NP-Herc prepared by covalent means (Figure 2.24).

| Nanoparticle | Valency |
|---|---|
| NP-7mer | 7 |
| NP-Herc (covalent) | 2 |
| NP-Herc (noncovalent) | 6 |
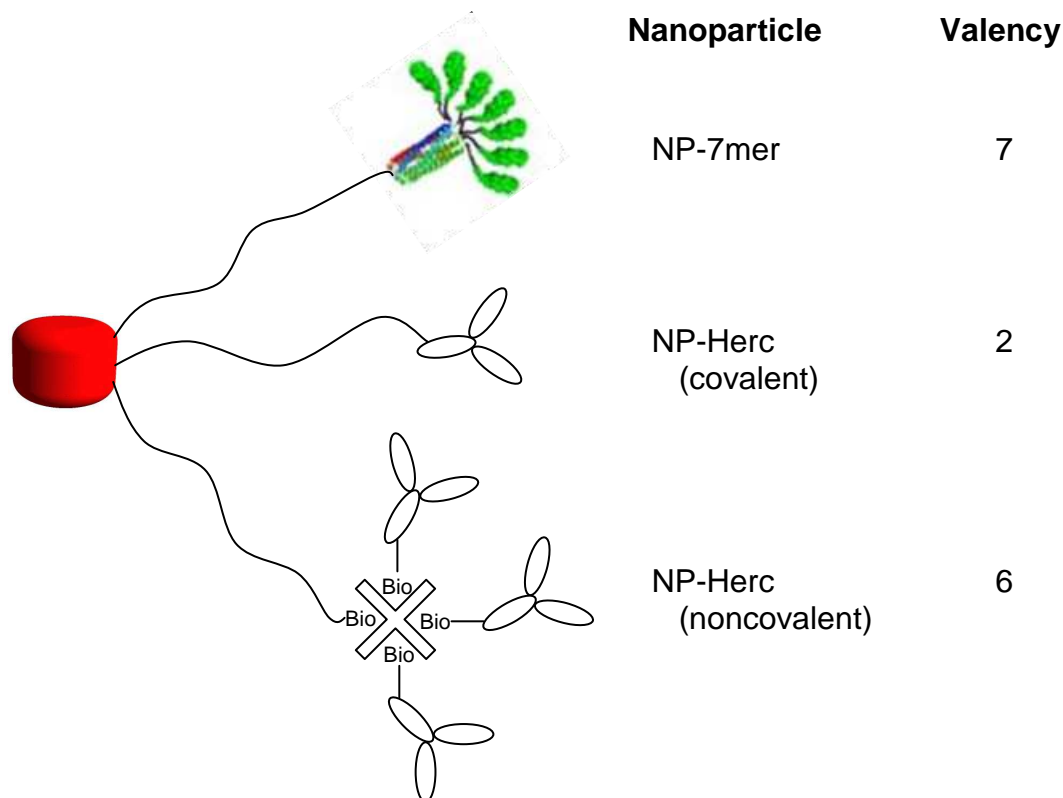
**Figure 2.24** Diagrams illustrating the maximal valency of NP-Herc and NP-7mer.

Additionally, specific targeting of NP-7mer and NP-Herc was visualized by confocal microscopy. NP-7mer, NP-Herc, and NP-IgG, all labeled with fluorescein, were incubated with BT474 cells. As expected, cells internalized NP-7mer, as observed by intracellular nanoparticle fluorescence seen in green (Figure 2.25), corroborating results from flow cytometry. These targeted nanoparticles bound to the HER2 receptor on BT474 cells, thus inducing receptor-mediated endocytosis. In contrast, NP-Herc were mostly observed at the periphery of cells, bound to the HER2 receptor but not internalized because the HER2 receptor is remarkably resistant to internalization.[84,85] Also, the low multivalent nature of NP-Herc relative to NP-7mer likely could not create sufficiently large antigen-antibody complexes to induce efficient internalization. As a

control, NP-IgG showed negligible internalization into cells due to their negative surface charge and nonspecific ligand.
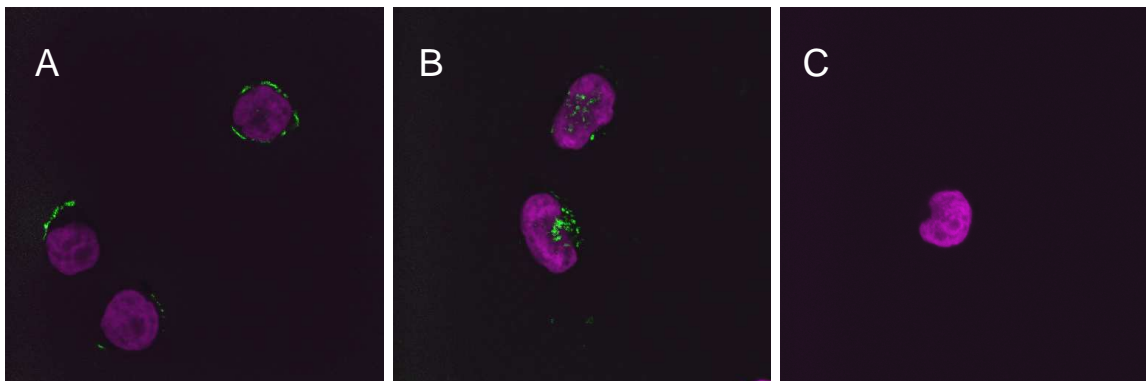


**Figure 2.25** Confocal micrscopy images of BT4747 cells with (A) NP-Herc, (B) NP-7mer, and (C) NP-IgG.

### 2.3.3.7 Kinetics of Internalization of Nanoparticles with Covalently Conjugated Ligands

To further elucidate the effect of surface chemistry and targeting ligands, the kinetics of internalization of these nanoparticles were investigated by flow cytometry. Targeted nanoparticles were incubated with BT474 cells at 37 °C for varied periods up to 4 h. NP-7mer internalized into cells more rapidly than NP-Herc. Different ligands, both targeting the HER2 receptor, resulted in dissimilar rates of nanoparticle uptake into BT474 cells. This is a result of the differing valency between the two targeted nanoparticles, which influences the size of the HER2 receptor-ligand complexes on the cellular surface. Previous studies have shown that the rate of internalization is proportional to the size of HER2-ligand lattices.[81,82] As NP-7mer are capable of binding more receptors and thus forming larger cellular surface complexes than NP-Herc, it is

expected and was observed that the rate of internalization of NP-7mer is more rapid than NP-Herc.
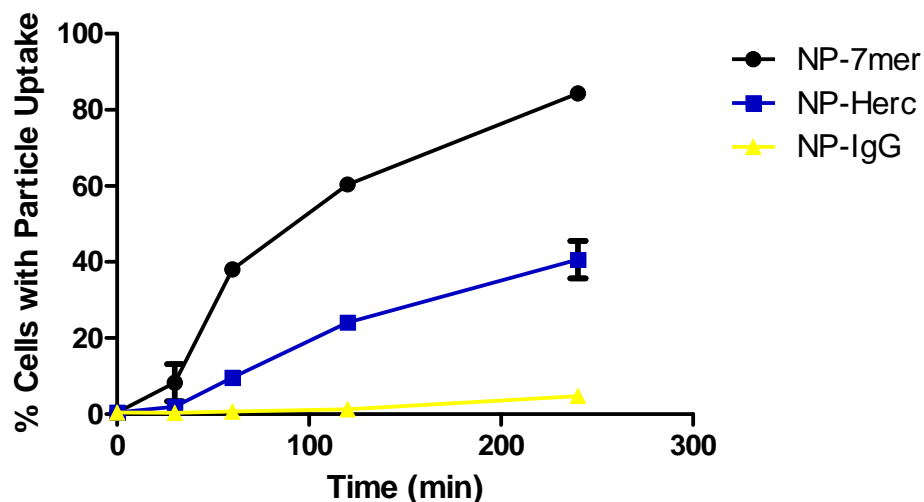


**Figure 2.26** Kinetics of internalization of nanoparticles conjugated with ligands for HER2 or IgG in BT474 cells.

### 2.3.3.8 Competition with Free Targeting Ligands

Additionally, the effect of competing free targeting ligands on internalization of targeted nanoparticles was investigated in BT474 cells. To confirm binding and uptake of NP-Herc and NP-7mer, BT474 cells were initially incubated with free Herceptin prior to exposure to nanoparticles (200 µg/mL) to allow the free ligands to bind to the HER2 receptors on the cellular surface, decreasing receptors available for the nanoparticles. Internalization of NP-Herc was greatly inhibited when cells were incubated with free Herceptin (Figure 2.26), indicating that NP-Herc are binding to the HER2 receptor and inducing receptor-mediated endocytosis. However, for NP-7mer, cellular uptake was only slightly inhibited with a drop of 80% to about 70% of cells with internalized

nanoparticles, indicating that the heptameric ligand does not bind the same epitope on the HER2 receptor as Herceptin. Control NP-IgG were unaffected by the addition of free Herceptin and exhibited minimal cellular uptake.
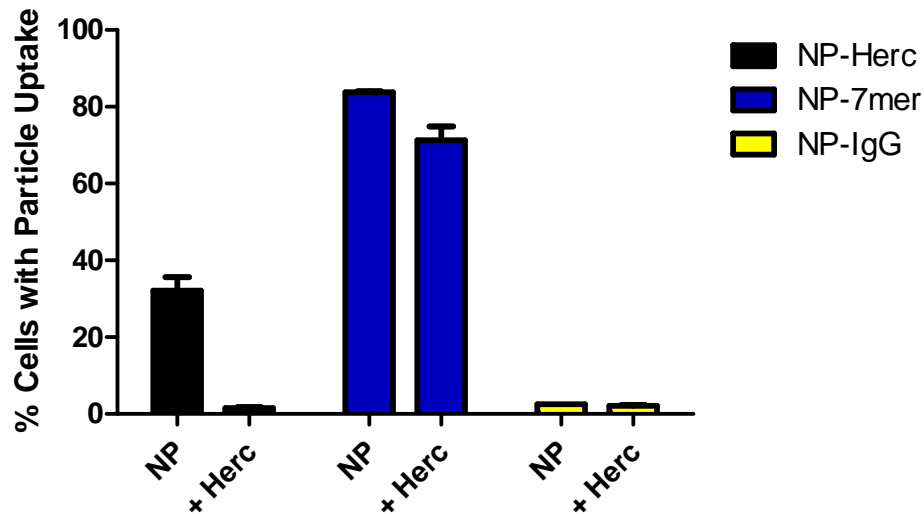


**Figure 2.27** Effect on internalization of targeted nanoparticles in BT474 cells with prior exposure to free Herceptin.

Because internalization of NP-7mer was minimally affected by free Herceptin, BT474 cells were also incubated with free heptamer before addition of nanoparticles. In this case, internalization of NP-7mer was inhibited to <50% (Figure 2.28), indicating that NP-7mer are also internalized through a receptor-mediated mechanism despite binding to the HER2 receptor in a different site than Herceptin. Interestingly, when BT474 cells were incubated with free heptamer prior to the addition of nanoparticles, internalization of NP-Herc and NP-IgG increased to 60% and 35%, respectively.
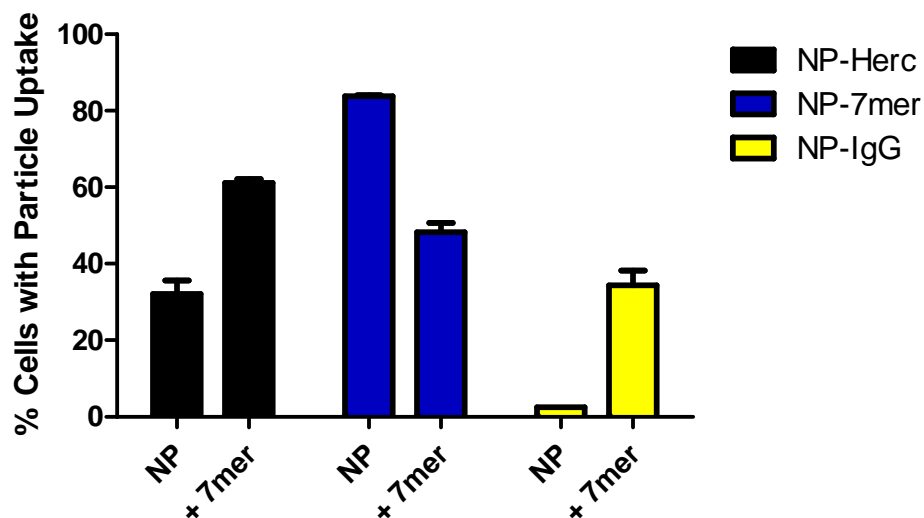
**Figure 2.28** Effect on internalization of targeted nanoparticles in BT474 cells with prior exposure to free heptamer.

The heptameric ligand can bind up to seven HER2 receptors to generate large cellular lattices of receptors and ligands. Seen previously, the cellular surface complexes formed by NP-7mer accelerate internalization. As the heptamer and Herceptin bind different epitopes of HER2, NP-Herc can bind to receptors within a cellular surface complex interconnected by heptameric ligands, thereby enhancing internalization of NP-Herc. Increased cellular uptake of NP-IgG was likely triggered by the same mechanism where large, preformed antigen-heptamer complexes heightened any nonspecific binding of NP-IgG. Similar results of enhanced HER2 receptor internalization have been reported in which BT474 cells incubated with antibodies that bind different epitopes stimulate internalization because of the formation of larger antigen-antibody complexes.[81] Targeting nanoparticles with multivalent ligands can trigger alternate cellular pathways that intensify the accumulation and potency of nanoparticle therapeutics.

## 2.3.4 Conclusions

Through the PRINT technology, HER2 receptor targeting nanoparticles were successfully designed and fabricated to study the potential of these nanoparticles for a targeted delivery system and the effects of multivalency on targeting. Nanoparticles possessed a negative surface charge that avoided nonspecific cellular uptake, but through noncovalent and covalent methods, Herceptin and heptameric ligands were conjugated to nanoparticles, enabling specific targeting and HER2 receptor-mediated endocytosis, despite the receptor's resistance to internalization. Cellular uptake of targeted nanoparticles was found to be dose dependent and also correlated with the expression level of the HER2 receptor in the cells. Furthermore, the multivalent nature of targeted nanoparticles influenced cellular targeting and internalization. When Herceptin was noncovalently conjugated onto nanoparticles, NP-Herc achieved high levels of uptake in BT474 cells through the numerous ligands on the surface from the multiple biotin binding sites. Similar levels of cellular uptake were achieved with NP-7mer because of the multivalency of the heptameric ligand that could bind and form large antigen-ligand complexes at the cellular surface. Thus, nanoparticles targeted with HER2 ligands demonstrate potential as improved therapeutics through specific targeting and induced internalization.

## 2.3.5 Future Work

### 2.3.5.1 Nanoparticles Targeting the HER2 Receptor

A barrier for delivery of nanoparticles is the length of *in vivo* circulation. Smaller spherical particle sizes from micro to nano have been found to increase circulation.[86,87] However, filamentous particles (>5 µm) were recently reported to have long circulation *in vivo*, detectable up to a week after injection.[88,89] Also, data indicates that cellular uptake by macrophages is decreased with elongated particles relative to spherical structures, thus indicating a method of reducing clearance by the reticuloendothelial clearance pathways so as to prolong circulation.[90-92] Thus, these properties of filamentous particles in conjunction with specific targeting may unlock great potential for therapeutic delivery of nanoparticles. To better elucidate the possibilities of nanoparticles targeted with HER2 ligands as improved nanotherapeutics, Herceptin-targeted cylindrical nanoparticles ($d = 200$ nm and $h = 200$ nm, AR = 1) were compared with elongated, rod-like nanoparticles (80 × 320 nm, AR = 4). Targeting ligands were conjugated via biotin-avidin linkages. NP-Herc and NP-IgG, in various nanoparticle concentrations of 0-200 µg/mL, were incubated with cancer cell lines of differing expression levels of the HER2 receptor. In BT474 cells, both types of NP-Herc exhibited similarly specific and high internalization around 90%, while there was an inconsiderable amount of cells with uptake of NP-IgG for either nanoparticle shape (Figure 2.29).
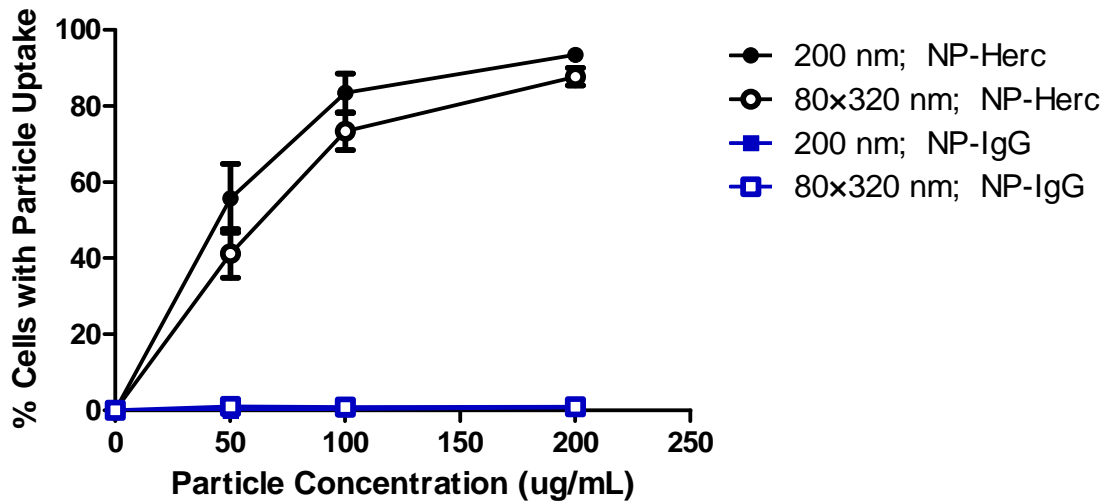
**Figure 2.29** Internalization of 200 nm cylindrical and $80 \times 320$ nm rod-like nanoparticles targeted with either Herceptin or IgG in BT474 cells.

In MCF7 cells, negligible difference in cellular uptake was observed between NP-Herc and NP-IgG (Figure 2.30). Less than 5% of MCF7 cells internalized any nanoparticles regardless of shape, aspect ratio, or surface ligands. This can be attributed to the minimal expression of the HER2 receptor in MCF7 cells.
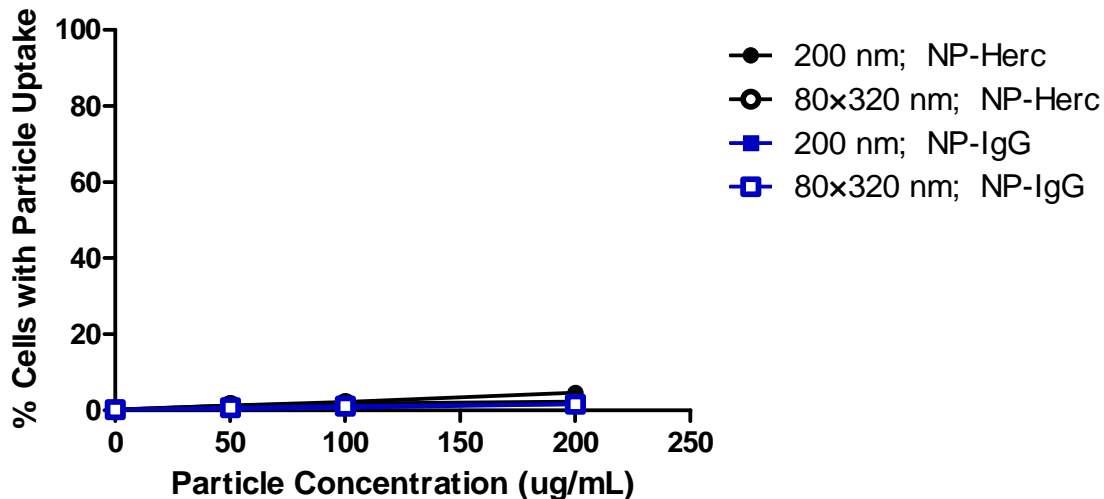
**Figure 2.30** Internalization of 200 nm cylindrical and $80 \times 320$ nm rod-like nanoparticles targeted with either Herceptin or IgG in MCF7 cells.

Regardless of the nanoparticle shape and aspect ratio, it was found that the extent of internalization of NP-Herc correlated well with the cellular level of the HER2 receptor. BT474 cells possess high amplification of the HER2 receptor so demonstrated increased nanoparticle uptake, whereas MCF7 cells, with low expression of HER2, exhibited low uptake of all nanoparticles. This indicates the high specificity of NP-Herc for binding to the HER2 receptor for cellular internalization despite elongated, nonspherical shapes as minimal differences in cellular uptake were observed between 200 nm cylindrical and 80 $\times$ 320 nm rod-like nanoparticles.

The effect of nanoparticle shape and aspect ratio on the kinetics of cellular internalization was also investigated. Targeted nanoparticles were incubated with BT474 and MCF7 cells at 37 °C and then analyzed for cellular uptake by flow cytometry at various time points (0-4 h). Shown in Figure 2.31, internalization of NP-Herc of either shape followed nearly identical profiles over the course of 4 h in BT474 cells. Control

NP-IgG of both shapes in BT474 cells also exhibited very low uptake throughout 4 h. In MCF7 cells, due to the low expression of the HER2 receptor, there was minimal uptake of both NP-Herc and NP-IgG in either shape over the time course.
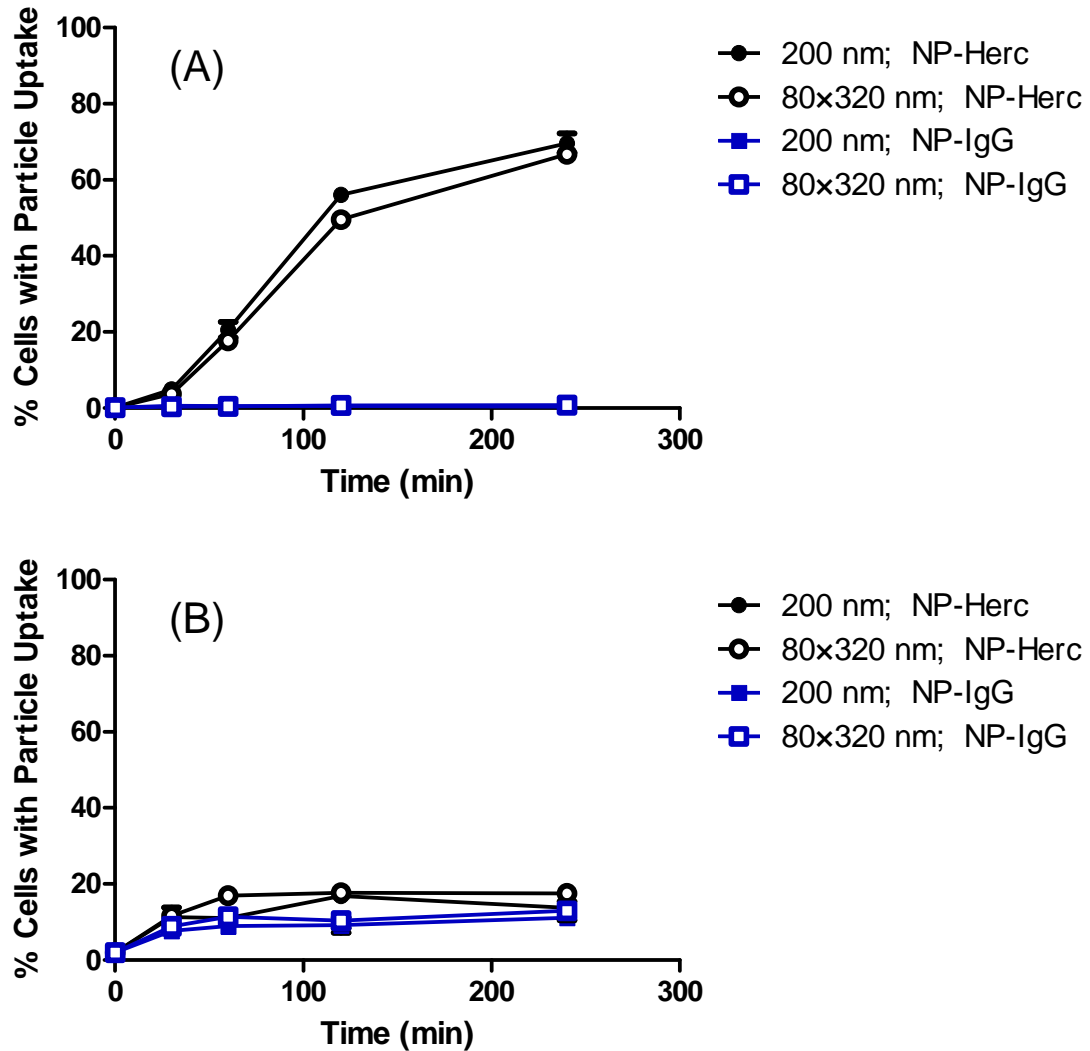


**Figure 2.31** Kinetics of internalization of 200 nm cylindrical and $80 \times 320$ nm rod-like NP-Herc and NP-IgG in (A) BT474 and (B) MCF7 cells.

These preliminary results suggest that, in this size range, targeted nanoparticles are minimally influenced by the shape or aspect ratio in regards to cellular uptake and kinetics. Instead, the predominant factor affecting cellular uptake of NP-Herc is the expression level of the HER2 receptor in diseased cells because nanoparticle internalization is regulated by HER2 receptor-mediated endocytosis. Further studies would be necessary to fully elucidate the effects of particle shape and size, but initial results are promising for the application of nonspherical nanoparticles as advanced targeted nanotherapeutics. Additional nanoparticle shapes and sizes should be investigated, specifically nanoparticles with greater aspect ratios, such as filamentous 80 × 2000 nm (AR = 25) or 80 × 5000 nm (AR = 62.5) nanoparticles. Targeting capabilities of these nanoparticles must be affirmed, in addition to *in vivo* pharmacokinetics resulting from the varied sizes to determine whether targeted filamentous particles exhibit similar prolonged circulation and accumulation at the tumor site as compared to untargeted counterparts.

### 2.3.5.2 Nanoparticles Targeting the HER1 Receptor

With the success of targeting PRINT nanoparticles with heptameric ligands for the HER2 receptor, targeting the HER1 receptor (EGFR, ErbB1), another member of the epidermal growth factor receptor family, was investigated. The HER1 receptor is overexpressed in 20-80% of breast cancers, among others, and both HER1 and HER2 receptor drive growth and progression of tumors.[31,93-95] Cylindrical nanoparticles ($d = 200$ nm and $h = 200$ nm) were covalently conjugated with engineered heptameric ligands (provided by Professor Rihe Liu from the UNC Eshelman School of Pharmacy) or

nonspecific control IgG. Targeted nanoparticles were incubated with A431 (epidermoid carcinoma) and SKOV3 (human ovarian adenocarcinoma) cells for 4 h at 37 °C. As seen in Figure 2.32, over 90% of A431 cells specifically internalized NP-7mer because of the high expression level of the HER1 receptor. However, NP-7mer did not exhibit significant cellular uptake in SKOV3 cells because of minimal expression of the receptor. For NP-IgG, there was low uptake in both cell lines as a result of the nonspecific ligand and negative surface charge.
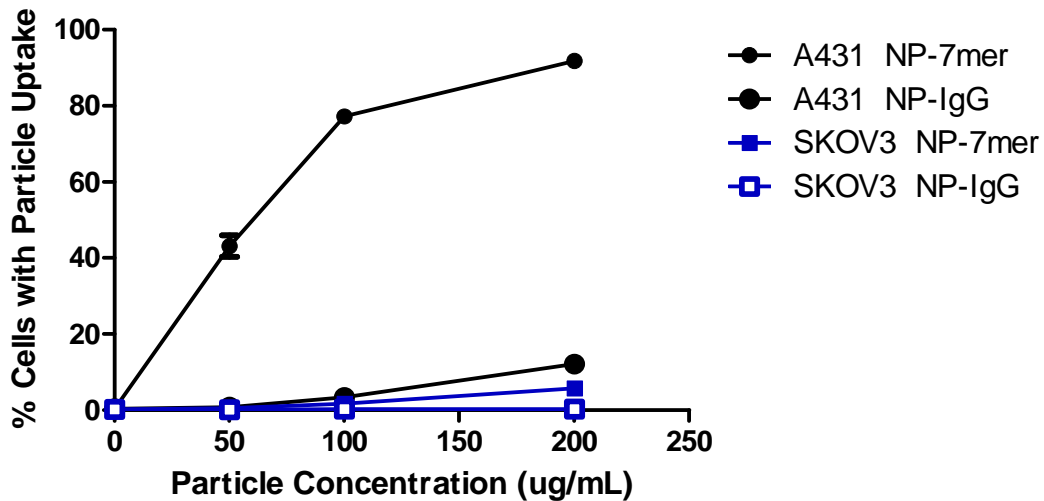


**Figure 2.32** Cellular internalization of cylindrical nanoparticles targeted with heptameric ligands for the HER1 receptor or IgG in A431 and SKOV3 cells.

Selective internalization of NP-7mer was also observed by confocal microscopy (Figure 2.33). NP-7mer, labeled with fluorescein, were prevalent throughout A431 cells as the nanoparticles bound to the HER1 receptor and were presumably internalized through receptor-mediated endocytosis. Conversely, NP-IgG were minimally internalized.
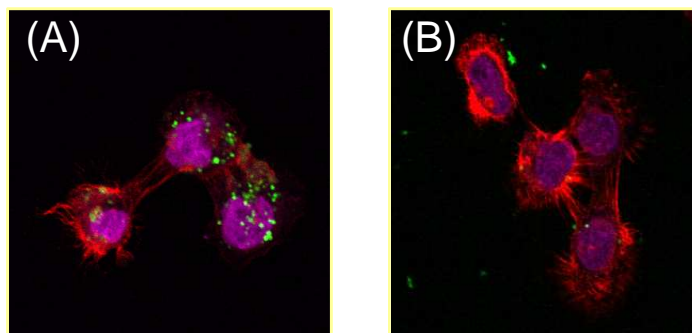
**Figure 2.33** Confocal microscopy images of (A) HER1 NP-7mer (green) and (B) NP-IgG in A431 cells.

These promising preliminary *in vitro* results from targeting with heptameric ligands for the HER1 receptor demonstrate the versatility of PRINT nanoparticles to be designed and fabricated to accommodate specific targets and diseases. Further investigation into HER1 targeting is necessary to confirm the target specificity of the nanoparticles, such as competition with free ligand as well as comparison to the approved monoclonal antibody against HER1, Erbitux (cetuximab). Furthermore, the multivalency of these nanoparticles may allow for the presence of various targeting agents (i.e., HER2 heptameric ligand, Herceptin, antibodies against the FR or TfR) on the nanoparticle surface to enhance target specificity for drug delivery, or therapeutic agents, such as chemotherapeutic drugs, can be conjugated to the nanoparticle surface while maintaining high specificity for tumor cells. Additional research is required to determine the potential of these nanoparticles as improved targeted drug delivery agents.

## 2.4 References

(1)     Peer, D.; Karp, J. M.; Hong, S.; Farokhzad, O. C.; Margalit, R.; Langer, R. *Nat Nano* **2007**, *2*, 751-760.

(2)     Gu, F. X.; Karnik, R.; Wang, A. Z.; Alexis, F.; Levy-Nissenbaum, E.; Hong, S.; Langer, R. S.; Farokhzad, O. C. *Nano Today* **2007**, *2*, 14-21.

(3)     Sinha, R.; Kim, G. J.; Nie, S.; Shin, D. M. *Molecular Cancer Therapeutics* **2006**, *5*, 1909-1917.

(4)     Maeda, H.; Wu, J.; Sawa, T.; Matsumura, Y.; Hori, K. *J Controlled Release* **2000**, *65*, 271-284.

(5)     Yuan, F.; Dellian, M.; Fukumura, D.; Leunig, M.; Berk, D. A.; Torchilin, V. P.; Jain, R. K. *Cancer Res* **1995**, *55*, 3752-3756.

(6)     Davis, M. E.; Chen, Z.; Shin, D. M. *Nat Rev Drug Discov* **2008**, *7*, 771-782.

(7)     Gabizon, A.; Tzemach, D.; Mak, L.; Bronstein, M.; Horowitz, A. T. *J Drug Target* **2002**, *10*, 539-548.

(8)     Gabizon, A.; Shmeeda, H.; Barenholz, Y. *Clin Pharmacokinet* **2003**, *42*, 419-436.

(9)     Nobs, L.; Buchegger, F.; Gurny, R.; Allémann, E. *J Pharm Sci* **2004**, *93*, 1980-1992.

(10)    Byrne, J. D.; Betancourt, T.; Brannon-Peppas, L. *Advanced Drug Delivery Reviews* **2008**, *60*, 1615-1626.

(11)    Adams, G. P.; Weiner, L. M. *Nat Biotech* **2005**, *23*, 1147-1157.

(12)    Miller, K.; Wang, M.; Gralow, J.; Dickler, M.; Cobleigh, M.; Perez, E. A.; Shenkier, T.; Cella, D.; Davidson, N. E. *N Engl J Med* **2007**, *357*, 2666-2676.

(13)    Romond, E. H.; Perez, E. A.; Bryant, J.; Suman, V. J.; Geyer, C. E.; Davidson, N. E.; Tan-Chiu, E.; Martino, S.; Paik, S.; Kaufman, P. A.; Swain, S. M.; Pisansky, T. M.; Fehrenbacher, L.; Kutteh, L. A.; Vogel, V. G.; Visscher, D. W.; Yothers, G.; Jenkins, R. B.; Brown, A. M.; Dakhil, S. R.; Mamounas, E. P.; Lingle, W. L.; Klein, P. M.; Ingle, J. N.; Wolmark, N. *N Engl J Med* **2005**, *353*, 1673-1684.

(14)    Coiffier, B.; Lepage, E.; Briàˉre, J.; Herbrecht, R.; Tilly, H.; Bouabdallah, R.; Morel, P.; Van Den Neste, E.; Salles, G.; Gaulard, P.; Reyes, F.; Lederlin, P.; Gisselbrecht, C. *N Engl J Med* **2002**, *346*, 235-242.

(15)    Cunningham, D.; Humblet, Y.; Siena, S.; Khayat, D.; Bleiberg, H.; Santoro, A.; Bets, D.; Mueser, M.; Harstrick, A.; Verslype, C.; Chau, I.; Van Cutsem, E. *N Engl J Med* **2004**, *351*, 337-345.

(16)    Carter, P. *Nat Rev Cancer* **2001**, *1*, 118-129.

(17)    Hudson, P. J.; Souriau, C. *Nat Med* **2003**, *9*, 129-134.

(18)    Farokhzad, O. C.; Karp, J. M.; Langer, R. *Expert Opinion on Drug Delivery* **2006**, *3*, 311-324.

(19)    Wilson, D. S.; Szostak, J. W. *Annu Rev Biochem* **1999**, *68*, 611-647.

(20)    White, R. R.; Sullenger, B. A.; Rusconi, C. P. *The Journal of Clinical Investigation* **2000**, *106*, 929-934.

(21)    Dhar, S.; Gu, F. X.; Langer, R.; Farokhzad, O. C.; Lippard, S. J. *Proceedings of the National Academy of Sciences* **2008**, *105*, 17356-17361.

(22)    Farokhzad, O. C.; Cheng, J.; Teply, B. A.; Sherifi, I.; Jon, S.; Kantoff, P. W.; Richie, J. P.; Langer, R. *Proceedings of the National Academy of Sciences* **2006**, *103*, 6315-6320.

(23)    Krag, D. N.; Shukla, G. S.; Shen, G.-P.; Pero, S.; Ashikaga, T.; Fuller, S.; Weaver, D. L.; Burdette-Radoux, S.; Thomas, C. *Cancer Res* **2006**, *66*, 7724-7733.

(24)    Shukla, G. S.; Krag, D. N. *J Drug Target* **2010**, *18*, 115-124.

(25)    Schiffelers, R. M.; Ansari, A.; Xu, J.; Zhou, Q.; Tang, Q.; Storm, G.; Molema, G.; Lu, P. Y.; Scaria, P. V.; Woodle, M. C. *Nucleic Acids Res* **2004**, *32*, e149.

(26)    Burke, P. A.; DeNardo, S. J.; Miers, L. A.; Lamborn, K. R.; Matzku, S.; DeNardo, G. L. *Cancer Res* **2002**, *62*, 4263-4272.

(27)    Bibby, D. C.; Talmadge, J. E.; Dalal, M. K.; Kurz, S. G.; Chytil, K. M.; Barry, S. E.; Shand, D. G.; Steiert, M. *Int J Pharm* **2005**, *293*, 281-290.

(28)    Eskens, F. A. L. M.; Dumez, H.; Hoekstra, R.; Perschl, A.; Brindley, C.; Böttcher, S.; Wynendaele, W.; Drevs, J.; Verweij, J.; van Oosterom, A. T. *Eur J Cancer* **2003**, *39*, 917-926.

(29)    Reardon, D. A.; Fink, K. L.; Mikkelsen, T.; Cloughesy, T. F.; O'Neill, A.; Plotkin, S.; Glantz, M.; Ravin, P.; Raizer, J. J.; Rich, K. M.; Schiff, D.; Shapiro, W. R.; Burdette-Radoux, S.; Dropcho, E. J.; Wittemer, S. M.; Nippgen, J.; Picard, M.; Nabors, L. B. *J Clin Oncol* **2008**, *26*, 5610-5617.

(30)    Smith, J. W. *Current Opinion in Investigational Drugs* **2003**, *4*, 741 - 745.

(31)     Nicholson, R. I.; Gee, J. M. W.; Harper, M. E. *Eur J Cancer* **2001**, *37, Supplement 4*, 9-15.

(32)     Lu, Y.; Low, P. S. *J Controlled Release* **2003**, *91*, 17-29.

(33)     Daniels, T. R.; Delgado, T.; Rodriguez, J. A.; Helguera, G.; Penichet, M. L. *Clin Immunol* **2006**, *121*, 144-158.

(34)     Bhirde, A. A.; Patel, V.; Gavard, J.; Zhang, G.; Sousa, A. A.; Masedunskas, A.; Leapman, R. D.; Weigert, R.; Gutkind, J. S.; Rusling, J. F. *ACS Nano* **2009**, *3*, 307-316.

(35)     Tseng, C.-L.; Wang, T.-W.; Dong, G.-C.; Yueh-Hsiu Wu, S.; Young, T.-H.; Shieh, M.-J.; Lou, P.-J.; Lin, F.-H. *Biomaterials* **2007**, *28*, 3996-4005.

(36)     Bartlett, D. W.; Su, H.; Hildebrandt, I. J.; Weber, W. A.; Davis, M. E. *Proceedings of the National Academy of Sciences* **2007**, *104*, 15549-15554.

(37)     Pun, S. H.; Tack, F.; Bellocq, N. C.; Cheng, J.; Grubbs, B. H.; Jensen, G. S.; Davis, M. E.; Brewster, M.; Janicot, M.; Janssens, B.; Floren, W.; Bakker, A. *Cancer Biology & Therapy* **2004**, *3*, 641-650.

(38)     Gabizon, A.; Shmeeda, H.; Horowitz, A. T.; Zalipsky, S. *Advanced Drug Delivery Reviews* **2004**, *56*, 1177-1192.

(39)     Oyewumi, M. O.; Yokel, R. A.; Jay, M.; Coakley, T.; Mumper, R. J. *Journal of Controlled Release* **2004**, *95*, 613-626.

(40)     Liu, Y.; Li, K.; Pan, J.; Liu, B.; Feng, S.-S. *Biomaterials* **2010**, *31*, 330-338.

(41)     Antony, A. C. *Annu Rev Nutr* **1996**, *16*, 501-521.

(42)     Sudimack, J.; Lee, R. J. *Advanced Drug Delivery Reviews* **2000**, *41*, 147-162.

(43)     Hilgenbrink, A. R.; Low, P. S. *J Pharm Sci* **2005**, *94*, 2135-2146.

(44)     Hartmann, L. C.; Keeney, G. L.; Lingle, W. L.; Christianson, T. J. H.; Varghese, B.; Hillman, D.; Oberg, A. L.; Low, P. S. *Int J Cancer* **2007**, *121*, 938-942.

(45)     Toffoli, G.; Cernigoi, C.; Russo, A.; Gallo, A.; Bagnoli, M.; Boiocchi, M. *Int J Cancer* **1997**, *74*, 193-198.

(46)     Weitman, S. D.; Lark, R. H.; Coney, L. R.; Fort, D. W.; Frasca, V.; Zurawski, V. R.; Kamen, B. A. *Cancer Res* **1992**, *52*, 3396-3401.

(47)     Kamen, B. A.; Capdevila, A. *Proceedings of the National Academy of Sciences* **1986**, *83*, 5983-5987.

(48)     Antony, A. C. *Blood* **1992**, *79*, 2807-20.

(49)   Lu, Y.; Low, P. S. *Advanced Drug Delivery Reviews* **2002**, *54*, 675-693.

(50)   Yoo, H. S.; Park, T. G. *J Controlled Release* **2004**, *100*, 247-256.

(51)   Low, P. S.; Henne, W. A.; Doorneweerd, D. D. *Accounts of Chemical Research* **2007**, *41*, 120-129.

(52)   Enlow, E. M.; Luft, J. C.; Napier, M. E.; DeSimone, J. M. *Nano Letters* **2011**, *11*, 808-813.

(53)   Gratton, S. E. A.; Ropp, P. A.; Pohlhaus, P. D.; Luft, J. C.; Madden, V. J.; Napier, M. E.; DeSimone, J. M. *Proceedings of the National Academy of Sciences* **2008**, *105*, 11613-11618.

(54)   Kelly, J. Y.; DeSimone, J. M. *J Am Chem Soc* **2008**, *130*, 5438-5439.

(55)   Merkel, T. J.; Jones, S. W.; Herlihy, K. P.; Kersey, F. R.; Shields, A. R.; Napier, M.; Luft, J. C.; Wu, H.; Zamboni, W. C.; Wang, A. Z.; Bear, J. E.; DeSimone, J. M. *Proceedings of the National Academy of Sciences* **2010**.

(56)   Parrott, M. C.; Finniss, M.; Luft, J. C.; Pandya, A.; Napier, M. E.; DeSimone, J. M. **2011**.

(57)   Parrott, M. C.; Luft, J. C.; Byrne, J. D.; Fain, J. H.; Napier, M. E.; DeSimone, J. M. *J Am Chem Soc* **2010**, *132*, 17928-17932.

(58)   Rolland, J. P.; Maynor, B. W.; Euliss, L. E.; Exner, A. E.; Denison, G. M.; DeSimone, J. M. *J Am Chem Soc* **2005**, *127*, 10096-10100.

(59)   Wang, J.; Tian, S.; Petros, R. A.; Napier, M. E.; DeSimone, J. M. *J Am Chem Soc* **2010**, *132*, 11306-11313.

(60)   Zhang, H.; et al. *New Journal of Physics* **2009**, *11*, 075018.

(61)   Harush-Frenkel, O.; Debotton, N.; Benita, S.; Altschuler, Y. *Biochem Biophys Res Commun* **2007**, *353*, 26-32.

(62)   Miller, C. R.; Bondurant, B.; McLean, S. D.; McGovern, K. A.; O'Brien, D. F. *Biochemistry (Mosc)* **1998**, *37*, 12875-12883.

(63)   Zauner, W.; Ogris, M.; Wagner, E. *Advanced Drug Delivery Reviews* **1998**, *30*, 97-113.

(64)   Fattorossi; A; Nisini; R; Pizzolo; J, G.; D'Amelio; R *Cytometry* **1989**, *10*, 320-325.

(65)   Gratton, S.; Napier, M.; Ropp, P.; Tian, S.; DeSimone, J. *Pharm Res* **2008**, *25*, 2845-2852.

(66)  Ross, J. S.; Fletcher, J. A.; Linette, G. P.; Stec, J.; Clark, E.; Ayers, M.; Symmans, W. F.; Pusztai, L.; Bloom, K. J. *Oncologist* **2003**, *8*, 307-325.

(67)  Slamon, D. J.; Clark, G. M.; Wong, S. G.; Levin, W. J.; Ullrich, A.; McGuire, W. L. *Science* **1987**, *235*, 177-182.

(68)  Slamon, D. J.; Godolphin, W.; Jones, L. A.; Holt, J. A.; Wong, S. G.; Keith, D. E.; Levin, W. J.; Stuart, S. G.; Udove, J.; Ullrich, A.; et, a. *Science* **1989**, *244*, 707-712.

(69)  Natali, P. G.; Nicotra, M. R.; Bigotti, A.; Venturo, I.; Slamon, D. J.; Fendly, B. M.; Ullrich, A. *Int J Cancer* **1990**, *45*, 457-461.

(70)  Tandon, A. K.; Clark, G. M.; Chamness, G. C.; Ullrich, A.; McGuire, W. L. *J Clin Oncol* **1989**, *7*, 1120-8.

(71)  Greenberg, P. A.; Hortobagyi, G. N.; Smith, T. L.; Ziegler, L. D.; Frye, D. K.; Buzdar, A. U. *J Clin Oncol* **1996**, *14*, 2197-205.

(72)  Slamon, D. J.; Leyland-Jones, B.; Shak, S.; Fuchs, H.; Paton, V.; Bajamonde, A.; Fleming, T.; Eiermann, W.; Wolter, J.; Pegram, M.; Baselga, J.; Norton, L. *New England Journal of Medicine* **2001**, *344*, 783-792.

(73)  Shukla, R.; Thomas, T. P.; Peters, J. L.; Desai, A. M.; Kukowska-Latallo, J.; Patri, A. K.; Kotlyar, A.; Baker, J. R. *Bioconjug Chem* **2006**, *17*, 1109-1115.

(74)  Steinhauser, I.; SpÃ¤nkuch, B.; Strebhardt, K.; Langer, K. *Biomaterials* **2006**, *27*, 4975-4983.

(75)  Cirstoiu-Hapca, A.; Bossy-Nobs, L.; Buchegger, F.; Gurny, R.; Delie, F. *Int J Pharm* **2007**, *331*, 190-196.

(76)  Wartlick, H.; Michaelis, K.; Balthasar, S.; Strebhardt, K.; Kreuter, J. r.; Langer, K. *J Drug Target* **2004**, *12*, 461-471.

(77)  Lee, A. L. Z.; Wang, Y.; Cheng, H. Y.; Pervaiz, S.; Yang, Y. Y. *Biomaterials* **2009**, *30*, 919-927.

(78)  Shukla, R.; Thomas, T. P.; Desai, A. M.; Kotlyar, A.; Park, S. J.; James R. Baker, J. *Nanotechnology* **2008**, *19*, 295102.

(79)  Anhorn, M. G.; Wagner, S.; Kreuter, J. r.; Langer, K.; von Briesen, H. *Bioconjug Chem* **2008**, *19*, 2321-2331.

(80)  Pasut, G.; Canal, F.; Dalla Via, L.; Arpicco, S.; Veronese, F. M.; Schiavon, O. *J Controlled Release* **2008**, *127*, 239-248.

(81)     Friedman, L. M.; Rinon, A.; Schechter, B.; Lyass, L.; Lavi, S.; Bacus, S. S.; Sela, M.; Yarden, Y. *Proc Natl Acad Sci U S A* **2005**, *102*, 1915-1920.

(82)     Zhu, W.; Okollie, B.; Artemov, D. *Cancer Biology & Therapy* **2007**, *6*, 1960-1966.

(83)     Guillemard, V.; Nedev, H. N.; Berezov, A.; Murali, R.; Saragovi, H. U. *DNA Cell Biol* **2005**, *24*, 351-358.

(84)     Hommelgaard, A. M.; Lerdrup, M.; van Deurs, B. *Mol Biol Cell* **2004**, *15*, 1557-1567.

(85)     Longva, K. E.; Pedersen, N. M.; Haslekås, C.; Stang, E.; Madshus, I. H. *Int J Cancer* **2005**, *116*, 359-367.

(86)     Ruenraroengsak, P.; Cook, J. M.; Florence, A. T. *J Controlled Release* **2010**, *141*, 265-276.

(87)     Alexis, F.; Pridgen, E.; Molnar, L. K.; Farokhzad, O. C. *Molecular Pharmaceutics* **2008**, *5*, 505-515.

(88)     Christian, D. A.; Cai, S.; Garbuzenko, O. B.; Harada, T.; Zajac, A. L.; Minko, T.; Discher, D. E. *Molecular Pharmaceutics* **2009**, *6*, 1343-1352.

(89)     Geng, Y.; Dalhaimer, P.; Cai, S.; Tsai, R.; Tewari, M.; Minko, T.; Discher, D. E. *Nature Nanotechnology* **2007**, *2*, 249-255.

(90)     Sharma, G.; Valenta, D. T.; Altman, Y.; Harvey, S.; Xie, H.; Mitragotri, S.; Smith, J. W. *J Controlled Release* **2010**, *147*, 408-412.

(91)     Champion, J.; Mitragotri, S. *Pharm Res* **2009**, *26*, 244-249.

(92)     Champion, J.; Walker, A.; Mitragotri, S. *Pharm Res* **2008**, *25*, 1815-1821.

(93)     Yarden, Y. *Eur J Cancer* **2001**, *37*, 3-8.

(94)     Cerra, M.; Cecco, L.; Montella, M.; Tuccillo, F.; Bonelli, P.; Botti, G. *The International journal of biological markers* **1995**, *10*, 136-42.

(95)     Seshadri, R.; McLeay, W. R. B.; Horsfall, D. J.; McCaul, K. *Int J Cancer* **1996**, *69*, 23-27.

# CHAPTER 3

## ENGINEERED TARGETED PRINT® NANOPARTICLES FOR DRUG DELIVERY

## 3.1  Degradable Silyl Ether Nanoparticles
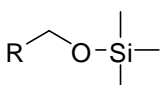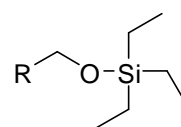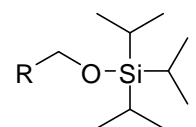
### 3.1.1  Introduction

Numerous advancements have emerged in the development of engineered drug delivery nanocarriers for more effective cancer therapeutics.  Improvements include stimuli-responsive drug delivery agents that achieve better targeted efficiency and treatment efficacy of the chemotherapeutic.[1]  Researchers have developed sophisticated systems that undergo cleavage or degradation catalyzed by biological triggers such as temperature and pH.[2-5]  In particular, hydrazones,[6-8] trityls,[9] aconityls,[10,11] vinyl ethers,[12,13] polyketals,[14,15] acetals,[16] poly(ortho esters),[17] and thiopropionates[18] exploit a pH gradient to trigger degradation.  However, these materials are limited by poor tunability, toxic degradation prodructs, or complex syntheses.

Thus, we reported the development of silyl ether-based biomaterials that are sensitive to pH.[19]  Silyl ethers are commonly employed as protecting groups in organic chemistry because the rate of deprotection can be tuned by varying the substituents on the silicon atom.[20]  Less hindered substituents create silyl ethers that are more susceptible to

acid catalyzed hydrolysis.  For instance, the relative stabilities of trimethyl silyl ether (TMS), triethyl silyl ether (TES), and triisopropyl silyl ether (TIS) to acid catalyzed hydrolysis are 1, 64, and 700,000, respectively (Table 3.1).[20]

**Table 3.1**  Chemical structures of silyl ethers and their relative stabilities to acid catalyzed hydrolysis.

|  | Trimethyl silyl ether (TMS) | Triethyl silyl ether (TES) | Triisopropyl silyl ether (TIS) |
|---|---|---|---|
| Chemical Structure | R—O–Si— | R—O–Si | R—O–Si |
| Relative Stability | 1 | 64 | 700,000 |

This example shows that the rate of deprotection can range over multiple orders of magnitude by merely modifying the substituents on the silicon atom.  More specifically, bifunctional silyl ethers, which consist of a C—O—Si(R)$_2$—O—C moiety, are commonly used for the protection of 1,2- and 1,3-diols.[21-23]  Typically, less hindered substituents, such as dimethyl, diethyl, and diisopropyl, are not utilized because they are excessively sensitive to acid catalyzed hydrolysis and thus, are not appropriate as protecting groups.  However, these same properties can be favorable for acid sensitive biomaterials.  As such, silyl ether chemistry was adapted to create stimuli-responsive materials for biomedical purposes.

Bifunctional silyl ether crosslinkers (Figure 3.1) were easily synthesized in one step from commercially available reagents to generate a collection of crosslinkers with varied substituents on the silicon atom.[19]  Crosslinkers were named according to their

substituents: dimethyl silyl ether (DMS), diethyl silyl ether (DES), diisopropyl silyl ether (DIS), and di-*tert*-butyl silyl ether (DTS).
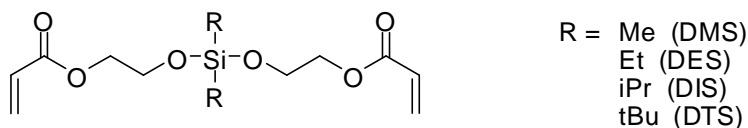


**Figure 3.1**  Generic chemical structure of silyl ether crosslinker.

These materials were used to fabricate microparticles by the PRINT process, and the particles were investigated for drug delivery purposes.  When 5 µm cubic particles were studied under varying pHs, it was found that all particles preferentially degraded under the acidic pH 5.0 and more slowly under the neutral pH 7.4.  This indicates that the particles, fabricated from the acid-sensitive crosslinkers, are more susceptible to degradation under endosomal conditions rather than physiological environments. Additionally, particles fabricated from the DMS crosslinker displayed an accelerated rate of degradation in just hours, while particles fabricated from the DES crosslinker degraded on the order of days.  Particles fabricated from the DIS crosslinker exhibited an even slower rate of degradation over months.  This demonstrates that the rate of degradation was effectively modulated by altering the substituent on the silicon atom of the silyl ether crosslinker.

Furthermore, the intracellular degradation of 3 µm hexnut particles prepared from the DMS and DTS crosslinkers was investigated with HeLa (human cervical cancer) cells. Particles prepared from the acid-sensitive DMS crosslinker degraded rapidly under intracellular conditions, initially swelling and deforming, and then fragmenting before

complete degradation, as observed by the growing widespread green fluorescence within the cells by confocal microscopy (Figure 3.2). In contrast, particles fabricated from the nondegrading DTS crosslinker exhibited no change under the same intracellular environment. This illustrates the potential of the crosslinkers as biomaterials for drug delivery carriers because the materials degrade under intracellular conditions and thus, may deliver chemotherapeutics more effectively within cancer cells.
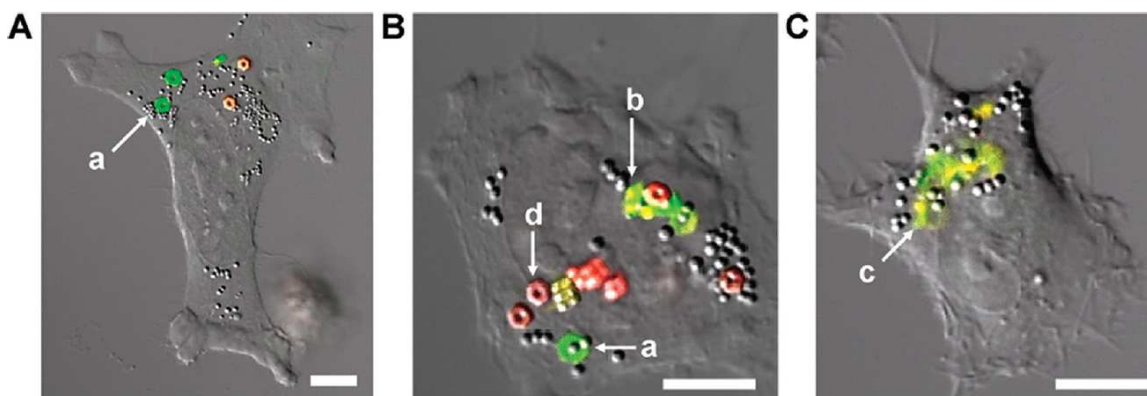


**Figure 3.2** Confocal imcroscopy images of the phases of rapid degradation of DMS particles (green): (a) swelling, (b) fragmentation, and (c) complete degradation. DTS particles (red) exhibited no change intracellularly (d). Scale bars = 10 µm.[19]

Based on the promising results of these bifunctional silyl ether crosslinkers, additional crosslinkers incorporating PEG (poly(ethylene glycol)) were synthesized. PEG is a biocompatible material and imparts hydrophilicity. This new class of bifunctional silyl ether crosslinkers was studied as biomaterials for improved drug delivery agents. Specifically, the $PEG_8DES$ ($PEG_8$ diethyl silyl ether) and $PEG_8DTS$ ($PEG_8$ di-*tert*-butyl silyl ether) crosslinkers were investigated (Figure 3.3).
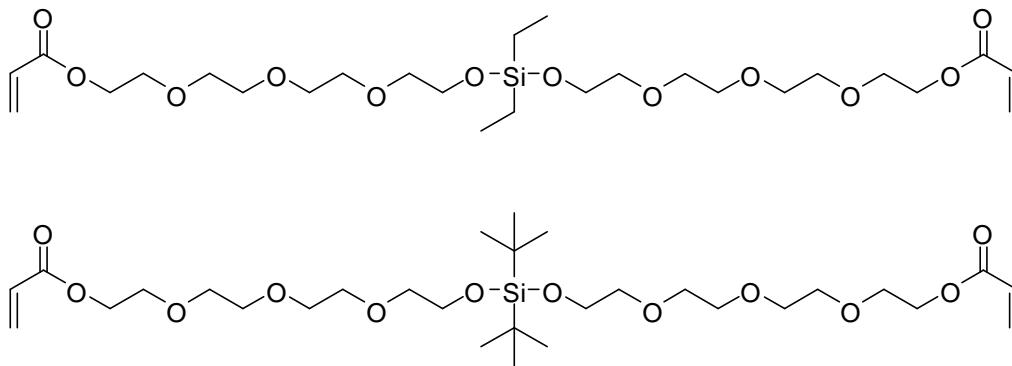
**Figure 3.3** Chemical structures of the PEG$_8$DES (top) and PEG$_8$DTS (bottom) silyl ether crosslinkers.

These materials were investigated with the chemotherapeutic agent docetaxel, which is the active component in Taxotere. Taxotere is a versatile therapeutic drug approved for the treatment of a variety of cancers, including breast, non-small cell lung, prostate, gastric, and head and neck.[24] By combining the acid-sensitive characteristics of the silyl ether-based crosslinkers along with active targeting ligands, we aimed to develop improved nanoparticulate cancer therapeutics that specifically treat diseased cells by intracellular degradation of the drug carrier and subsequent release of the drug docetaxel.

### 3.1.2 Experimental

### 3.1.2.1 Chemicals and Reagents

Biotinylated OKT9 and isotype control mouse IgG were purchased from eBioscience. Herceptin (Genentech) was purchased from the UNC Hospitals. UltraAvidin was purchased from Leinco Technologies. Biotin-poly(ethylene glycol)-

succinimidyl carboxymethyl ester (3400 g/mol for PEG; NHS-PEG$_{3400}$-biotin) was purchased from Laysan Bio. Anhydrous dimethylformamide (DMF) and pyridine were purchased from Acros. Acetic anhydride was purchased from Fisher Scientific. All other reagents were purchased from Sigma Aldrich.

### 3.1.2.2 Cells and Culture

Ramos, BT474, HeLa, and H460 cells were from UNC LCCC Tissue Culture Facility. Ramos and H460 cells were maintained in RPMI 1640 with 10% FBS. BT474 cells were maintained in RPMI 1640 with 10% FBS, 1.5 g/L sodium bicarbonate, 4.5 g/L glucose, 10 mM HEPES, 1.0 mM sodium pyruvate, and 0.02 mg/mL human insulin. HeLa cells were maintained in MEM with 10% FBS. All media and supplements were from Gibco.

### 3.1.2.3 Fabrication of PRINT Nanoparticles

Cylindrical nanoparticles ($d$ = 200 nm and $h$ = 200 nm) were fabricated using the PRINT technique. Nanoparticles were prepared from a starting monomer solution (5% wt/vol in isopropanol) consisting of 87 wt % of bifunctional silyl ether PEG$_8$DES or PEG$_8$DTS crosslinker, 10 wt % of 2-aminoethyl methacrylate hydrochloride, 2 wt % of fluorescein $o$-acrylate, and 1 wt % of 2,2-diethoxyacetophenone. A monomer film was cast upon a sheet of poly(ethylene terephthalate) (PET) by spreading 90 µL of monomer solution with a mayer rod (#2, R.D. Specialties), and it was dried with cool air using a heat gun to remove the solvent isopropanol. The monomer film and humidified patterned mold, provided by Liquidia Technologies, were laminated together under pressure (40

PSI) and then delaminated, by gently splitting the mold and PET, to yield a mold with filled cavities. The filled mold was laminated with a fresh sheet of PET and then exposed to UV irradiation ($\lambda = 365$ nm, power 90 mW/cm$^2$) for 4 min under a nitrogen purge. The mold was removed, leaving nanoparticles transferred on the sheet of PET. This was due to the higher surface energy of the PET. Cold Dulbecco's phosphate buffered saline (DPBS; 400 µL) was placed on the PET, and nanoparticles were collected mechanically with a cell scraper. The harvested particles were washed twice with cold DPBS by centrifugation.

### 3.1.2.4 Fabrication of Docetaxel Encapsulated PRINT Nanoparticles

The same fabrication procedure as described for blank nanoparticles was followed. The nanoparticles were prepared from a starting monomer solution (5% wt/vol in isopropanol) consisting of 86 wt % of bifunctional silyl ether PEG$_8$DES or PEG$_8$DTS crosslinker, 10 wt % of 2-aminoethyl methacrylate hydrochloride, 2 wt % of fluorescein *o*-acrylate, 1 wt % of 2,2-diethoxyacetophenone, and either 1 wt % of docetaxel.

### 3.1.2.5 Herceptin/OKT9/IgG Conjugation to PRINT Nanoparticles

Nanoparticles were conjugated with Herceptin, OKT9, or IgG through a biotin-avidin linkage. Nanoparticles in anhydrous DMF (500 µL at 2 mg/mL) were reacted with 5 mg of NHS-PEG$_{3400}$-biotin in the presence of 10 µL anhydrous of pyridine; the nanoparticle dispersion was shaken on a vortex for 2 h. Acetic anhydride (10 µL) was added to the dispersion, which was shaken for 10 min, to quench unreacted amines on the

nanoparticle surface. The nanoparticles were washed twice with cold DPBS by centrifugation. UltraAvidin (50 µL, 10 mg/mL) was added to the nanoparticles in DPBS (2 mg/mL). The dispersion was shaken for 1 h. The nanoparticles were washed twice with cold DPBS by centrifugation. To target the nanoparticles, 50 µg of Herceptin, OKT9, or IgG was added to the nanoparticle dispersion and was shaken for 30 min at room temperature and then kept overnight at 4 °C. The nanoparticles were washed twice with cold DPBS by centrifugation and then resuspended in DPBS.

### 3.1.2.6  Physical Characterization of Nanoparticles

Scanning electron microscopy samples were prepared by pipetting 10 µL of nanoparticle solution onto a glass slide. Samples were dried and coated with 2 nm of gold palladium with a Cressington 108 auto sputter coater (Cressington Scientific Instruments). Samples were imaged with a scanning electron microscope (Hitachi S-4700). The size (dynamic light scattering, DLS) and charge ($\zeta$-potential) of the nanoparticles were determined for 20 µg/mL nanoparticle samples in a 1 mM potassium chloride solution with a Malvern Instruments Nano ZS.

### 3.1.2.7  Quantitative *In Vitro* Cellular Targeting

BT474, HeLa, and H460 cells were plated at 10,000 cells/well in a 96-well plate and allowed to adhere overnight at 37 °C and 5% $CO_2$. Ramos cells were used at 100,000 cells/well. Nanoparticles in OPTI-MEM were incubated with cells at 37 °C and 5% $CO_2$ for specified amounts of time and then removed. The cells were washed twice

with DPBS, trypsinized, and prepared for analysis by flow cytometry with a 0.2% trypan blue solution containing 10% FBS in DPBS. Samples were analyzed with a Dako CyAn flow cytometer.

### 3.1.2.8 Confocal Microscopy

BT474 cells were plated on cover slips in a 6-well plate ($5 \times 10^4$ cells/well) overnight at 37 °C and 5% $CO_2$. Cells were incubated with 50 µg/mL of nanoparticles in OPTI-MEM for 4 h at 37 °C. Cells were fixed, made permeable with 0.1% triton-X100 in PBS for 3 min, and incubated with Alexa Fluor 555 phalloidin (Invitrogen) for 1 h at room temperature without light. Cells were washed with DPBS, and cover slips were mounted onto glass slides with FluorSave Reagent (Calbiochem), and cells were imaged with a confocal laser scanning microscope (Olympus Fluoview FV500).

### 3.1.2.9 Cytotoxicity of Silyl Ether-Based Nanoparticles

BT474, HeLa, and H460 cells were plated at 5,000 cells/well in a 96-well plate and allowed to adhere overnight at 37 °C and 5% $CO_2$. Nanoparticles in complete media were incubated with cells at 37 °C and 5% $CO_2$ for 72 h and removed. Cell viability was determined using Promega CellTiter-Glo® Luminescent Cell Viability Assay according to the manufacturer's instructions. Bioluminescence was measured by a SpectraMax M5 plate reader (Molecular Devices).

### 3.1.3  Results and Discussion

### 3.1.3.1  Nanoparticle Fabrication and Conjugation with Herceptin/OKT9/IgG

The PRINT technology is a versatile technique for the fabrication of particles. Previously described,[19,25-32] it affords absolute control over particle size, shape, composition, and surface chemistry.  As such, the process was easily adapted for the fabrication of nanoparticles composed of novel crosslinkers consisting of bifunctional silyl ethers, $PEG_8$ diethyl silyl ether ($PEG_8DES$) and $PEG_8$ di-*tert*-butyl silyl ether ($PEG_8DTS$; Figure 3.3).  Cylindrical nanoparticles ($d$ = 200 nm and $h$ = 200 nm), comprised mostly of the novel silyl ether crosslinkers, were fabricated. $PEG_8DES$ served as an acid sensitive nanoparticle matrix, while $PEG_8DTS$ acted as the stable, nondegradable control.  In addition to the crosslinker, 2-aminoethyl methacrylate hydrochloride, fluorescein *o*-acrylate, and 2,2-diethyoxyacetophenone were included within the nanoparticles (Table 3.2).

**Table 3.2** Composition of bifunctional silyl ether-based nanoparticles.

| Monomers | Wt % |
| --- | --- |
| $PEG_8DES$ or $PEG_8DTS$ | 87 |
| 2-Aminoethyl methacrylate hydrochloride | 10 |
| Fluorescein *o*-acrylate | 2 |
| 2,2-Diethoxyacetophenone | 1 |

Amine functional handles for nanoparticle surface modification were incorporated into the nanoparticles through 2-aminoethyl methacrylate hydrochloride, while fluorescein *o*-acrylate provided a fluorescent label so that the nanoparticles could be visualized and tracked with cells *in vitro*. As seen in Figure 3.4, nanoparticles composed of the novel silyl ether crosslinkers were successfully fabricated.
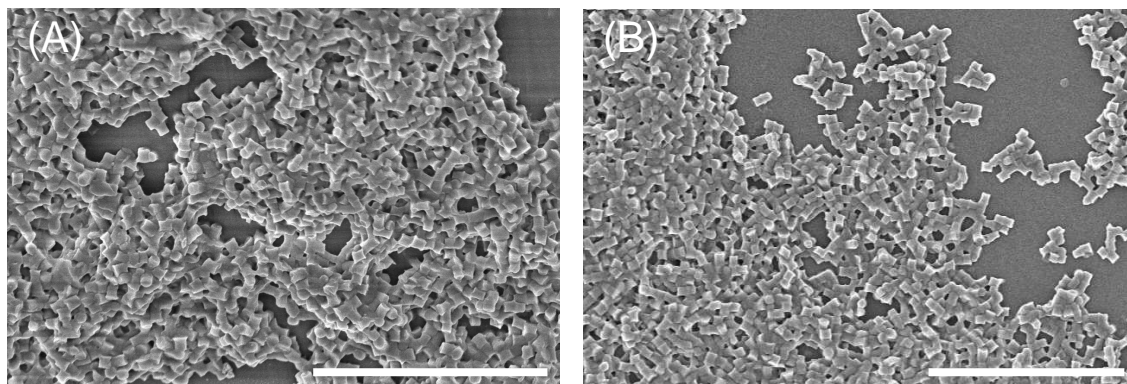


**Figure 3.4** SEMs of cylindrical 200 nm (A) PEG$_8$DES and (B) PEG$_8$DTS nanoparticles. Scale bar is 3 µm.

Both crosslinkers polymerized with co-monomers to form isolated cylindrical nanoparticles, demonstrating the versatility of the PRINT technology to fabricate particles composed of a desired material so as to elicit specific behaviors, properties, or traits in the particles.

Unmodified, pre-functionalized nanoparticles fabricated from the PEG$_8$DES and PEG$_8$DTS crosslinkers had a hydrodynamic diameter around 300 nm and a positive $\zeta$-potential of approximately +26 mV (Table 3.3). Amines from the monomer 2-aminoethyl methacrylate hydrochloride imparted the cationic nature of the pre-functionalized nanoparticles and were reacted with NHS-PEG$_{3400}$-biotin to functionalize

the nanoparticles for targeting as previously described.  In order to avoid nonspecific cellular uptake of positively charged particles, unreacted amines were quenched with acetic anhydride to ensure a negative $\zeta$-potential of -12.0 ± 0.2 mV and -14.5 ± 0.4 mV for nanoparticles prepared from the $PEG_8DES$ and $PEG_8DTS$ crosslinkers, respectively. After conversion to a negative charge, biotinylated nanoparticles were targeted with monoclonal antibodies through noncovalent biotin-avidin linkages.  Avidin was first coupled to the surface of the nanoparticles, followed by the targeting ligands Herceptin, OKT9, or IgG to yield Herceptin-targeted nanoparticles (NP-Herc), OKT9-targeted nanoparticles (NP-OKT), and IgG-targeted nanoparticles (NP-IgG), respectively.  Final targeted nanoparticles (NP-Herc, NP-OKT9, NP-IgG) maintained negative $\zeta$-potentials. Also, throughout the surface functionalization and targeting of these silyl ether-based nanoparticles, the size of the nanoparticles was maintained around ~300 nm.

**Table 3.3** Hydrodynamic diameters and zeta potentials of cylindrical 200 nm PEG$_8$DES and PEG$_8$DTS nanoparticles.

| Silyl Ether Crosslinker | Nanoparticle | Diameter (nm) | PDI | $\zeta$-Potential (mV) |
|---|---|---|---|---|
| PEG$_8$DES | Pre-functionalized | $311 \pm 16$ | 0.178 | $+25.6 \pm 0.3$ |
| | Biotinylated | $306 \pm 12$ | 0.155 | $-12.0 \pm 0.2$ |
| | NP-Herc | $299 \pm 4$ | 0.125 | $-7.1 \pm 0.7$ |
| | NP-OKT9 | $302 \pm 17$ | 0.083 | $-8.3 \pm 0.6$ |
| | NP-IgG | $298 \pm 10$ | 0.164 | $-6.3 \pm 0.3$ |
| PEG$_8$DTS | Pre-functionalized | $288 \pm 3$ | 0.086 | $+27.3 \pm 0.9$ |
| | Biotinylated | $300 \pm 1$ | 0.178 | $-14.5 \pm 0.4$ |
| | NP-Herc | $303 \pm 15$ | 0.133 | $-15.1 \pm 0.4$ |
| | NP-OKT9 | $294 \pm 3$ | 0.143 | $-14.3 \pm 0.9$ |
| | NP-IgG | $297 \pm 6$ | 0.163 | $-15.5 \pm 0.75$ |

### 3.1.3.2 Quantitative *In Vitro* Cellular Uptake

Nanoparticle uptake was investigated in BT474 (human breast cancer) and Ramos (human Burkitt's lymphoma) cells. BT474 cells display high expression of the HER2 receptor (human epidermal growth factor receptor 2), which is present in approximately 30% of breast cancers.[33,34] Both BT474 and Ramos cells overexpress the transferrin receptor (TfR).[31,35] The TfR is a prevalent protein amongst a variety of cancer cells because it is necessary for intracellular transport of iron, which is required for DNA synthesis and active proliferation.[36] Both the HER2 and TfR are highly amplified in cancerous cells relative to normal cells, and therefore, are appealing targets for cancer therapeutics.

Nanoparticles composed of the silyl ether crosslinker PEG$_8$DES were targeted with Herceptin and OKT9. Herceptin (trastuzumab) is a humanized monoclonal antibody

developed by Genentech that is approved as an immunotherapy with breast cancer patients.[37] It binds to the extracellular region of HER2 to inhibit tumor growth and thus, is a potential targeting ligand for therapies aimed at HER2-positive cancers.[38,39] OKT9 is a monoclonal antibody that binds with the TfR, and IgG is a nonspecific, control antibody. Both NP-Herc and NP-OKT9, in addition to NP-IgG and pre-functionalized nanoparticles, were incubated with BT474 cells at various concentrations (0-200 µg/mL) for 4 h at 37 °C. Samples were analyzed using a flow cytometry technique to quantify the percentage of cells with internalized particles.[40] Pre-functionalized nanoparticles internalized rapidly but indiscriminately into BT474 cells because of their positive surface charge. Over 95% of BT474 cells readily internalized $PEG_8DES$ pre-functionalized nanoparticles at all particle concentrations (Figure 3.5). Also, NP-Herc and NP-OKT9 exhibited nanoparticle uptake in a dose dependent manner with over 90% of BT474 cells having internalized nanoparticles because BT474 cells have amplified levels of both the HER2 and TfR. Uptake of control $PEG_8DES$ NP-IgG was much lower (<30%), owing to the negative ζ-potential of and nonspecific ligands on the nanoparticles. Through attachment of targeting ligands to the surface of silyl ether-based nanoparticles, specific internalization of NP-Herc and NP-OKT9 was observed despite the negative surface charge of the nanoparticles. Herceptin and OKT9 bound to the HER2 and TfR, respectively, to facilitate receptor-mediated endocytosis of the nanoparticles.
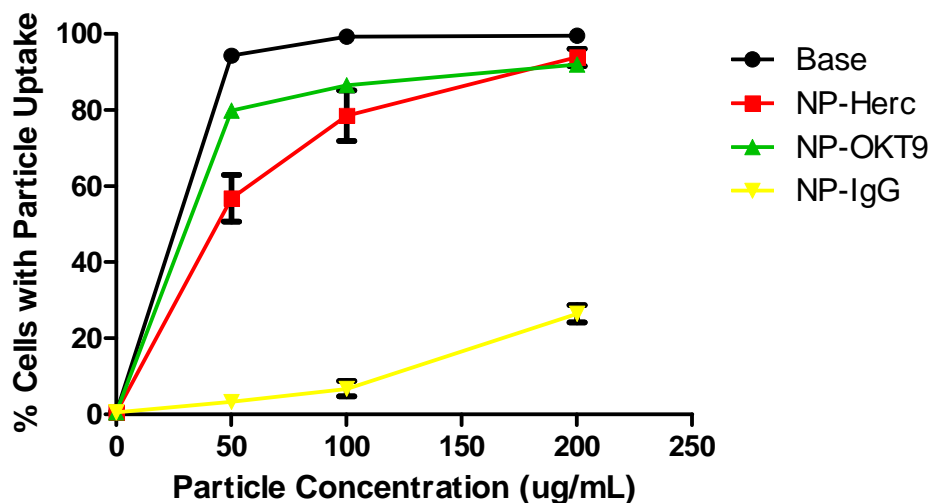
**Figure 3.5** Internaliztion of nanoparticles fabricated from the $PEG_8DES$ crosslinker in BT474 cells.

Additionally, silyl ether-based nanoparticles were functionalized with OKT9 to target the TfR expressed on Ramos cells. As seen in Figure 3.6, the positively-charged $PEG_8DES$ base nanoparticles internalized rapidly into the cells with over 95% of Ramos cells having associated nanoparticles. Approximately 90% of Ramos cells also internalized NP-OKT9 in a dose dependent manner, while control silyl ether-based NP-IgG bound minimally to the cells. NP-OKT9 bound to the TfR overexpressed in Ramos cells, inducing subsequent receptor-mediated endocytosis. This demonstrates selective targeting of NP-OKT9 relative to NP-IgG.
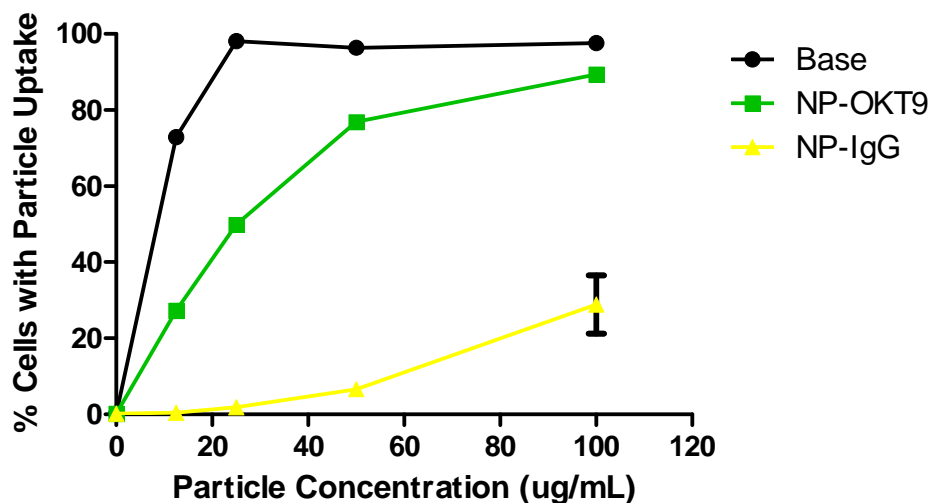
**Figure 3.6** Internalization of nanoparticles fabricated from the PEG$_8$DES crosslinker in Ramos cells.

In both BT474 breast cancer and Ramos Burkitt's lymphoma cell lines, nanoparticles, composed of the silyl ether crosslinker PEG$_8$DES, demonstrated *in vitro* uptake trends similar to PEG-based targeted nanoparticles. Silyl ether pre-functionalized nanoparticles were internalized into both cell lines quickly but nonspecifically and in a dose dependent fashion due to their positive ζ-potential, as was previously observed with PEG-based nanoparticles. Targeted nanoparticles, fabricated from the silyl ether crosslinker, selectively internalized into cells, analogous to PEG-based nanoparticles. Based on these results, silyl ether-based nanoparticles with surface properties similar to PEG-based nanoparticles exhibited comparable *in vitro* trends.

### 3.1.3.3  Confocal Microscopy

In addition to flow cytometry, targeting of silyl ether-based nanoparticles was visualized by confocal microscopy. Targeted and control nanoparticles fabricated from

the PEG$_8$DES crosslinker, fluorescently labeled through fluorescein *o*-acrylate, were incubated with BT474 breast cancer cells. Shown in Figure 3.7, nanoparticle internalization, seen in green, was observed with NP-Herc and NP-OKT9 but minimally with NP-IgG. This is indicative of the selective binding of NP-Herc to the HER2 receptor and of NP-OKT9 to the TfR, which induces receptor-mediated endocytosis. As was previously observed by flow cytometry, BT474 cells did not internalize an appreciable amount of NP-IgG as a result of the nonspecific ligands on the nanoparticles and the negative surface charge. Confocal micrscopy images corroborated the results determined by flow cytometry.
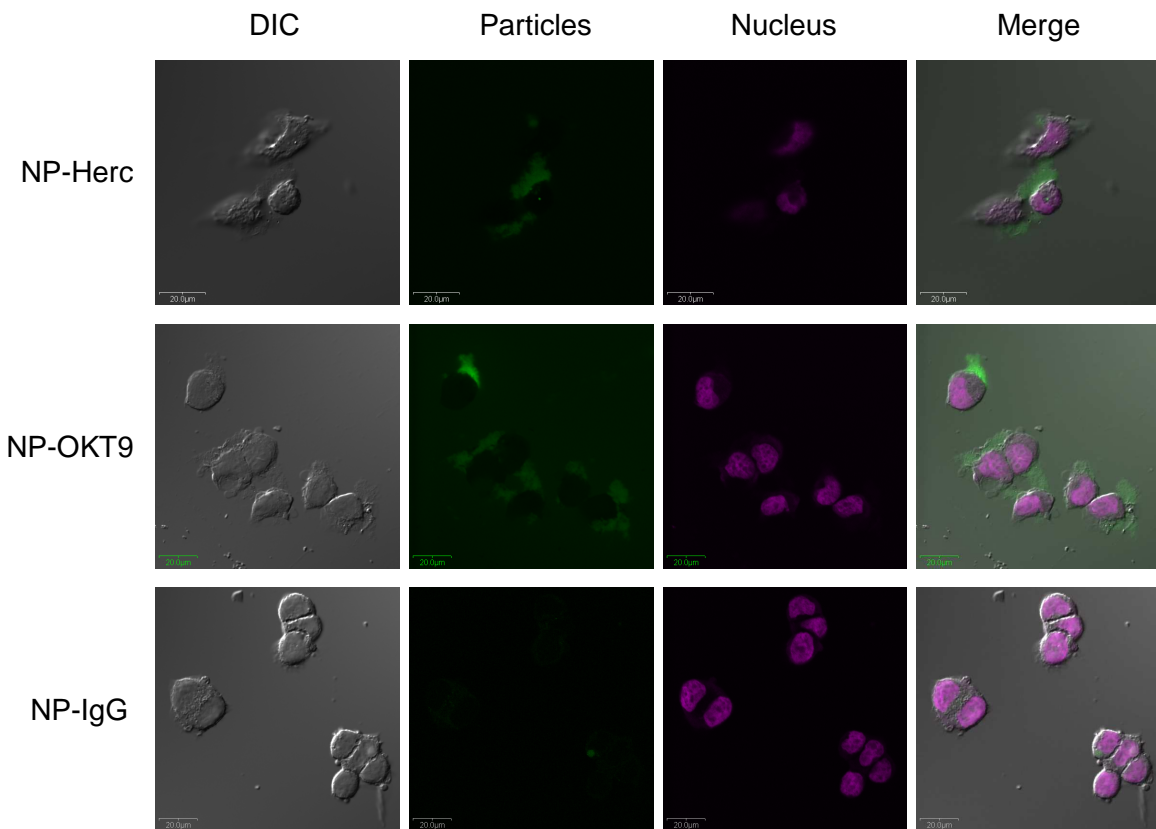


**Figure 3.7** Confocal microscopy images of specific internalization of nanoparticles (green), fabricated from the PEG$_8$DES crosslinker, in BT474 cells.

111

Furthermore, the observed green fluorescence from targeted silyl ether-based nanoparticles differed from that in previous images of PEG-based nanoparticles. Prior images of PEG-based nanoparticles consisted of prominent punctate areas of fluorescence from the fluorescein-labeled nanoparticles. Instead of distinct, spotted fluorescence, dispersed and diffuse fluorescence was noted from nanoparticles fabricated with the PEG$_8$DES crosslinker. This difference may be attributed to the intracellular degradation of the silyl ether-based nanoparticles. As demonstrated previously, microparticles composed of dimethyl silyl ether (DMS) degraded rapidly under intracellular conditions, observed as widespread fluorescence in the cell through confocal microscopy.[19] So the susceptibility of nanoparticles, fabricated from the PEG$_8$DES crosslinker, to acid-catalyzed hydrolysis may be detected by confocal microscopy. Active degradation of these nanoparticles stimulated by acidic intracellular conditions is a favorable property for nanocarriers whereby the therapeutic payload can be locally released at the site of disease.

### 3.1.3.5 Cytotoxicity of Blank Silyl Ether-Based Nanoparticles

To ensure the nontoxicity of this nanoparticulate drug delivery system developed from novel silyl ether biomaterials, cytotoxicity of silyl ether-based nanoparticles and their degradation products were investigated in BT474 (breast cancer), HeLa (human cervical adenocarcinoma), and H460 (human large cell lung carcinoma) cells. Ramos cells were not investigated because prior studies revealed that similar PEG-based nanoparticles, without any drugs and targeted with OKT9, were cytotoxic to Ramos cells

due to the multivalent nature of the nanoparticles.[31]  Pre-functionalized nanoparticles, comprised of $PEG_8DES$ and $PEG_8DTS$, were incubated with each cell line for 72 h at 37 °C, after which the viability of cells was evaluated with a bioluminescence assay detecting ATP generation.  In all three cell lines, the pre-functionalized nanoparticles did not elicit significant cytotoxicity (Figure 3.8).  There was minimal difference in toxicity for nanoparticles fabricated from the $PEG_8DES$ and $PEG_8DTS$ crosslinkers as well.  The results suggest that nanoparticles fabricated from these novel silyl ether crosslinkers and the degradation byproducts are well-tolerated by the cells.
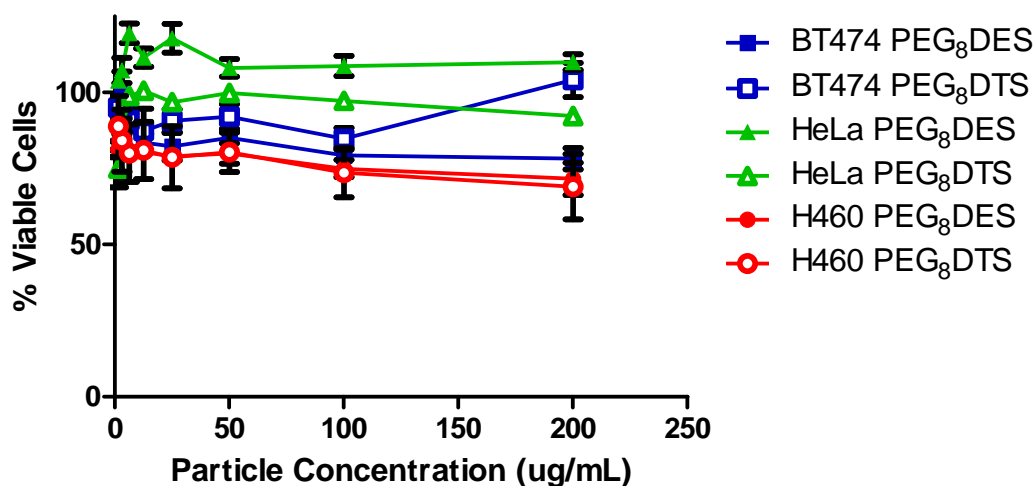


**Figure 3.8**  Cell viability of BT474, HeLa, and H460 cells after incubation with pre-functionalized nanoparticles fabricated from the $PEG_8DES$ and $PEG_8DTS$ crosslinkers.

To further investigate the potential of silyl ether-based nanoparticles as a drug delivery system, the viability of BT474 cells with targeted nanoparticles, fabricated from the $PEG_8DES$ crosslinker, was studied.    NP-Herc, NP-OKT9, and NP-IgG were incubated with BT474 cells for 72 h at 37 °C and then analyzed for cellular viability.

Similar to the pre-functionalized nanoparticles, the targeted versions exhibited minimal cytotoxicity across a range of nanoparticle concentrations (Figure 3.9). Based on these results, silyl ether crosslinkers are promising materials for therapeutic targeted nanocarriers because their blank nanoparticle formulations and degradation byproducts do not exhibit cytotoxicity in a range of cancer cells and nanoparticle concentrations. This supports the potential for silyl ether-based nanoparticles targeted for the HER2 and TfR as improved drug delivery agents.
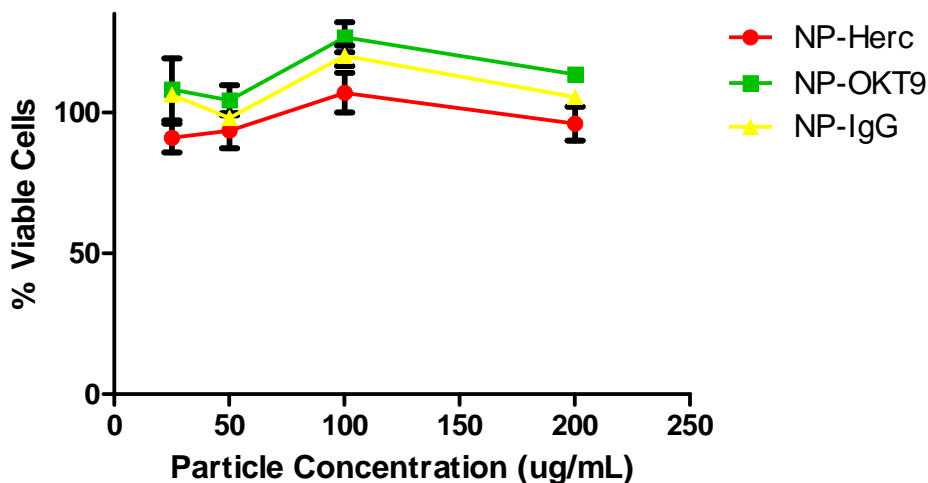


**Figure 3.9** Cell viability of BT474 cells after incubation with targeted nanoparticles fabricated from the PEG$_8$DES crosslinker.

### 3.1.3.6 Fabrication of Silyl Ether-Based Nanoparticles Loaded with Docetaxel

As nanoparticles fabricated from the PEG$_8$DES and PEG$_8$DTS crosslinkers were not cytotoxic in either pre-functionalized or targeted formulations and demonstrated intracellular degradation, silyl ether chemistry is a viable approach for biomaterials used in drug delivery. To further investigate the efficacy of silyl ether-based nanoparticles as

drug delivery agents, they were applied to the delivery of docetaxel. Docetaxel is a chemotherapeutic antimicrotubule agent, approved as Taxotere for the treatment of breast, non-small cell lung, prostate, gastric, and head and neck cancers.[24] Docetaxel has also demonstrated promise over other drugs including doxorubicin and paclitaxel.[41] However, like other chemotherapeutics, docetaxel is plagued by systemic toxicities and thus adverse side effects, so it is an attractive candidate for enhanced efficacy by encapsulation within nanocarriers.

Docetaxel was loaded into nanoparticles, comprised of the PEG$_8$DES and PEG$_8$DTS crosslinkers, with 1 wt % by addition to the preparticle solution (Table 3.4).

**Table 3.4** Composition of docetaxel-containing silyl ether-based nanoparticles.

| Monomers | Wt % |
| --- | --- |
| PEG$_8$DES or  PEG$_8$DTS | 86 |
| 2-Aminoethyl methacrylate hydrochloride | 10 |
| Fluorescein $o$-acrylate | 2 |
| 2,2-Diethoxyacetophenone | 1 |
| Docetaxel | 1 |

Nanoparticles encapsulating the chemotherapeutic were fabricated following the same procedure as blank particles. Addition of docetaxel did not adversely affect the formation of cylindrical nanoparticles by the PRINT process as seen by SEMs in Figure 3.10. Surface functionalization of the nanoparticles and targeting with Herceptin, OKT9, and IgG were also performed under the same conditions as blank nanoparticles.
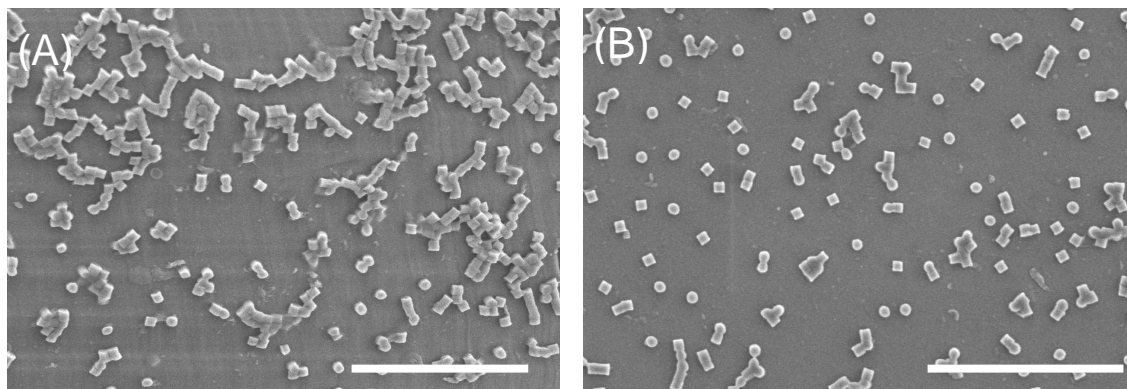
**Figure 3.10** SEMs of cylindrical 200 nm nanoparticles, fabricated from the (A) PEG$_8$DES and (B) PEG$_8$DTS crosslinkers, containing docetaxel. Scale bar is 3 µm.

**3.1.3.7 Cytotoxicity of Targeted Silyl Ether Nanoparticles Loaded with Docetaxel**

Similar to other cancers, HeLa cells express amplified levels of the TfR,[31] which was used as the target for 1 wt % docetaxel-loaded nanoparticles. Nanoparticles were fabricated from the PEG$_8$DES crosslinker, functionalized, and targeted with OKT9 and IgG. They were incubated with HeLa cells for 72 h at 37 °C and evaluated for cytotoxicity thereafter. Dose dependent cytotoxicity was observed for both NP-OKT9 and NP-IgG fabricated from the PEG$_8$DES crosslinker (Figure 3.11).
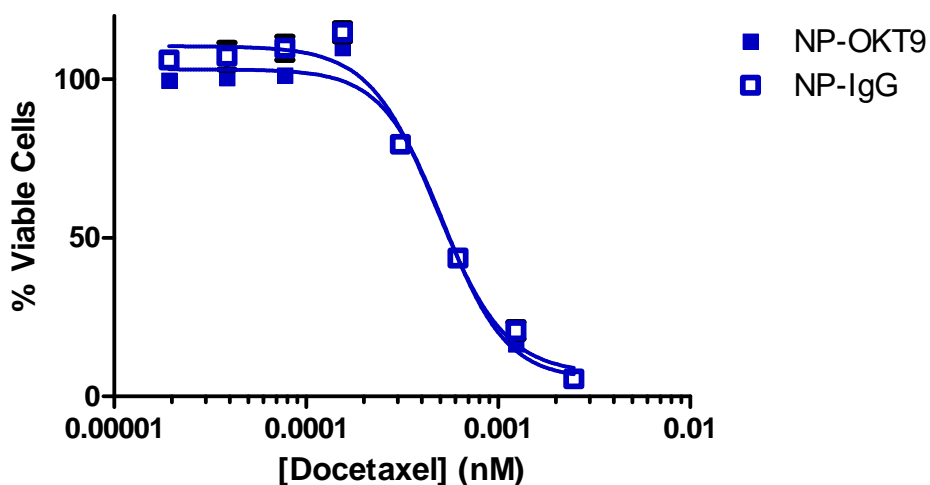
**Figure 3.11** Cytotoxicity of targeted nanoparticles, fabricated from the PEG$_8$DES crosslinker, loaded with docetaxel in HeLa cells.

However, no difference in cytotoxicity between NP-OKT9 and NP-IgG was observed. In fact, the cytotoxic profiles were nearly identical within each nanoparticle composition (Table 3.5).

**Table 3.5** IC$_{50}$ values of targeted nanoparticles, fabricated from the PEG$_8$DES crosslinker, loaded with docetaxel in HeLa cells.

| Nanoparticle | IC$_{50}$ (nM) |
|---|---|
| NP-OKT9 | $5.2 \times 10^{-4}$ |
| NP-IgG | $4.8 \times 10^{-4}$ |

It was expected that NP-OKT9 would bind specifically with the TfR on the cellular surface of HeLa cells and internalize the nanoparticles to promote the intracellular degradation of the nanoparticles under acidic conditions. It was also anticipated that

HeLa cells would not internalize NP-IgG because of the negative surface charge and nonspecific control targeting ligands on the nanoparticles. Instead, targeting ligands on the nanoparticle surface did not influence the cytotoxicity in HeLa cells. This is potentially because docetaxel was poorly retained within the nanoparticles. In hydrogel particles, the predominant mechanism of drug release is passive diffusion.[42] Thus, cytotoxicity observed from NP-OKT9 likely was not associated with TfR-mediated endocytosis and the subsequent intracellular degradation of the nanoparticles for release of docetaxel. Instead, docetaxel may diffuse out of NP-OKT9 and NP-IgG, resulting in similar cytotoxicity profiles regardless of the targeting moieties on the nanoparticle surface.

Because docetaxel was encapsulated within the nanoparticles, loss of the drug during surface functionalization and targeting was a concern for these bifunctional silyl ether-based nanoparticles. To further understand release of docetaxel and the cytotoxicity profiles observed, pre-functionalized nanoparticles were fabricated from the PEG$_8$DES crosslinker and loaded with 1 wt % of docetaxel. One set of pre-functionalized nanoparticles was set aside while another set was washed in a similar manner to nanoparticles undergoing functionalization and targeting. Pre-functionalized nanoparticles were incubated with HeLa cells for 72 h at 37 °C and then analyzed for cell viability. As seen in Figure 3.12, blank nanoparticles without any encapsulated docetaxel did not elicit strong cytotoxic responses over a large concentration range, suggesting the nanoparticle composition of PEG$_8$DES and its degradation byproducts are well-tolerated by HeLa cells. Drug-loaded pre-functionalized nanoparticles without extensive washing exhibited cytotoxicity at all concentrations. However, when the same nanoparticles were

processed through multiple washings, they showed dose dependent toxicity. Through repeated washes, encapsulated docetaxel diffused out of the silyl ether hydrogel nanoparticles. This suggests that docetaxel is not well retained within the nanoparticles and readily diffuses out of the nanoparticles, also corroborating the minimal difference in cytotoxicity results observed from NP-OKT9 and NP-IgG.
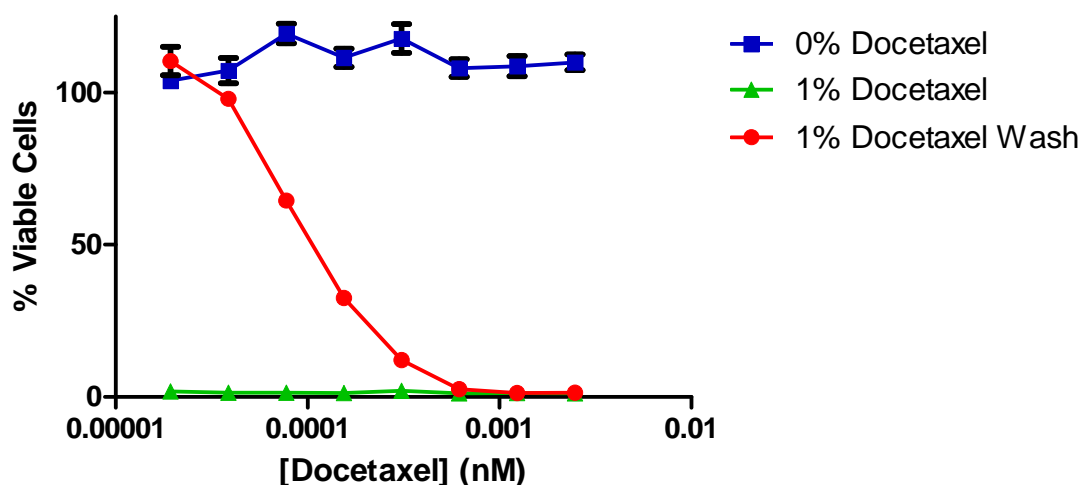


**Figure 3.12** Cytotoxicity of washed and unwashed pre-functionalized nanoparticles, fabricated from the PEG$_8$DES crosslinker, loaded with 1 wt % docetaxel in HeLa cells. Blank (0% docetaxel) nanoparticles were dosed at the same nanoparticle concentrations as the drug-loaded nanoparticles.

Consequently, nanoparticles fabricated from the silyl ether crosslinkers may not be appropriate nanocarriers for docetaxel or other small molecules therapeutics as the cargo freely diffuses from within the nanoparticles. Nonethless, utilizing silyl ether chemistry as acid-sensitive moieties that are responsive to environmental triggers possesses great potential. Instead of nanoparticles comprised of silyl ether crosslinkers, we exploit the sensitivity of silyl ethers for drug delivery by incorporation of the

functionality into a prodrug and explore its delivery through targeted nanoparticles in the following sections.

### 3.1.4 Conclusions

Bifunctional silyl ether crosslinkers $PEG_8DES$ and $PEG_8DTS$ were investigated as biomaterials for drug delivery nanoparticles. The crosslinkers were used to successfully fabricate cylindrical nanoparticles ($d = 200$ nm and $h = 200$ nm) through the PRINT technology. This reinforces the versatility of the PRINT platform as novel materials, including these silyl ethers, can be readily incorporated into particles. Furthermore, the silyl ether-based nanoparticles were functionalized with Herceptin and OKT9 and investigated *in vitro* for cellular targeting of the HER2 and TfR. Both NP-Herc and NP-OKT9 demonstrated specific uptake relative to control NP-IgG in BT474 and Ramos cells, suggesting nanoparticle internalization through receptor-mediated endocytosis. After internalization, targeted nanoparticles prepared from the $PEG_8DES$ crosslinker degraded intracellularly, as observed by diffuse fluorescence throughout the cells by confocal microscopy. This indicated that the nanoparticles are responsive to the stimuli of acidic conditions within the cells. Moreover, cytotoxicity of blank pre-functionalized and targeted nanoparticles indicated that the silyl ether-based materials and its degradation byproducts are well-tolerated by BT474, HeLa, and H460 cells. Specific cellular targeting and internalization, acid-catalyzed hydrolysis, and relative nontoxicity of the nanoparticles are promising traits of drug delivery vehicles for cancer therapeutics.

Efficacy of the silyl ether-based nanoparticles was investigated by encapsulation of the chemotherapeutic agent docetaxel. Both NP-OKT9 and NP-IgG exhibited dose-dependent cytotoxicity but negligible differences between targeted and control formulations. These results were due to poor retention of encapsulated docetaxel within the nanoparticles due to passive diffusion. Loss of the therapeutic payload during the targeting of the nanoparticles produced less cytotoxic pre-functionalized nanoparticles as compared to those with less processing. The potential of nanoparticles fabricated from the silyl ether crosslinkers as drug delivery vehicles is overshadowed by the rapid passive diffusion of docetaxel out of the nanoparticles.

### 3.1.5 Future Work

Although targeted nanoparticles fabricated from the bifunctional silyl ether crosslinkers $PEG_8DES$ and $PEG_8DTS$ were not ideal drug delivery vehicles for docetaxel, silyl ether-based crosslinkers still have much promise as stimuli-responsive materials for biomedical purposes. The hydrogel nanoparticles may not be appropriate for the delivery of small molecules drugs, such as docetaxel, because of uncontrolled passive diffusion of the drug out of the nanoparticles, but they could be utilized for macromolecular cargoes, including peptides,[43] proteins,[44] and oligonucleotides.[45] The hydrodynamic radii of macromolecules would promote sustained release from hydrogels instead of the rapid diffusion of small molecules.[42] Furthermore, silyl ether crosslinkers could be utilized as stimuli-responsive materials for biomedical devise. Initial investigations have been promising. The previously reported DMS crosslinker was molded into rudimentary biomedical devices of sutures and stents; both devices showed accelerated degradation

under acidic conditions.[19]  Because silyl ether chemistry provides precise control over the rate of degradation, based on the substituents on the silicon atom, biomedical devices prepared from these materials can truly be tailored to fit the application and needs of patients.

## 3.2  Nanoparticles Containing Degradable Silyl Ether Prodrugs

### 3.2.1  Introduction

Gemcitabine (2',2'-difluorodeoxycytidine, dFdC, Gemzar, Figure 3.13) is a versatile chemotherapeutic drug with proven anticancer efficacy against a variety of cancers including pancreatic,[46] lung,[47] breast,[48] ovarian, and head and neck.[49]  It is a pyrimidine nucleoside analogue that must be delivered into cells through nucleoside transporters (NTs) in order to inhibit cell growth.[50,51]
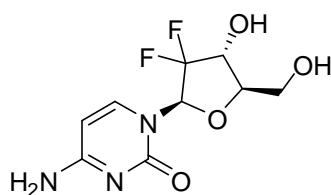


**Figure 3.13**  Chemical structure of gemcitabine.

Once internalized, gemcitabine is phosphorylated by deoxycytidine kinase (dCK) to its monophosphate form and then further into the active diphosphate and triphosphate

metabolites. The active triphosphate derivative is incorporated into DNA, inhibiting DNA synthesis and thus, arresting cellular growth in the early S phase.[52]

Despite its clinical relevance, gemcitabine faces some challenges. As a hydrophilic, polar drug, it possesses poor membrane permeability. Similar to other nucleoside analogues, gemcitabine requires active transport processes via NTs for delivery into cells.[51,53] Still another limitation of gemcitabine is that it is rapidly metabolized in the blood, liver, kidneys, and other organs by cytidine deaminase into the inactive 2',2'-difluorodeoxyuridine, which is subsequently excreted in urine.[54,55] Therefore, gemcitabine has a short plasma half-life of only 8-17 min in humans.[53,56,57] This adversely affects the bioavailability and thus reduces the efficacy of the drug.

Current efforts to improve upon gemcitabine have ranged from aerosols[58-62] to conjugates[63-68] to nanocarriers.[54,55,69-75] In particular, gemcitabine prodrugs have been designed and synthesized with various lipids with the aim of protecting gemcitabine from rapid deamination to its inactive uridine metabolite. Gemcitabine has been modified with fatty acids[63,76,77] and also with saturated and monounsaturated 18-20 carbon atom chains[64] to yield select prodrugs with higher *in vitro* cytotoxicity profiles than the original drug, in addition to reduced degradation by cytidine deaminase. Although these gemcitabine prodrugs overcame the limitation of metabolizing to the inactive metabolite, they included their own set of challenges, namely poor aqueous solubility and problems with administration.[53]

To address this new set of challenges, liposomes and nanoparticles have been utilized as drug delivery agents for gemcitabine because lipophilic derivatives of gemcitabine are easily encapsulated into lipophilic environments of some

nanocarriers.[54,55,71,78]    Liposomes and nanoparticles have enhanced the *in vitro* cytotoxicity of the chemotherapeutic drug through increased cellular penetration[55] and also have improved the *in vivo* antitumor activity through the differential pharmacokinetic profiles of the small molecule drug and nanocarriers.[75,78,79] Entrapping gemcitabine within liposomes and nanoparticles mitigated the plasma degradation and inactivation of gemcitabine by cytidine deaminase.[54] Recent advancements involve the attachment of ligands specific for overexpressed cellular receptors to the surface of liposomes and nanoparticles to actively target cancer cells. These studies demonstrated that gemcitabine encapsulated in nanoparticles that target the epidermal growth factor receptor (EGFR)[70,71,80] or HER2 receptor[69] possessed improved therapeutic effects. Targeted nanocarriers promoted greater intracellular accumulation of the drug than untargeted nanocarriers to further enhance *in vitro* cytotoxicity and *in vivo* antitumor activity.

In this study, we investigated the potential of PRINT nanoparticles, targeting the transferrin receptor (TfR), as drug delivery agents for the enhancement of gemcitabine efficacy. We have previously shown that PRINT nanoparticles, conjugated with ligands that bind the TfR, selectively internalized into cancer cells with amplified TfR expression and even exhibited cytotoxicity to Ramos (B-cell lymphoma) cells due to the multivalent nature of the nanoparticles.[31]   In addition, we have synthesized novel gemcitabine prodrugs (Figure 3.14), consisting of an acrylate functionality through which the prodrug can be covalently entrapped within the nanoparticles, and also a silyl ether functionality that imparts acid sensitivity such that the prodrug can degrade under endocytic conditions.[30]
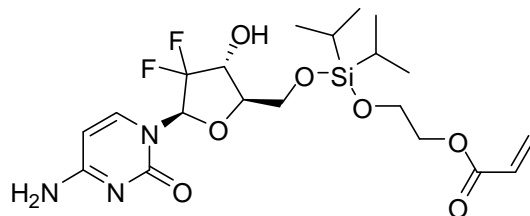
**Figure 3.14** Chemical structure of diisopropyl silyl ether prodrug.

We leveraged these two approaches of targeted nanoparticles and a novel prodrug to improve the therapeutic effect of gemcitabine. Our design aims to protect gemcitabine and enhance drug accumulation intracellularly through the targeted nanoparticles in addition to reducing nonspecific systemic toxicity with the acid-labile prodrug.

### 3.2.2 Experimental

### 3.2.2.1 Chemicals and Reagents

Biotinylated OKT9 and isotype control mouse IgG were purchased from eBioscience. UltraAvidin was purchased from Leinco Technologies. Biotin-poly(ethylene glycol)-succinimidyl carboxymethyl ester (5000 g/mol for PEG; NHS-PEG$_{5000}$-biotin) was purchased from Laysan Bio. Anhydrous dimethylformamide (DMF) and pyridine were purchased from Acros. Poly(ethylene glycol) dimethacrylate (1000 g/mol for PEG; PEG$_{1000}$ dimethacrylate) was purchased from PolySciences. Acetic anhydride, HPLC grade water and acetonitrile, and pH 5.0 buffer were purchased from Fisher Scientific. All other reagents were purchased from Sigma Aldrich.

### 3.2.2.2 Cells and Culture

H460 cells were from ATCC. HEK293 cells were from UNC LCCC Tissue Culture Facility. H460 cells were maintained in RPMI 1640 with 10% FBS, and HEK293 cells were maintained in MEM alpha with 10% FBS. All media were supplemented with 50 units/mL penicillin and 50 µg/mL streptomycin. All media and supplements were from Gibco.

### 3.2.2.3 Fabrication of PRINT Nanoparticles

Cylindrical nanoparticles ($d$ = 200 nm and $h$ = 200 nm) were fabricated using the PRINT technique. Nanoparticles were prepared from a starting monomer solution (5% wt/vol in DMF) consisting of 78 wt % of $PEG_{1000}$ dimethacrylate, 20 wt % of 2-aminoethyl methacrylate hydrochloride, 1 wt % of fluorescein $o$-acrylate, and 1 wt % of 1-hydroxycyclohexyl phenyl ketone. A monomer film was cast upon a sheet of poly(ethylene terephthalate) (PET) by spreading 90 µL of monomer solution with a mayer rod (#2, R.D. Specialties), and it was dried with heat using a heat gun to remove the solvent DMF. The monomer film and patterned mold, provided by Liquidia Technologies, were laminated together under pressure (40 PSI) and then delaminated, by gently splitting the mold and PET, to yield a mold with filled cavities. The filled mold was laminated with a fresh sheet of PET and then exposed to UV irradiation ($\lambda$ = 365 nm, power 90 mW/cm$^2$) for 4 min under a nitrogen purge. The mold was removed, leaving nanoparticles transferred on the sheet of PET. This was due to the higher surface energy

of the PET. Cold Dulbecco's phosphate buffered saline (DPBS; 400 µL) was placed on the PET, and nanoparticles were collected mechanically with a cell scraper. The harvested particles were washed twice with cold DPBS by centrifugation.

### 3.2.2.4  Fabrication of Prodrug-Loaded PRINT Nanoparticles

The same fabrication procedure as described for blank nanoparticles was followed. The nanoparticles were prepared from a starting monomer solution (5% wt/vol in DMF) consisting of 58 wt % of $PEG_{1000}$ dimethacrylate, 20 wt % of diisopropyl silyl ether gemcitabine prodrug, 20 wt % of 2-aminoethyl methacrylate hydrochloride, 1 wt % of fluorescein o-acrylate, and 1 wt % of 1-hydroxycyclohexyl phenyl ketone.

### 3.2.2.5  OKT9/IgG Conjugation to PRINT Nanoparticles

Nanoparticles were conjugated with OKT9 or IgG through a biotin-avidin linkage. Nanoparticles in anhydrous DMF (500 µL at 2 mg/mL) were reacted with 5 mg of NHS-$PEG_{5000}$-biotin in the presence of 10 µL anhydrous of pyridine; the nanoparticle dispersion was shaken on a vortex for 2 h. Acetic anhydride (10 µL) was added to the dispersion, which was shaken for 10 min, to quench unreacted amines on the nanoparticle surface. The nanoparticles were washed twice with cold DPBS by centrifugation. UltraAvidin (50 µL, 10 mg/mL) was added to the nanoparticles in DPBS (2 mg/mL). The dispersion was shaken for 1 h. The nanoparticles were washed twice with cold DPBS by centrifugation. To target the nanoparticles, 100 µL of OKT9 or IgG was added to the nanoparticle dispersion and was shaken for 30 min at room temperature and then

kept overnight at 4 °C.  The nanoparticles were washed twice with cold DPBS by centrifugation and then resuspended in DPBS.

### 3.2.2.6  Physical Characterization of Nanoparticles

Scanning electron microscopy samples were prepared by pipetting 10 µL of nanoparticle solution onto a glass slide.  Samples were dried and coated with 2 nm of gold palladium with a Cressington 108 auto sputter coater (Cressington Scientific Instruments).  Samples were imaged with a scanning electron microscope (Hitachi S-4700).  The size (dynamic light scattering, DLS) and charge ($\zeta$-potential) of the nanoparticles were determined for 20 µg/mL nanoparticle samples in a 1 mM potassium chloride solution with a Malvern Instruments Nano ZS.

### 3.2.2.7  Quantitative *In Vitro* Cellular Targeting and Kinetics

H460 cells were plated at 10,000 cells/well in a 96-well plate and allowed to adhere overnight at 37 °C and 5% $CO_2$.  Nanoparticles in OPTI-MEM were incubated with cells at 37 °C and 5% $CO_2$ for specified amounts of time and then removed.  The cells were washed twice with DPBS, trypsinized, and prepared for analysis by flow cytometry with a 0.2% trypan blue solution containing 10% FBS in DPBS.  Samples were analyzed with a Dako CyAn flow cytometer.  Similar procedures were followed for HEK293 cells, which were plated at 30,000 cells/well in a 96-well plate.

### 3.2.2.8  Inhibition of Nanoparticle Cellular Targeting

H460 cells were plated at 10,000 cells/well in a 96-well plate and allowed to adhere overnight at 37 °C and 5% $CO_2$.  Free OKT9 or IgG, at varying concentrations in complete media, was dosed onto cells.  The cells were incubated at 37 °C for 30 min, after which free targeting ligands were removed.  Nanoparticles in OPTI-MEM, at 200 µg/mL, were incubated with cells at 37 °C for 4 h and then removed.  The cells were washed twice with DPBS, trypsinized, and prepared for analysis by flow cytometry with a 0.2% trypan blue solution containing 10% FBS in DPBS.  Samples were analyzed with a Dako CyAn flow cytometer.

### 3.2.2.9  Kinetics of Gemcitabine Released from Nanoparticles

Aliquots of nanoparticles loaded with prodrug were shaken in a buffer solution pH 7.4 or pH 5.0 at 37 °C.  At specified times, a suspension of nanoparticles was centrifuged to pellet the particles, and an aliquot of the supernatant was analyzed by high-performance liquid chromatography (HPLC, Agilent Technologies Series 1200) with a C18 reverse phase column (Zorbax Eclipse XDB-C18, 4.6×150 mm, 5 micron).  A mobile phase of water and acetonitrile on a gradient of water to water:acetonitrile (97.5:2.5) over 15 min with a flow rate of 1 mL/min and a detection wavelength of 267 nm was employed.

### 3.2.2.10  Qualitative *In Vitro* Cellular Targeting and Trafficking

H460 and HEK293 cells were plated on cover slips in a 6-well plate ($5 \times 10^4$ cells/well) overnight at 37 °C and 5% $CO_2$.  Cells were incubated with 50 µg/mL of nanoparticles in OPTI-MEM for 4 or 24 h in addition to Lysotracker Red DND-99 (Invitrogen) at 37 °C.  Cells were fixed, made permeable with 0.1% triton-X100 in PBS for 3 min, and incubated with Alexa Fluor 555 phalloidin (Invitrogen) for 1 h at room temperature without light.  Cells were washed with DPBS, and cover slips were mounted onto glass slides with FluorSave Reagent (Calbiochem), and cells were imaged with a confocal laser scanning microscope (Olympus Fluoview FV500).

### 3.2.2.11  Cytotoxicity of Prodrug-Loaded Nanoparticles

H460 cells were plated at 5,000 cells/well in a 96-well plate and allowed to adhere overnight at 37 °C and 5% $CO_2$.  Nanoparticles in OPTI-MEM were incubated with cells at 37 °C and 5% $CO_2$ for 1 h and removed.  The cells were washed twice with DPBS, and complete media was added to the cells, which were incubated at 37 °C for 72 h.  Cell viability was determined using Promega CellTiter-Glo® Luminescent Cell Viability Assay according to the manufacturer's instructions.  Bioluminescence was measured by a SpectraMax M5 plate reader (Molecular Devices).

### 3.2.3  Results and Discussion

### 3.2.3.1 PRINT Particle Fabrication and Conjugation with OKT9/IgG

The PRINT technology is a robust particle fabrication approach that facilitates independent control over particle size, shape, matrix composition, and surface chemistry and has been described previously.[19,25-29,31,32] Through this technique, cylindrical nanoparticles ($d$ = 200 nm and $h$ = 200 nm), primarily composed of poly(ethylene glycol) (PEG, 1000 g/mol) dimethacrylate, were fabricated (Figure 3.15).
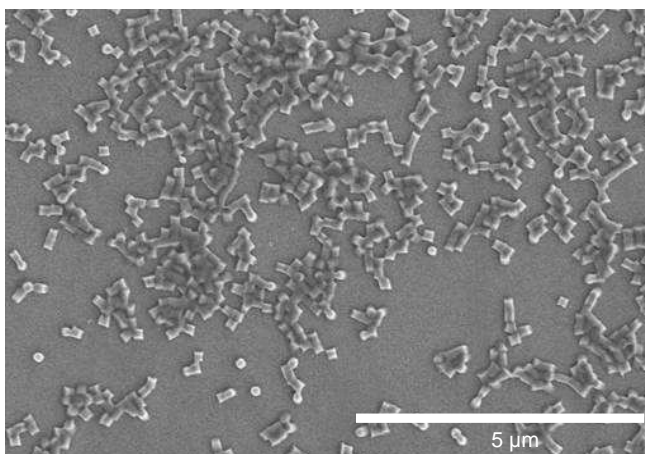


**Figure 3.15** SEM of 200 nm cylindrical PRINT nanoparticles.

The nanoparticles were also prepared to include 20 wt % of 2-aminoethyl methacrylate hydrochloride and 1 wt % of fluorescein $o$-acrylate (Table 3.6). The 2-aminoethyl methacrylate hydrochloride provided a functional handle through which the nanoparticle surface could be modified. Fluorescein $o$-acrylate labeled the nanoparticles to enable fluorescent monitoring and visualization of nanoparticles with cells.

**Table 3.6** Composition of blank and prodrug-loaded PRINT nanoparticles.

| Monomers | No Prodrug (Wt %) | With Prodrug (Wt %) |
|---|---|---|
| PEG$_{1000}$ dimethacrylate | 78 | 58 |
| 2-Aminoethyl methacrylate hydrochloride | 20 | 20 |
| Fluorescein $o$-acrylate | 1 | 1 |
| 1-Hydroxycyclohexyl phenyl ketone | 1 | 1 |
| Diisopropyl silyl ether gemcitabine prodrug | 0 | 20 |

The pre-functionalized nanoparticles with no surface modification had a hydrodynamic diameter of 277 nm with a narrow polydispersity index of 0.037. They were also cationic and possessed a positive ζ-potential (+25.6 ± 0.4 mV) due to the amine surface functionality (Table 3.7). It has been shown that positively charged nanoparticles are internalized rapidly but nonspecifically into cells[27,81-83] and can induce cytotoxicity.[84] Conversely, negatively charged particles exhibit decreased cellular uptake,[27,81-83] so nanoparticles with a negative ζ-potential and targeting ligands can effectively circumvent nonspecific cellular internalization while targeting specific diseased cells.[31]

**Table 3.7** Hydrodynamic dimaeter and zeta potential of 200 nm PRINT nanoparticles.

| Nanoparticle | Diameter (nm) | PDI | ζ-Potential (mV) |
|---|---|---|---|
| Pre-functionalized | 277 ± 4 | 0.037 | +25.6 ± 0.4 |
| Biotinylated | 309 ± 7 | 0.071 | -10.0 ± 0.7 |
| Avidinated | 304 ± 2 | 0.104 | -5.31 ± 0.4 |
| NP-OKT9 | 310 ± 4 | 0.114 | -15.3 ± 0.7 |
| NP-IgG | 301 ± 3 | 0.085 | -14.8 ± 0.8 |

Thus, the surface of the pre-functionalized nanoparticles was functionalized and enhanced with targeting ligands as previously described. To evade nonspecific uptake into cells, the pre-functionalized nanoparticles were initially reacted with NHS-PEG$_{5000}$-biotin, followed by acetic anhydride to quench any unreacted amines. Quenching of unreacted amines shifted the positive $\zeta$-potential to negative (biotinylated nanoparticle $\zeta$-potential = -10.0 mV, Table 3.7) to avoid nonspecific cellular internalization. Targeting ligands were then attached via biotin-avidin linkages. Biotinylated nanoparticles were reacted with avidin, and thereafter, the targeting ligands (OKT9) or the control ligands (IgG) were conjugated to the nanoparticle surface. OKT9 is an anti-human transferrin receptor monoclonal antibody, and IgG is a control mouse antibody of the same isotype. Both OKT9-targeted nanoparticles (NP-OKT9) and IgG-targeted nanoparticles (NP-IgG) maintained hydrodynamic diameters of ~300 nm and negative $\zeta$-potentials of about -15 mV (Table 3.7) for minimizing nonspecific cellular internalization.

### 3.2.3.2  Quantitative *In Vitro* Cellular Uptake and Kinetics

Cellular internalization of the nanoparticles without prodrug was investigated in H460 (human large cell lung carcinoma) and HEK293 (transformed human embryonic kidney) cells. H460 cells display amplified expression of the transferrin receptor (TfR), in contrast to HEK293 cells that have minimal cellular levels of the receptor.[31] Transferrin binds to iron for transport through the TfR. Thus, the TfR is critical in the transport of iron, which is involved in metabolism, respiration, and DNA synthesis, and expression of the TfR is regulated by intracellular iron levels. Consequently, the TfR is

highly expressed on actively proliferating cancerous cells and at low levels on normal cells. Therefore, the TfR is an attractive target for cancer treatments.[36]

Pre-functionalized nanoparticles, as well as NP-OKT9 and NP-IgG, at various concentrations (0-200 µg/mL), were incubated with H460 and HEK293 cells at 37 °C over a range of times (1-8 h). Samples were analyzed using a flow cytometry technique to quantify the percentage of cells with bound and internalized nanoparticles.[40] When pre-functionalized nanoparticles were investigated with H460 and HEK293 cells, nanoparticles were rapidly internalized into cells in a dose dependent manner (Figure 3.16). In both cell lines, over 80% of cells had internalized pre-functionalized nanoparticles after 8 h. In H460 cells, time-dependent nanoparticle uptake was observed, while minimal differences in uptake were observed amongst the incubation times for HEK293 cells. Regardless of the amount of time for nanoparticle incubation, HEK293 cells exhibited significant internalization of nanoparticles (>90%). This rapid nanoparticle uptake into cells was expected as we have previously shown that PRINT particles with positive $\zeta$-potential are easily internalized nonspecifically.[27,83]
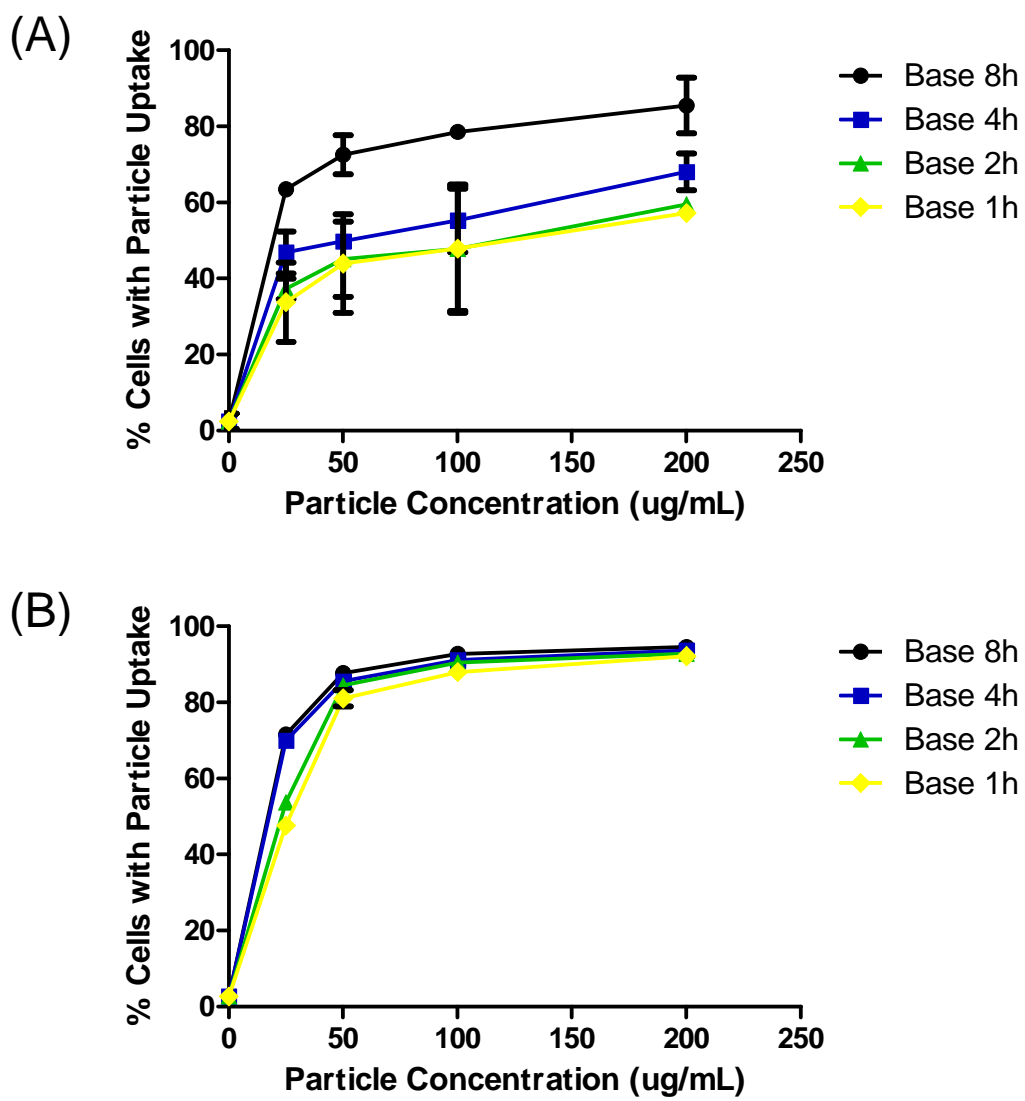
**Figure 3.16** Pre-functionalized nanoparticle uptake as a function of nanoparticle concentration and time in (A) H460 cells and (B) HEK293 cells.

Despite the significant cellular internalization of pre-functionalized nanoparticles, positively charged particles are internalized nonspecifically[27,81-83] and can induce cytotoxic effects.[84] Consequently, the pre-functionalized nanoparticles were engineered to have a negative $\zeta$-potential to evade nonspecific cellular uptake and conjugated with targeting ligands for the TfR to enhance selective drug delivery. When incubated with

H460 cells, which have amplified expression of TfR, NP-OKT9 exhibited selective targeting in a nanoparticle dose and time dependent fashion. As seen in Figure 3.17, up to 57% of cells had associated NP-OKT9 at 1 h. Targeting was saturated at 4 h with ~80% of cells with bound NP-OKT9. In contrast, because of their negative charge and nonspecific ligand, NP-IgG did not exhibit an appreciable level of uptake (<7%) in H460 cells at all nanoparticle concentrations and incubations times. Conversely, despite a negative ζ-potential, the addition of the specific targeting ligand OKT9 enabled NP-OKT9 to bind selectively to H460 cells through targeting of the TfR. Negatively charged particles can override nonspecific cellular uptake, but with a targeting ligand, the particles can now induce specific internalization.[31]
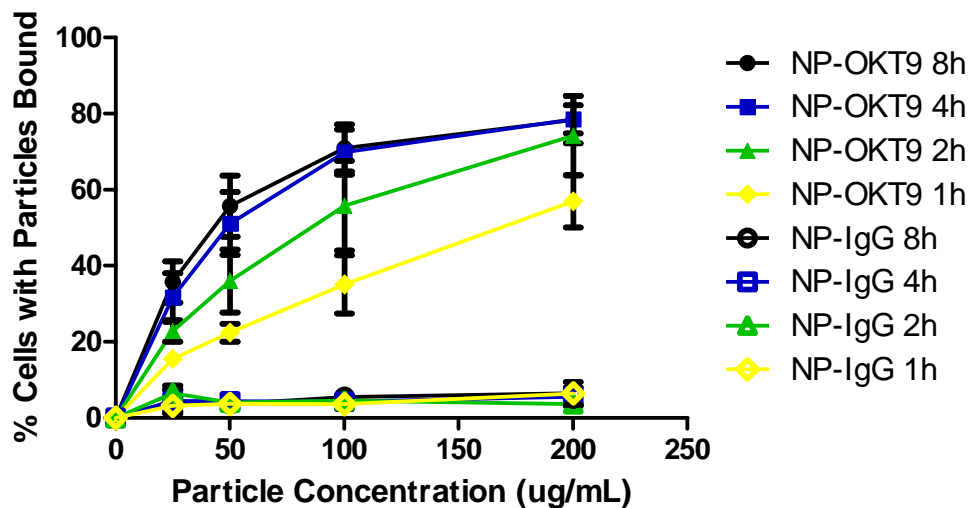


**Figure 3.17** Association of OKT9- and IgG-targeted nanoparticles in H460 cells as a function of nanoparticle concentration and time.

Additionally, targeting of NP-OKT9 and NP-IgG in HEK293 cells was investigated. When NP-OKT9 were incubated with cells, low cellular binding of nanoparticles was observed (Figure 3.18).
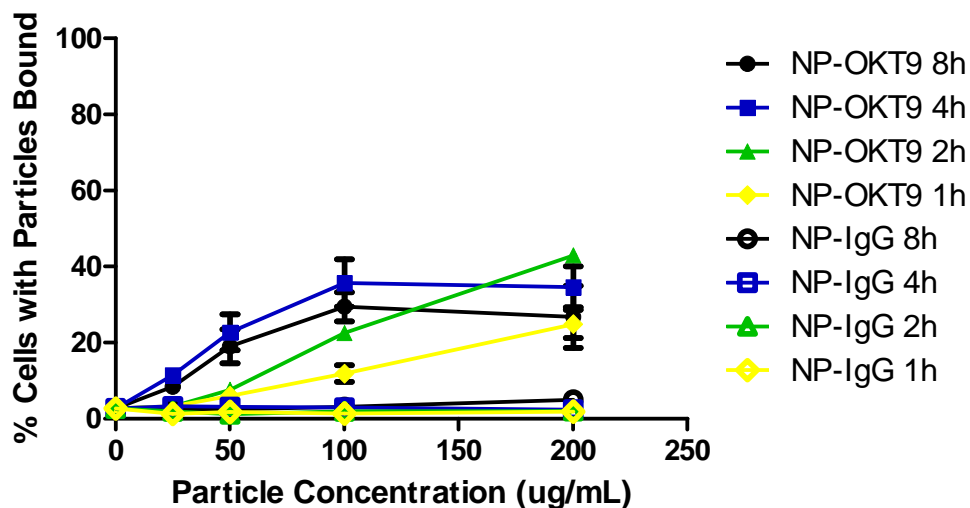


**Figure 3.18** Association of OKT9- and IgG-targeted nanoparticles in HEK293 cells as a function of nanoparticle concentration and time.

Unlike H460 cells, HEK293 cells have low levels of TfR expression,[31] so the extent of NP-OKT9 uptake in H460 and HEK293 correlates well to the TfR expression on the cells. H460 cells internalized more NP-OKT9 and also at a quicker rate than HEK293 cells because H460 cells have greater expression of TfR. On the other hand, control nanoparticles NP-IgG exhibited similarly minimal uptake ($<6\%$) in HEK293 cells. The difference observed in cellular binding of NP-OKT9 in H460 and HEK293 cells demonstrate the potential of targeted nanoparticles to preferentially bind and internalize into diseased cells for specific delivery of the therapeutic payload.

### 3.2.3.3 Inhibition of Nanoparticle Cellular Targeting

To confirm binding and uptake of NP-OKT9 in H460 cells, competition with free targeting ligand was investigated. H460 cells were incubated with varying concentrations of free OKT9 prior to exposure to nanoparticles without prodrug so that the TfR on the cellular surface could be bound by free ligands thereby decreasing those available to bind with targeted nanoparticles. H460 cells dosed with free OKT9 exhibited lower binding with NP-OKT9 in a concentration dependent manner. An increased concentration of free OKT9 led to greater inhibition in binding of NP-OKT9 (Figure 3.19).
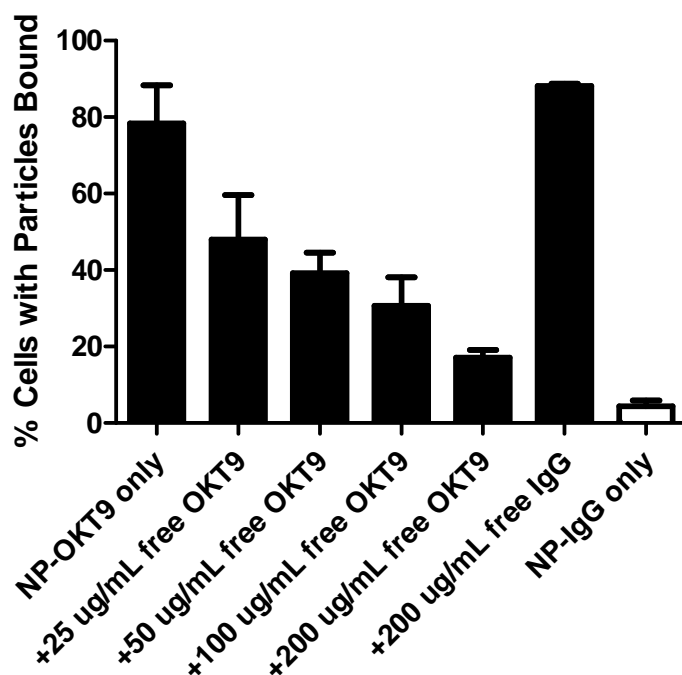
**Figure 3.19** Inhibition of binding of NP-OKT9 to H460 cells by free targeting antibodies.

Targeting was suppressed to <20% when cells were exposed to 200 µg/mL of free OKT9 before incubation with NP-OKT9. Binding of NP-OKT9 was inhibited in a dose-

dependent manner with free OKT9, but addition of the nonspecific IgG isotype control antibody to H460 cells did not influence binding of NP-OKT9. The selective binding of NP-OKT9 and its suppression only with free OKT9 indicate that the targeted nanoparticles are specifically targeting the TfR for subsequent internalization through transferrin receptor-mediated endocytosis. As such, highly specific NP-OKT9 targeted for the TfR demonstrate potential as drug delivery vehicles to enhance therapeutic efficacy.

### 3.2.3.4  Kinetics of Gemcitabine Released from Nanoparticles

Novel asymmetric bifunctional silyl ether prodrugs of gemcitabine were reported previously from our group.[30] Silyl ether chemistry is ideal for the synthesis of various prodrugs as silyl ethers are acid sensitive[20] and degrade under acidic environments within the body. Moreover, the rate of degradation of these prodrugs and subsequent release of the drug are tunable by modifying the substituents on the silicon atom. Further, degradation of these prodrugs releases the parent drug without any trace of chemical modification. For these reasons, novel asymmetric bifunctional silyl ether prodrugs of gemcitabine were synthesized and incorporated into PRINT nanoparticles.[30] The stability of each prodrug of gemcitabine was investigated under neutral (pH 7.4) and acidic (pH 5.0) environments. Each derivative exhibited more rapid degradation and subsequent release of gemcitabine under acidic conditions compared to pH 7.4 due to the silyl ether functionality. Additionally, it was shown that gemcitabine prodrugs with less steric bulk around the silicon atom were more sensitive to acid, so prodrugs with *tert*-butyl groups were very stable relative to those with isopropyl or ethyl moieties. The diethyl silyl ether

gemcitabine prodrug degraded rapidly within hours while the diisopropyl derivative exhibited sustained released over several days. This demonstrates that the release of gemcitabine can be controlled based upon the substituents on the silicon atom.

The diisopropyl silyl ether gemcitabine prodrug (Figure 3.14) was incorporated into our TfR-targeted nanoparticulate system because it demonstrated sensitivity to acidic conditions as well as extended release of the chemotherapeutic over several days.[30] Gemcitabine is also hydrophilic and highly soluble in water, so it is difficult to retain the drug within hydrogel nanoparticles because rapid and significant loss of the drug would likely occur in aqueous environments.[53] Thus, recent efforts by others involved encapsulating lipophilic derivatives of the drug into hydrophobic pockets of liposomes[54] or nanoparticles.[55,71,78] Our novel silyl ether gemcitabine prodrug circumvented the issue of loss in aqueous environments through its acrylate functionality which allowed the prodrug to be covalently conjugated into the nanoparticle to avoid loss of the cargo by diffusion while the silyl ether moiety enabled the controlled release of gemcitabine.

Targeted nanoparticles, loaded with the silyl ether gemcitabine prodrug, were incubated in physiological (pH 7.4) or endocytic (pH 5.0) environments at 37 °C to investigate the effect of targeting on the prodrug as well as the degradation of the prodrug and subsequent release of gemcitabine. Supernatants from aliquots of nanoparticle suspensions were analyzed by high-performance liquid chromatography (HPLC). As seen in Figure 3.20, gemcitabine was released from targeted nanoparticles more rapidly under an acidic environment than under a neutral pH.
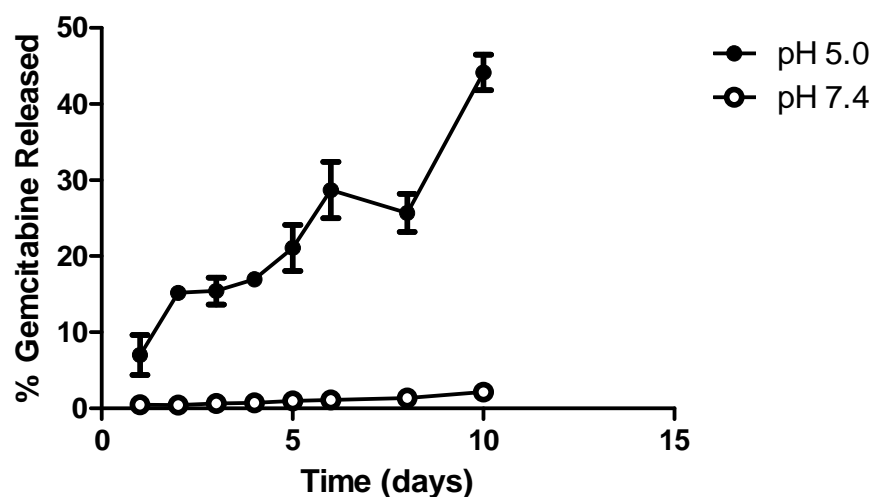
**Figure 3.20** Release of gemcitabine from targeted nanoparticles loaded with silyl ether prodrug at acidic (5.0) and neutral (7.4) pH over time.

Based on this data, the half-life of drug release from targeted nanoparticles at pH 5.0 was 15 days, whereas the half-life at pH 7.4 was 381 days. Rapid release of gemcitabine from the targeted nanoparticles was derived from the silyl ether functionality in the prodrug. Silyl ether moieties are known to be susceptible to acid.[20] The more rapid release of gemcitabine from nanoparticles under endocytic conditions also demonstrated that functionalizing the surface of the nanoparticles with targeting ligands did not adversely influence the behavior of the silyl ether prodrug. The differential and more rapid degradation rate of the silyl ether prodrug and consequent release of gemcitabine from targeted nanoparticles under endocytic environments demonstrate the possibility of an engineered drug delivery system to specifically deliver the drug intracellularly and thus improve bioavailability.

### 3.2.3.5 Qualitative *In Vitro* Cellular Uptake and Trafficking

Targeting of NP-OKT9 without prodrug with H460 cells was also visualized by confocal microscopy, through which intracellular accumulation of nanoparticles in acidic vesicles was observed. Inside these acidic compartments, prodrug degradation can be activated for release of gemcitabine from nanoparticles. Cells were treated with fluorescein-labeled nanoparticles. As expected, NP-OKT9 were associated with H460 cells through specific targeting of OKT9 to the TfR, while NP-IgG did not bind to the cells (Figure 3.21).
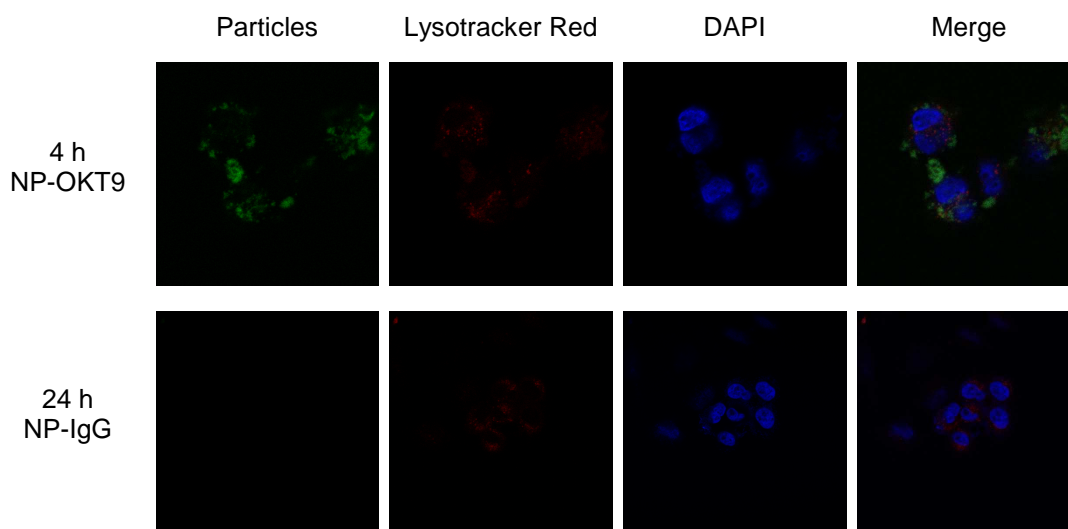


**Figure 3.21** Confocal microscopy images of specific targeting of NP-OKT9 (green) and minimal association of NP-IgG with H460 cells.

To investigate the intracellular fate of NP-OKT9, H460 cells were treated with NP-OKT9 and Lysotracker Red, which labels acidic vesicles within cells. NP-OKT9 were found to bind the TfR, internalize into H460 cells, and colocalize with Lysotracker Red, indicating

that after internalization, NP-OKT9 accumulated into acidic compartments, such as endosomes and/or lysosomes, of the cells (Figure 3.22).
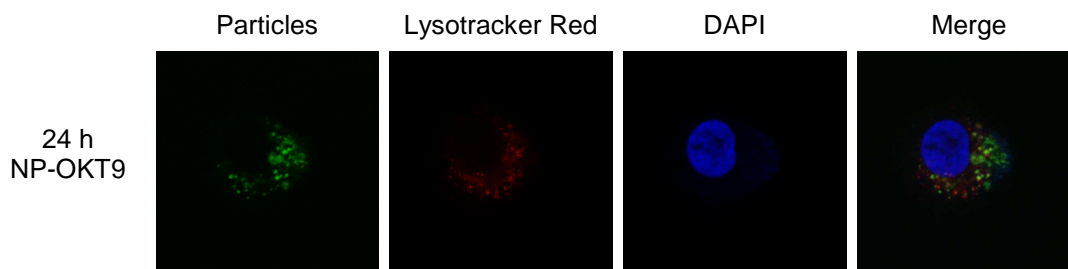


**Figure 3.22** Confocal microscopy images of specific targeting of NP-OKT9 (green) and intracellular trafficking into acidic compartments (red) in H460 cells.

The intracellular pathway of internalized targeted nanoparticles may be similar to that of the TfR with transferrin. As the mechanism for iron delivery, the TfR does not undergo the endosome-lysosome pathway so as to avoid degradation of the TfR. Instead, it is recycled back to the plasma membrane following internalization.[36] Intracellular TfR are incorporated into endocytic vesicles that interact transiently with EEA1 (early endosome antigen 1)-enriched endosomes and then move into juxtanuclear recycling compartments free of EEA1.[85] As seen in Figure 3.22, the targeted nanoparticles internalized through receptor-mediated endocytosis and accumulated in acidic vesicles intracellularly. This is consistent with results observed previously in Ramos cells where TfR-targeted nanoparticles internalized into acidic environments free of EEA1.[31] Targeted PRINT nanoparticles were endocytosed through the TfR into acidic compartments. As prodrug-loaded nanoparticles released gemcitabine more rapidly under acidic conditions than a neutral pH (Figure 3.20), acidic vesicles within cells are

143

the preferred sites of accumulation where prodrug degradation can be triggered for drug release. Effective delivery of gemcitabine can be achieved through this approach of combining both an acid-sensitive prodrug and targeted nanoparticles.

### 3.2.3.6 Cytotoxicity of Prodrug-Loaded Nanoparticles

Nanoparticles were fabricated with the diisopropyl silyl ether gemcitabine prodrug through the PRINT process by which the prodrug was polymerized into the nanoparticle. Covalently reacting the prodrug into the nanoparticles enabled convenient incorporation and retention of a water soluble drug into a hydrogel matrix. As the prodrug is sensitive to acid, gemcitabine was released from the nanoparticles more rapidly under endocytic conditions than a neutral environment. Through targeting the TfR, NP-OKT9 were found to accumulate intracellularly in acidic vesicles where the degradation of the prodrug can be stimulated. To investigate intracellular degradation of the prodrug *in vitro* and subsequent release of gemcitabine, cytotoxicity of prodrug-loaded nanoparticles was evaluated by a bioluminescence assay detecting ATP generation. Nanoparticles were incubated with H460 cells for 1 h at 37 °C for nanoparticles to target and bind to cells. Unbound nanoparticles were removed so as to minimize nonspecific cytotoxicity from the degradation of the prodrug and subsequent release of the drug from the nanoparticles. Viability of the cells was determined after 72 h. As shown in Figure 3.23, NP-OKT9 and unmodified pre-functionalized nanoparticles both exhibited similar cytotoxicity profiles.
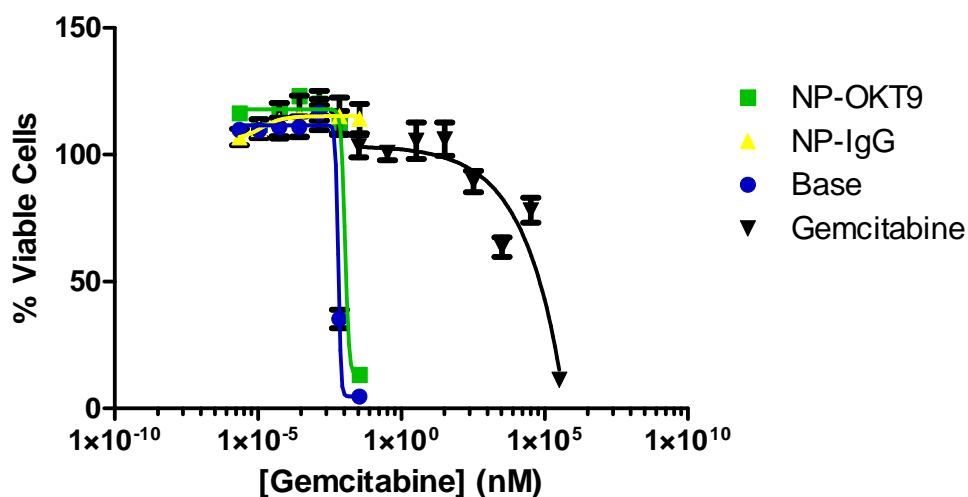
**Figure 3.23** Cytotoxicity of gemcitabine and nanoparticles loaded with silyl ether prodrug in H460 cells.

Both sets of nanoparticles were cytotoxic in subnanomolar concentrations, and the $IC_{50}$ of NP-OKT9 (0.018 nM) was nearly three times less toxic than pre-functionalized nanoparticles (Table 3.8). For NP-OKT9, cytotoxicity stemmed from the specific binding of OKT9 to the TfR and the subsequent receptor-mediated endocytosis of the nanoparticles into acidic vesicles within the cells where prodrug degradation could occur. Likewise, the pre-functionalized nanoparticles exhibited a similar cytotoxic profile ($IC_{50}$ = 0.0064 nM) to NP-OKT9, but instead, they internalized quickly albeit indiscriminately due to their positive $\zeta$-potential. Although the pre-functionalized nanoparticles exhibited a similar cytotoxicity profile to NP-OKT9, targeted nanoparticles with a negative surface charge are a more ideal therapeutic for *in vivo* purposes, as indicated by the NCI Nanotechnology Characterization Laboratory's criteria for the model nanoparticle therapeutic.

**Table 3.8** IC$_{50}$ values of gemcitabine and PRINT nanoparticles loaded with silyl ether gemcitabine prodrug in H460 cells.

|  | IC$_{50}$ (nM) | Relative Response |
|---|---|---|
| Pre-functionalized Nanoparticles | $6.37 \times 10^{-3}$ | 1.00 |
| NP-OKT9 | $1.82 \times 10^{-2}$ | 2.86 |
| Gemcitabine | $4.09 \times 10^{4}$ | $6.42 \times 10^{6}$ |

Moreover, NP-OKT9 and pre-functionalized nanoparticles demonstrated far improved efficacy relative to free gemcitabine. Gemcitabine was six orders of magnitude less cytotoxic than pre-functionalized nanoparticles. The chemotherapeutic is categorized as an antimetabolite. It is a nucleoside analog that once internalized, inhibits DNA synthesis, thereby arresting cell growth that leads to apoptosis.[52] Therefore, the efficacy of gemcitabine is foremost dependent on its transport into cells. The chemotherapeutic is typically internalized into cells through nucleoside transporters (NTs).[50,51] In our system, the mechanism of internalization of gemcitabine was different. The drug was shielded from the usual cellular uptake mechanism through incorporation into a nanoparticulate drug delivery system. Uptake of gemcitabine was dictated by the nanoparticles. Positive pre-functionalized nanoparticles were internalized nonspecifically because of their positive ζ-potential and were previously shown to traffick into cells through clathrin- and caveolae-mediated endocytosis.[27] NP-OKT9 were delivered intracellularly into cells through TfR-mediated endocytosis rather than NTs. Targeted nanoparticles trafficked into acidic compartments where the low pH environment promotes rapid degradation of the silyl ether prodrug and subsequent release of gemcitabine. Despite the lower concentration of dosed drug, the nanoparticles exhibited

well improved potency over free gemcitabine as a result of the method of delivery and internalization. Studies have shown that incorporating lipophilic gemcitabine derivatives into liposomes and polymeric nanospheres can magnify the effectiveness of the drug.[54,55,75,78,79] A few have also investigated nanocarriers targeting the EGFR[70,71,80] and HER2 receptor,[69] and demonstrated enhanced performance of gemcitabine through targeting. NP-OKT9 make up a new class of advanced drug delivery agents that are responsive to environmental stimuli and can selectively target diseased cells with amplified expression of the TfR. Bypassing the usual influx mechanism of NTs greatly enhanced the efficacy of gemcitabine when the chemotherapeutic was incorporated into TfR-targeted nanoparticles as an acid-sensitive prodrug that degraded under endocytic conditions.

### 3.2.4 Conclusions

TfR-targeted nanoparticles with diisopropyl silyl ether gemcitabine prodrug were shown to be more efficacious *in vitro* than gemcitabine alone, suggesting that NP-OKT9 are a promising platform for drug delivery. Nanoparticles demonstrated improved therapeutic efficacy through active targeting with OKT9 and the acid-sensitive silyl ether gemcitabine prodrug. They specifically targeted H460 cells, which have high expression of the TfR, and thus induced receptor-mediated endocytosis for internalization of the nanoparticles. Additionally, targeted nanoparticles loaded with the prodrug demonstrated preferential release of gemcitabine under acidic conditions compared to a neutral pH, indicating that the silyl ether prodrug was unaffected by incorporation into nanoparticles and the processing to conjugate targeting ligands. Intracellular accumulation of NP-

OKT9, through TfR-mediated endocytosis, into acidic vesicles promotes the acid catalyzed degradation of the silyl ether prodrug to release gemcitabine. The efficacy of these targeted nanoparticles was investigated through cytotoxicity studies. Targeted nanoparticles exhibited far improved therapeutic potency with a significantly lower $IC_{50}$ than gemcitabine alone. This is because the usual cellular uptake mechanism of gemcitabine was bypassed through targeting, and an acid-sensitive silyl ether gemcitabine prodrug, capable of degradation under acidic environments, was employed. NP-OKT9 are effective drug delivery agents that can specifically target cancer cells and deliver its cargo intracellularly to achieve enhanced therapeutic potency.

### 3.2.5  Future Work

NP-OKT9 have demonstrated the potential to advance cancer therapy. Nanoparticles conjugated with OKT9 can target a variety of cancers that have amplified levels of the TfR. When loaded with a silyl ether gemcitabine prodrug, they demonstrated enhanced efficacy against H460 large cell lung cancer cells *in vitro*. Thus, they are promising drug delivery nanocarriers that may improve upon conventional chemotherapeutics. NP-OKT9 were engineered and fabricated to shield gemcitabine to limit systemic distribution and consequently nonspecific toxicities, in addition to protecting the drug from potential plasma degradation. They were also designed to enhance the bioavailability of gemcitabine through targeting so as to increase drug efficacy. *In vivo* studies are required to better understand these behaviors of the targeted nanoparticles and the degradation of the silyl ether prodrug.

Moreover, TfR-targeted nanoparticles loaded with silyl ether gemcitabine prodrugs may be a possible therapeutic for gemcitabine-resistant cancers. Gemcitabine is typically internalized into cells through nucleoside transporters (NTs), in particular the human equilibrative nucleoside transporter 1 (hENT1).[51,52] Studies have shown that cells deficient in hENT1 are highly resistant to gemcitabine.[50] Without hENT1, cells have difficulty internalizing nucleoside analogs, so the expression level of hENT1 is a predictive marker for cellular sensitivity to gemcitabine.[50,51,53] As NP-OKT9 are internalized via receptor-mediated endocytosis, hENT1 would not be necessary for chemotherapy uptake and the usual internalization mechanism would be circumvented. Further investigation into targeted uptake and efficacy of nanoparticles loaded with silyl ether gemcitabine prodrugs in drug-resistant cells would provide more insight.

Furthermore, the possibility of acid-sensitive silyl ether prodrugs is not limited to gemcitabine. Derivatives of camptothecin and dasatinib have been synthesized and reported.[30] Additional chemotherapeutics can be modified with silyl ether chemistry to create prodrugs designed to degrade under endocytic conditions. The possibilities of silyl ether chemistry and its adaptation for prodrugs are still largely undiscovered. As the PRINT process is amenable to fabricating particles from new materials, novel silyl ether prodrugs can be easily incorporated into particles for drug delivery carriers that may improve upon current chemotherapeutics. Together silyl ether prodrugs and the PRINT platform have the potential to address a multitude of cancers.

## 3.3  References

(1)     Ganta, S.; Devalapally, H.; Shahiwala, A.; Amiji, M. *J Controlled Release* **2008**, *126*, 187-204.

(2)     Zhang, L.; Guo, R.; Yang, M.; Jiang, X.; Liu, B. *Advanced Materials* **2007**, *19*, 2988-2992.

(3)     Cammas, S.; Suzuki, K.; Sone, C.; Sakurai, Y.; Kataoka, K.; Okano, T. *J Controlled Release* **1997**, *48*, 157-164.

(4)     Na, K.; Bae, Y. H. *Pharm Res* **2002**, *19*, 681-688.

(5)     Soppimath, K. S.; Tan, D. C. W.; Yang, Y. Y. *Advanced Materials* **2005**, *17*, 318-323.

(6)     Kale, A. A.; Torchilin, V. P. *Bioconjug Chem* **2007**, *18*, 363-370.

(7)     Stefano, G. D.; Lanza, M.; Kratz, F.; Merina, L.; Fiume, L. *Eur J Pharm Sci* **2004**, *23*, 393-397.

(8)     Beyer, U.; Roth, T.; Schumacher, P.; Maier, G.; Unold, A.; Frahm, A. W.; Fiebig, H. H.; Unger, C.; Kratz, F. *J Med Chem* **1998**, *41*, 2701-2708.

(9)     Patel, V. F.; Hardin, J. N.; Mastro, J. M.; Law, K. L.; Zimmermann, J. L.; Ehlhardt, W. J.; Woodland, J. M.; Starling, J. J. *Bioconjug Chem* **1996**, *7*, 497-510.

(10)    Yoo, H. S.; Lee, E. A.; Park, T. G. *J Controlled Release* **2002**, *82*, 17-27.

(11)    Shen, W.-C.; Ryser, H. J. P. *Biochem Biophys Res Commun* **1981**, *102*, 1048-1054.

(12)    Gümüşderelioğlu, M.; Kesgin, D. *Int J Pharm* **2005**, *288*, 273-279.

(13)    Shin, J.; Shum, P.; Thompson, D. H. *J Controlled Release* **2003**, *91*, 187-200.

(14)    Heffernan, M. J.; Murthy, N. *Bioconjug Chem* **2005**, *16*, 1340-1342.

(15)    Sankaranarayanan, J.; Mahmoud, E. A.; Kim, G.; Morachis, J. M.; Almutairi, A. *ACS Nano* **2010**, *4*, 5930-5936.

(16)    Gillies, E. R.; Fréchet, J. M. J. *Bioconjug Chem* **2005**, *16*, 361-368.

(17)    Toncheva, V.; Schacht, E.; Ng, S. Y.; Barr, J.; Heller, J. *J Drug Target* **2003**, *11*, 345-353.

(18)     Oishi, M.; Nagasaki, Y.; Itaka, K.; Nishiyama, N.; Kataoka, K. *J Am Chem Soc* **2005**, *127*, 1624-1625.

(19)     Parrott, M. C.; Luft, J. C.; Byrne, J. D.; Fain, J. H.; Napier, M. E.; DeSimone, J. M. *Journal of the American Chemical Society* **2010**, *132*, 17928-17932.

(20)     Wuts, P. G. M.; Greene, T. W. *Greene's Protective Groups in Organic Synthesis*; 4th ed.; Wiley-Interscience: New York, 2006.

(21)     Furusawa, K.; Katsura, T. *Tetrahedron Lett* **1985**, *26*, 887-890.

(22)     Kumagai, D.; Miyazaki, M.; Nishimura, S.-I. *Tetrahedron Lett* **2001**, *42*, 1953-1956.

(23)     Trost, B. M.; Caldwell, C. G. *Tetrahedron Lett* **1981**, *22*, 4999-5002.

(24)     Montero, A.; Fossella, F.; Hortobagyi, G.; Valero, V. *The Lancet Oncology* **2005**, *6*, 229-239.

(25)     Rolland, J. P.; Maynor, B. W.; Euliss, L. E.; Exner, A. E.; Denison, G. M.; DeSimone, J. M. *J Am Chem Soc* **2005**, *127*, 10096-10100.

(26)     Enlow, E. M.; Luft, J. C.; Napier, M. E.; DeSimone, J. M. *Nano Letters* **2011**, *11*, 808-813.

(27)     Gratton, S. E. A.; Ropp, P. A.; Pohlhaus, P. D.; Luft, J. C.; Madden, V. J.; Napier, M. E.; DeSimone, J. M. *Proceedings of the National Academy of Sciences* **2008**, *105*, 11613-11618.

(28)     Kelly, J. Y.; DeSimone, J. M. *Journal of the American Chemical Society* **2008**, *130*, 5438-5439.

(29)     Merkel, T. J.; Jones, S. W.; Herlihy, K. P.; Kersey, F. R.; Shields, A. R.; Napier, M.; Luft, J. C.; Wu, H.; Zamboni, W. C.; Wang, A. Z.; Bear, J. E.; DeSimone, J. M. *Proceedings of the National Academy of Sciences* **2010**.

(30)     Parrott, M. C.; Finniss, M.; Luft, J. C.; Pandya, A.; Napier, M. E.; DeSimone, J. M. **2011**.

(31)     Wang, J.; Tian, S.; Petros, R. A.; Napier, M. E.; DeSimone, J. M. *Journal of the American Chemical Society* **2010**, *132*, 11306-11313.

(32)     Zhang, H.; et al. *New Journal of Physics* **2009**, *11*, 075018.

(33)     Slamon, D. J.; Leyland-Jones, B.; Shak, S.; Fuchs, H.; Paton, V.; Bajamonde, A.; Fleming, T.; Eiermann, W.; Wolter, J.; Pegram, M.; Baselga, J.; Norton, L. *N Engl J Med* **2001**, *344*, 783-792.

(34)   Park, J. W.; Hong, K.; Kirpotin, D. B.; Colbern, G.; Shalaby, R.; Baselga, J.; Shao, Y.; Nielsen, U. B.; Marks, J. D.; Moore, D.; Papahadjopoulos, D.; Benz, C. C. *Clin Cancer Res* **2002**, *8*, 1172-1181.

(35)   Pardo, L. A.; del Camino, D.; Sanchez, A.; Alves, F.; Bruggemann, A.; Beckh, S.; Stuhmer, W. *EMBO J* **1999**, *18*, 5540-5547.

(36)   Daniels, T. R.; Delgado, T.; Rodriguez, J. A.; Helguera, G.; Penichet, M. L. *Clinical Immunology* **2006**, *121*, 144-158.

(37)   Hortobagyi, G. N. *Semin Oncol* **2001**, *28, Supplement 18*, 43-47.

(38)   Nahta, R.; Esteva, F. J. *Cancer Lett* **2006**, *232*, 123-138.

(39)   Molina, M. A.; Codony-Servat, J.; Albanell, J.; Rojo, F.; Arribas, J. n.; Baselga, J. *Cancer Res* **2001**, *61*, 4744-4749.

(40)   Fattorossi; A; Nisini; R; Pizzolo; J, G.; D'Amelio; R *Cytometry* **1989**, *10*, 320-325.

(41)   Lyseng-Williamson, K. A.; Fenton, C. *Drugs* **2005**, *65*, 2513-2531.

(42)   Hamidi, M.; Azadi, A.; Rafiei, P. *Advanced Drug Delivery Reviews* **2008**, *60*, 1638-1649.

(43)   Wang, N.; Wu, X. S. *Pharm Dev Technol* **1997**, *2*, 135-142.

(44)   Jana, S. S.; Bharali, D. J.; Mani, P.; Maitra, A.; Gupta, C. M.; Sarkar, D. P. *FEBS Lett* **2002**, *515*, 184-188.

(45)   Vinogradov, S.; Batrakova, E.; Kabanov, A. *Colloids and Surfaces B: Biointerfaces* **1999**, *16*, 291-304.

(46)   Eckel, F.; Schneider, G. n.; Schmid, R. M. *Expert Opinion on Investigational Drugs* **2006**, *15*, 1395-1410.

(47)   Anderson, H.; Lund, B.; Bach, F.; Thatcher, N.; Walling, J.; Hansen, H. H. *Journal of Clinical Oncology* **1994**, *12*, 1821-1826.

(48)   Carmichael, J.; Possinger, K.; Phillip, P.; Beykirch, M.; Kerr, H.; Walling, J.; Harris, A. L. *Journal of Clinical Oncology* **1995**, *13*, 2731-2736.

(49)   Catimel, G.; Vermorken, J. B.; Clavel, M.; de Mulder, P.; Judson, I.; Sessa, C.; Piccart, M.; Bruntsch, U.; Verweij, J.; Wanders, J.; Franklin, H.; Kaye, S. B.; For the, E. E. C. T. G. *Annals of Oncology* **1994**, *5*, 543-547.

(50)   Achiwa, H.; Oguri, T.; Sato, S.; Maeda, H.; Niimi, T.; Ueda, R. *Cancer Science* **2004**, *95*, 753-757.

(51)     Mackey, J. R.; Mani, R. S.; Selner, M.; Mowles, D.; Young, J. D.; Belt, J. A.; Crawford, C. R.; Cass, C. E. *Cancer Research* **1998**, *58*, 4349-4357.

(52)     Veltkamp, S. A.; Pluim, D.; van Eijndhoven, M. A. J.; Bolijn, M. J.; Ong, F. H. G.; Govindarajan, R.; Unadkat, J. D.; Beijnen, J. H.; Schellens, J. H. M. *Molecular Cancer Therapeutics* **2008**, *7*, 2415-2425.

(53)     Reddy, L. H.; Couvreur, P. *Current Pharmaceutical Design* **2008**, *14*, 1124-1137.

(54)     Immordino, M. L.; Brusa, P.; Rocco, F.; Arpicco, S.; Ceruti, M.; Cattel, L. *J Controlled Release* **2004**, *100*, 331-346.

(55)     Stella, B.; Arpicco, S.; Rocco, F.; Marsaud, V. r.; Renoir, J.-M.; Cattel, L.; Couvreur, P. *International Journal of Pharmaceutics* **2007**, *344*, 71-77.

(56)     Abbruzzese, J. L.; Grunewald, R.; Weeks, E. A.; Gravel, D.; Adams, T.; Nowak, B.; Mineishi, S.; Tarassoff, P.; Satterlee, W.; Raber, M. N. *Journal of Clinical Oncology* **1991**, *9*, 491-498.

(57)     Reid, J. M.; Qu, W.; Safgren, S. L.; Ames, M. M.; Krailo, M. D.; Seibel, N. L.; Kuttesch, J.; Holcenberg, J. *Journal of Clinical Oncology* **2004**, *22*, 2445-2451.

(58)     Koshkina, N. V.; Kleinerman, E. S. *International Journal of Cancer* **2005**, *116*, 458-463.

(59)     Rodriguez, C. O.; Crabbs, T. A.; Wilson, D. W.; Cannan, V. A.; Skorupski, K. A.; Gordon, N.; Koshkina, N.; Kleinerman, E.; Anderson, P. M. *Journal of Aerosol Medicine and Pulmonary Drug Delivery* **2009**, *23*, 197-206.

(60)     Gagnadoux, F. d. r.; Leblond, V. r.; Vecellio, L.; Hureaux, J.; Le Pape, A.; Boisdron-Celle, M. l.; Montharu, J. r.; Majoral, C.; Fournier, J.; Urban, T.; Diot, P.; Racineux, J.-L.; Lemarié, E. *Cancer Chemotherapy and Pharmacology* **2006**, *58*, 237-244.

(61)     Gagnadoux, F.; Pape, A. L.; Lemarié, E.; Lerondel, S.; Valo, I.; Leblond, V.; Racineux, J. L.; Urban, T. *European Respiratory Journal* **2005**, *26*, 657-661.

(62)     Gordon, N.; Kleinerman, E. S. *Journal of Aerosol Medicine and Pulmonary Drug Delivery* **2010**, *23*, 189-196.

(63)     Bergman, A. M.; al, e.; et al. *ChemInform* **2005**, *36*, no-no.

(64)     Myhren, F.; Borretzen, B.; Dalen, A.; Sandvold, M. L.; Conpharma AS. (Parkveien 55, Oslo, 0256, NO): 2004.

(65)     Pasut, G.; Canal, F.; Dalla Via, L.; Arpicco, S.; Veronese, F. M.; Schiavon, O. *Journal of Controlled Release* **2008**, *127*, 239-248.

(66) Arias, J. L.; Reddy, L. H.; Couvreur, P. *Langmuir* **2008**, *24*, 7512-7519.

(67) Wu, W.; Sigmond, J.; Peters, G. J.; Borch, R. F. *Journal of Medicinal Chemistry* **2007**, *50*, 3743-3746.

(68) Bender, D. M.; Bao, J.; Dantzig, A. H.; Diseroad, W. D.; Law, K. L.; Magnus, N. A.; Peterson, J. A.; Perkins, E. J.; Pu, Y. J.; Reutzel-Edens, S. M.; Remick, D. M.; Starling, J. J.; Stephenson, G. A.; Vaid, R. K.; Zhang, D.; McCarthy, J. R. *Journal of Medicinal Chemistry* **2009**, *52*, 6958-6961.

(69) Arya, G.; Vandana, M.; Acharya, S.; Sahoo, S. K. *Nanomedicine: Nanotechnology, Biology and Medicine* **2011**.

(70) Kim, I.-Y.; Kang, Y.-S.; Lee, D. S.; Park, H.-J.; Choi, E.-K.; Oh, Y.-K.; Son, H.-J.; Kim, J.-S. *Journal of Controlled Release* **2009**, *140*, 55-60.

(71) Sandoval, M. A.; Sloat, B. R.; Lansakara-P, D. S. P.; Kumar, A.; Rodriguez, B. L.; Kiguchi, K.; DiGiovanni, J.; Cui, Z. *Journal of Controlled Release* **2011**.

(72) Yang, J.; Park, S. B.; Yoon, H.-G.; Huh, Y. M.; Haam, S. *International Journal of Pharmaceutics* **2006**, *324*, 185-190.

(73) Celano, M.; Calvagno, M.; Bulotta, S.; Paolino, D.; Arturi, F.; Rotiroti, D.; Filetti, S.; Fresta, M.; Russo, D. *BMC Cancer* **2004**, *4*, 63.

(74) Bornmann, C.; Graeser, R.; Esser, N.; Ziroli, V.; Jantscheff, P.; Keck, T.; Unger, C.; Hopt, U.; Adam, U.; Schaechtele, C.; Massing, U.; von Dobschuetz, E. *Cancer Chemotherapy and Pharmacology* **2008**, *61*, 395-405.

(75) Moog, R. M.; Burger, A. B.; Brandl, M. B.; Schüler, J. S. l.; Schubert, R. S.; Unger, C. U.; Fiebig, H. F.; Massing, U. M. *Cancer Chemotherapy and Pharmacology* **2002**, *49*, 356-366.

(76) Whitehouse, P. A.; Cooper, A. J.; Johnson, C. D. *Pancreatology* **2003**, *3*, 367-374.

(77) Wynter, M. P.; Russell, S. T.; Tisdale, M. J. *In Vivo* **2004**, *18*, 543-548.

(78) Sloat, B. R.; Sandoval, M. A.; Li, D.; Chung, W.-G.; Lansakara-P, D. S. P.; Proteau, P. J.; Kiguchi, K.; DiGiovanni, J.; Cui, Z. *International Journal of Pharmaceutics* **2011**, *409*, 278-288.

(79) Wang, C.-X.; Huang, L.-S.; Hou, L.-B.; Jiang, L.; Yan, Z.-T.; Wang, Y.-L.; Chen, Z.-L. *Brain Research* **2009**, *1261*, 91-99.

(80) Patra, C. R.; Bhattacharya, R.; Wang, E.; Katarya, A.; Lau, J. S.; Dutta, S.; Muders, M.; Wang, S.; Buhrow, S. A.; Safgren, S. L.; Yaszemski, M. J.; Reid, J. M.; Ames, M. M.; Mukherjee, P.; Mukhopadhyay, D. *Cancer Research* **2008**, *68*, 1970-1978.

(81)    Miller, C. R.; Bondurant, B.; McLean, S. D.; McGovern, K. A.; O'Brien, D. F. *Biochemistry* **1998**, *37*, 12875-12883.

(82)    Harush-Frenkel, O.; Debotton, N.; Benita, S.; Altschuler, Y. *Biochemical and Biophysical Research Communications* **2007**, *353*, 26-32.

(83)    Gratton, S.; Napier, M.; Ropp, P.; Tian, S.; DeSimone, J. *Pharmaceutical Research* **2008**, *25*, 2845-2852.

(84)    Zauner, W.; Ogris, M.; Wagner, E. *Advanced Drug Delivery Reviews* **1998**, *30*, 97-113.

(85)    Leonard, D.; Hayakawa, A.; Lawe, D.; Lambright, D.; Bellve, K. D.; Standley, C.; Lifshitz, L. M.; Fogarty, K. E.; Corvera, S. *Journal of Cell Science* **2008**, *121*, 3445-3458.